SYNTHESIS AND CHARACTERIZATION OF Cu-MCM-41 AND Ni-MCM-41 TYPE CATALYTIC MATERIALS

A THESIS SUBMITTED TO
THE GRADUATE SCHOOL OF NATURAL AND APPLIED SCIENCES
OF
MIDDLE EAST TECHNICAL UNIVERSITY

BY

ASLI NALBANT

IN PARTIAL FULFILLMENT OF THE REQUIREMENTS
FOR
THE DEGREE OF MASTER OF SCIENCE
IN
CHEMICAL ENGINEERING

JANUARY 2005

Approval of the Graduate School of Natural and Applied Sciences

Prof. Dr. Canan Özgen
Director

I certify that this thesis satisfies all the requirements as a thesis for the degree of Master of Science.

Prof. Dr. Nurcan Baç
Head of Department

This is to certify that we have read this thesis and that in our opinion it is fully adequate, in scope and quality, as a thesis and for the degree of Master of Science.

Prof. Dr. Suna Balcı
Co-Supervisor

Prof. Dr. Timur Doğu
Supervisor

Examining Committee Members

Prof. Dr. Hayrettin Yücel (METU, CHE) _____

Prof. Dr. Timur Doğu (METU, CHE) _____

Prof. Dr. Tunçer H. Özdamar (Ankara Univ., CHE) _____

Prof. Dr. Gülşen Doğu (Gazi Univ., CHE) _____

Assoc. Prof. Gürkan Karakaş (METU, CHE) _____

I hereby declare that all information in this document has been obtained and presented in accordance with academic rules and ethical conduct. I also declare that, as required by these rules and conduct, I have fully cited and referenced all material and results that are not original to this work.

Name, Last name: Aslı Nalbant

Signature :

ABSTRACT

SYNTHESIS AND CHARACTERISATION OF Cu-MCM-41 AND Ni-MCM-41 TYPE CATALYTIC MATERIALS

Nalbant, Aslı
M.S., Department of Chemical Engineering
Supervisor: Prof. Dr. Timur DOĞU
Co-Supervisor: Prof. Dr. Suna BALCI

January 2005, 128 pages

Discovery of mesoporous materials by Mobil researchers in 1992 opened a new field in catalytic applications. The materials designated as M41S family are MCM-41 with one-dimensional hexagonal structure, MCM-48 with three-dimensional cubic structure and MCM-51 with unstable lamellar structure. This family of materials have high surface areas up to 1500 m^2/g, narrow pore size distributions with pore sizes varying from 20 to 100 Å. These materials can be activated by incorporation of metals or active compounds into their structures.

In this study, copper and nickel incorporated MCM-41 type catalytic materials were synthesized via different methods namely, impregnation, high temperature and low temperature direct synthesis methods. The Cu-MCM-41, and Ni-MCM-41, as well as synthesized MCM-41 were characterized by using XRD, TEM, N_2 sorption, SEM, XRF, EDS, AAS and TPR.

MCM-41 was synthesized with high temperature direct synthesis method. High surface area values up to 1400 m^2/g of MCM-41 mesoporous materials were obtained with high pore volumes up to 1.17 cc/g.

Cu-MCM-41 type catalytic materials were synthesized with three different methods. Impregnation and high temperature direct synthesis methods gave better results than those of low temperature direct synthesis method. In impregnation, relatively high surface area values (730 m^2/g) were obtained with Cu/Si mole ratio as high as 0.3 in the product. For the case of high temperature direct synthesis products, Cu/Si mole ratios as high as 0.26 were obtained with somewhat smaller surface areas (400 m^2/g). Low temperature direct synthesis method is the least favorable method in metal loading.

Ni-MCM-41 type of catalytic materials were synthesized by impregnation and high temperature direct syntheses methods. Ni incorporation by high temperature direct synthesis method gave high surface area values (560-930 m^2/g) having Ni/Si mole ratios of 0.12-0.28.

Keywords: MCM-41, copper, nickel, mesoporous molecular sieves

ÖZ

Cu-MCM-41 VE Ni-MCM-41 TİPİ KATALİTİK MALZEMELERİN SENTEZLENMESİ VE KARAKTERİZASYONU

Nalbant, Aslı
Yüksek Lisans, Kimya Mühendisliği
Tez Yöneticisi: Prof. Dr. Timur DOĞU
Ortak Tez Töneticisi: Prof. Dr. Suna BALCI

Ocak 2005, 128 sayfa

Mezo gözenekli malzemelerin 1992 yılında Mobil araştırmacıları tarafından sentezi katalitik uygulamalarında yeni ufuklar açtı. M41S ailesi olarak adlandırılan bu malzemeler, tek boyutlu altıgen yapısıyla MCM-41, üç boyutlu kübik yapısıyla MCM-48 ve lamellar yapısıyla MCM-50'dir. 1500 m^2/g 'a varan yüzey alanları, çapları 20 ila 100 Å arasında değişen düzenli gözenek dağılımları ve yüksek ısıl kararlılıkları bu malzemelerin başlıca özellikleridir. M41S ailesindeki malzemelerin kendilerine ait katalitik özellikleri bulunmadığından, metaller ve aktif bileşiklerin yapılarına katılmasıyla aktiflik kazanırlar.

Bu çalışmada bakır ve nikel katkılı MCM-41 tipi katalitik malzemeler çeşitli sentez yöntemleriyle sentezlendi. Bu yöntemler, sonradan ekleme, yüksek sıcaklıkta doğrudan ekleme, ve düşük sıcaklıkta doğrudan ekleme

olarak adlandırılabilirler. Sentezlenen MCM-41, Cu-MCM-41 ve Ni-MCM-41 XRD, TEM, N_2 adsorplanması, SEM, XRF, EDS, AAS ve TPR yöntemleriyle karakterize edildi.

MCM-41 yüksek sıcaklık doğrudan ekleme yöntemiyle sentezlendi. 1400 m^2/g' a varan yüksek yüzey alanı gösteren MCM-41 gözenekli malzemelerde 1.17 cc/g' a varan gözenek hacimleri elde edildi.

Cu-MCM-41 katalitik malzemeler 3 farklı yöntemle sentezlendi. Sonradan ekleme ve yüksek sıcaklıkta doğrudan ekleme yöntemleri düşük sıcaklıkta doğrudan ekleme yöntemine oranla daha iyi sonuç verdi. Sonradan ekleme yönteminde yüksek yüzey alanları (730 m^2/g) ile 0.3 Cu/Si mol oranı elde edildi. Yüksek sıcaklıkta doğrudan ekleme yönteminde ise, ürünlerdeki Cu/Si mol oranı 0.26 gibi yüksek bir değer gösterirken yüzey alanlarında kismi düşüş gözlendi (400 m^2/g). Düşük sıcaklıkta doğrudan ekleme yöntemi metal yükleme açısından en az terci edilen yöntem oldu.

Ni-MCM-41 tipi katalitik malzemeler yüksek sıcaklık doğrudan ekleme ve sonradan ekleme yöntemleriyle sentezlendi. Nikelin yüksek sıcaklık doğrudan sentezleme yöntemi ile eklenmesi sonucunda yüksek yüzey alanlari (560-930 m^2/g) ve 0.12 ve 0.28 Cu/Si mol oranları elde edildi.

Anahtar kelimeler: MCM-41, bakır, nikel, mezo gözenekli moleküler yapı

To Mehmet Melikoğlu,

ACKNOWLEDGEMENTS

I wish to express my deepest gratitude to my supervisor Prof. Dr. Timur Doğu for his guidance, advice, criticism, and encouragements throughout the research. Also I wish to express my gratitude to my co-supervisor Prof. Dr. Suna Balcı for her valuable advice.

I would like to express my sincere appreciation to Prof. Dr. Hayrettin Yücel for his suggestions and comments and Prof. Dr. Tunçer Özdamar for the nickel(II) nitrate hexahydrate supply. I acknowledge the kind permission of Assoc. Prof. Gürkan Karakaş for the TPR analysis in his laboratory. Also I would like to thank Burcu Mirkelamoğlu for her help during these analyses. Special thanks go to Yeşim Güçbilmez for sharing her valuable knowledge.

I would like to thank Mr. Serkan Türk from ÇMB (Çimento Müstahsilleri Birliği) for XRD analyses, Mr. Tarık Baykara and Mr. Orhan İpek from TUBITAK Marmara Araştırma Merkezi (MAM) Malzeme ve Kimya Teknolojleri Araştırma Enstitüsü (MKTAE) for TEM and SEM analyses, Mrs. Gülten Bayrakçı from Microstructure Laboratory of Chemical Engineering Department and Prof. Dr. Çiğdem Erçelebi from Central Laboratory of METU for N_2 sorption analysis, Mr. İhsan Yavuz from MTA (Maden Tetkik Arama) for XRF analyses, Mr. Cengiz Tan from Metallurgical and Materials Engineering Department of METU for EDS analyses, Ms. Kerime Güney from Instrumental Analysis Laboratory of Chemical Engineering Department of METU for AAS analyses and deionized water supply.

I present my sincere gratitude to Mehmet Melikoğlu for his valuable support, patience, help and encouragement. Without him, it would not be possible to end my study in such a short time. I offer sincere thanks to Tülay and Kazım Melikoğlu for being near me during these years.

Finally, I would like to thank my family, and my grandfather Mehmet Göçeoğlu for their patience and support.

This study was supported by the Turkish State Planning Organization (DPT) Grant No: DPT.0-04-DPT.2003K120920-0.5.

TABLE OF CONTENTS

PLAGIARISM iii

ABSTRACT iv

ÖZ vi

DEDICATION viii

ACKNOWLEDGEMENTS ix

TABLE OF CONTENTS xi

LIST OF TABLES xiv

LIST OF FIGURES xvii

NOMENCLATURE xx

CHAPTER

1 INTRODUCTION 1

2 M41S MOLECULAR SIEVES MATERIALS 3

2.1 Historical Development of M41S Molecular Sieves Materials 3

2.2 M41S Family 3

2.2.1 MCM-41 4

2.2.2 MCM-48 6

2.2.3 MCM-50 7

2.3 Cu-MCM-41 and Ni-MCM-41 Type Catalytic Materials 7

3 CHARACTERIZATION OF M41S MOLECULAR SIEVES MATERIALS 10

3.1 X-ray Diffraction 10

3.2 Transmission Electron Microscopy 12

3.3 N_2 Sorption 13

3.4 Scanning Electron Microscopy 16

3.5 X-ray Fluorescence 17

3.6 Energy Dispersive Spectroscopy 17

4 EXPERIMENTAL 18

4.1 Chemicals 18

4.1.1 Source of Silica 19
4.1.2 Source of Surfactant 19
4.1.3 Source of Solvent 19
4.1.4 Source of Acid 19
4.1.5 Source of Metal 19
4.2 Synthesis of MCM-41 20
4.3 Synthesis of Cu-MCM-41 Type Catalytic Materials 22
4.3.1 Impregnation Method 22
4.3.2 High Temperature Direct Synthesis Method 23
4.3.3 Low Temperature Direct Synthesis Method 24
4.4 Synthesis of Ni-MCM-41 Type Catalytic Materials 26
4.4.1 High Temperature Direct Synthesis Method 26
4.4.2 Impregnation Method 27
4.5 Characterization 28
4.5.1 X-ray Diffraction 28
4.5.2 Transmission Electron Microscopy 28
4.5.3 N_2 Sorption 28
4.5.4 Scanning Electron Microscopy 29
4.5.5 X-ray Fluorescence 29
4.5.6 Energy Dispersive Spectroscopy 29
4.5.7 Atomic Absorption Spectroscopy 29
4.5.8 Temperature Programmed Reduction 30
5 RESULTS AND DISCUSSION 31
5.1 Synthesis Results 31
5.2 Characterization Results 33
5.2.1 X-ray Diffraction 34
5.2.2 Transmission Electron Microscopy 39
5.2.3 N_2 Sorption 40
5.2.4 Scanning Electron Microscopy 52
5.2.5 X-ray Fluorescence 53
5.2.6 Energy Dispersive Spectroscopy 54
5.2.7 Atomic Absorption Spectroscopy 55
5.2.8 Temperature Programmed Reduction 58
5.3 Economics 60
6 CONCLUSIONS AND RECOMMENDATIONS 61
REFERENCES 63

APPENDICES 67

A MSDS OF CHEMICALS 67

B CHARACTERIZATION DATA 77

B.1 X-ray Diffraction 77

B.2 Transmission Electron Microscopy 90

B.3 N_2 Sorption 91

B.4 Scanning Electron Microscopy 117

B.5 X-ray Fluorescence 120

B.6 Energy Dispersive Spectroscopy 121

B.7 Atomic Absorption Spectroscopy 126

B.8 Temperature Programmed Reduction 127

LIST OF TABLES

4.1 Synthesis differences of MCM-41 mesoporous materials 21

5.1 Summary of the Synthesized Materials 32

5.2 Summary of the Characterization Techniques 33

5.3 Summary of Physical Properties 51

5.4 XRF results of Cu-MCM-41 type catalytic materials 53

5.5 XRF results of Ni-MCM-41 type catalytic materials 53

5.6 EDS results of Cu-MCM-41 type catalytic materials 54

5.7 EDS results of Ni-MCM-41 type catalytic materials 54

5.8 AAS results of Cu-MCM-41 type catalytic materials 55

5.9 AAS results of Ni-MCM-41 type catalytic materials 55

5.10 Summary of Metal Content 56

5.11 Cost analyses of materials 60

5.12 Cost of synthesized materials 60

A.1 MSDS of Sodium Silicate Solution 67

A.2 Physical and Chemical Properties of Sodium Silicate Solution 68

A.3 MSDS of Sodium Metasilicate 69

A.4 Physical and Chemical Properties of Sodium Metasilicate 70

A.5 MSDS of Hexadecyltrimethyl ammonium bromide 71

A.6 Physical and Chemical Properties of Hexadecyltrimethyl ammonium bromide 72

A.7 MSDS of Copper (II) nitrate trihydrate 73

A.8 Physical and Chemical Properties of Copper (II) nitrate trihydrate 74

A.9 MSDS of Nickel (II) nitrate hexahydrate 75

A.10 Physical and Chemical Properties of Nickel (II) nitrate hexahydrate 76

B.1 XRD plot of MCM-41(I) 77
B.2 XRD plot of MCM-41(II) 78
B.3 XRD plot of MCM-41(III) 79
B.4 XRD plot of MCM-41(IV) 80
B.5 XRD plot of Cu-Imp(I) 81
B.6 XRD plot of Cu-Imp(II) 82
B.7 XRD plot of Cu-HT(I) 83
B.8 XRD plot of Cu-HT(II) 84
B.9 XRD plot of Cu-LT(I) 85
B.10 XRD plot of Cu-LT(II) 86
B.11 XRD plot of Ni-HT(I) 87
B.12 XRD plot of Ni-HT(II) 88
B.13 XRD plot of Ni-Imp(I) 89
B.14 N_2 Sorption Data of MCM-41(I) 91
B.15 N_2 Sorption Data of MCM-41(II) 93
B.16 N_2 Sorption Data of MCM-41(III) 95
B.17 N_2 Sorption Data of MCM-41(IV) 97
B.18 N_2 Sorption Data of Cu-Imp(I) 99
B.19 N_2 Sorption Data of Cu-Imp(II) 101
B.20 N_2 Sorption Data of Cu-HT(I) 103
B.21 N_2 Sorption Data of Cu-HT(II) 104
B.22 N_2 Sorption Data of Cu-LT(I) 106
B.23 N_2 Sorption Data of Cu-LT(II) 108
B.24 N_2 Sorption Data of Ni-HT(I) 110
B.25 N_2 Sorption Data of Ni-HT(II) 112
B.26 N_2 Sorption Data of Ni-Imp(I) 114
B.27 Summary of N_2 Sorption Data 116
B.28 XRF analyses of Cu-MCM-41 type catalytic materials 120

B.29 XRF analyses of Ni-MCM-41 type catalytic materials 120
B.30 AAS analyses of Cu-MCM-41 type catalytic materials 126
B.31 AAS analyses of Ni-MCM-41 type catalytic materials 126

LIST OF FIGURES

2.1 LCT Mechanism proposed by Beck et al. (1992) 5

2.2 Structure of MCM-48 (Schumacher et al., 2000) 6

2.3 Structure of MCM-50 (Behrens et al., 1997) 7

3.1 XRD of calcined MCM-41 (Beck et al., 1992) 11

3.2 XRD of calcined MCM-48 (Beck et al., 1992) 11

3.3 Types of Adsorption Isotherms 14

3.4 Types of Hysteresis 15

4.1 Schematic Representation of the Synthesis of MCM-41 21

4.2 Schematic Representations of the Syntheses of Cu-MCM-41 Type Catalytic Materials 25

4.3 Schematic Representations of the Syntheses of Ni-MCM-41 Type Catalytic Materials 27

5.1 Success of experiments in terms of synthesized materials 31

5.2 XRD plot of MCM-41(I) 34

5.3 XRD plot of MCM-41(II) 34

5.4 XRD plot of MCM-41(III) 34

5.5 XRD plot of MCM-41(IV) 34

5.6 XRD plot of Cu-Imp(I) 36

5.7 XRD plot of Cu-Imp(II) 36

5.8 XRD plot of Cu-HT(I) 36

5.9 XRD plot of Cu-HT(II) 36

5.10 XRD plot of Cu-LT(I) 36

5.11 XRD plot of Cu-LT(II) 36

5.12 XRD plot of Ni-HT(I) 38

5.13 XRD plot of Ni-HT(II) 38
5.14 XRD plot of Ni-Imp(I) 38
5.15 TEM of MCM-41(I) 39
5.16 TEM of Cu-Imp(I) 39
5.17 TEM of Cu-HT(I) 39
5.18 TEM of Cu-LT(I) 39
5.19 N_2 Adsorption/Desorption Isotherms of Synthesized MCM-41 Mesoporous Materials 40
5.20 N_2 Adsorption/Desorption Isotherms of Synthesized Cu-MCM-41 Type Catalytic Materials 42
5.21 N_2 Adsorption/Desorption Isotherms of Synthesized Ni-MCM-41 Type Catalytic Materials 43
5.22 N_2 Adsorption Pore Size Distribution (APSD) and Desorption Pore Size Distribution (DPSD) of MCM-41 Mesoporous Materials 45
5.23 N_2 Adsorption Pore Size Distribution (APSD) and Desorption Pore Size Distribution (DPSD) of Cu-MCM-41 Type Catalytic Materials 46-47
5.24 N_2 Adsorption Pore Size Distribution (APSD) and Desorption Pore Size Distribution (DPSD) of Ni-MCM-41 Type Catalytic Materials 48
5.25 SEM of MCM-41(I) 52
5.26 SEM of Cu-Imp(I) 52
5.27 SEM of Cu-HT(I) 52
5.28 SEM of Cu-LT(I) 52
5.29 TPR of Cu-Imp(I) 58
5.30 TPR of Cu-HT(I) 58
5.31 TPR of Cu-LT(II) 59
B.1 TEM of Cu-LT(I) 90
B.2 TEM of Cu-LT(I) 90
B.3 TEM of Cu-LT(I) 90

B.4 SEM of MCM-41(I) 117
B.5 SEM of MCM-41(I) 117
B.6 SEM of Cu-Imp(I) 117
B.7 SEM of Cu-Imp(I) 117
B.8 SEM of Cu-Imp(I) 117
B.9 SEM of Cu-Imp(I) 117
B.10 SEM of Cu-HT(I) 118
B.11 SEM of Cu-HT(I) 118
B.12 SEM of Cu-LT(I) 118
B.13 SEM of Cu-LT(I) 118
B.14 SEM of Cu-LT(I) 118
B.15 SEM of Cu-LT(I) 118
B.16 SEM of Cu-LT(I) 119
B.17 EDS of Cu-Imp(I) 121
B.18 EDS of Cu-Imp(II) 121
B.19 EDS plot of Cu-HT(I) 122
B.20 EDS plot of Cu-HT(II) 122
B.21 EDS plot of Cu-LT(I) 123
B.22 EDS plot of Cu-LT(II) 123
B.23 EDS plot of Ni-HT(I) 124
B.24 EDS plot of Ni-HT(II) 124
B.25 EDS plot of Ni-Imp(I) 125
B.26 TPR of Cu-Imp(I) 127
B.27 TPR of Cu-HT(I) 127
B.28 TPR of Cu-LT(II) 128

NOMENCLATURE

Abbreviations

AAS : Atomic Absorption Spectroscopy

EDS : Energy Dispersive Spectroscopy

IUPAC : International Union of Pure and Applied Chemistry

MCM : Mobil Composition of Matter

SEM : Scanning Electron Microscopy

TEM : Transmission Electron Microscopy

TPR : Temperature Programmed Reduction

XPS : X-ray Photoelectron Spectroscopy

XRD : X-ray Diffraction

XRF : X-ray Fluorescence

CHAPTER 1

INTRODUCTION

According to International Union of Pure and Applied Chemistry (IUPAC) definition, materials are classified into three categories in terms of their pore sizes (IUPAC, 1972):

- Microporous Materials

(pore diameters $\leq$ 20 Å)

- Mesoporous materials

(20 Å $<$pore diameters $<$500 Å)

- Macroporous materials

(pore diameters $\geq$ 500 Å)

Zeolites are the members of microporous materials and provide excellent catalytic properties. However, their applications are limited by the relatively small pore openings. Porous glasses and porous gels have larger pores but they have disordered pore systems with broad pore-size distributions (Ciesla and Schüth, 1999).

In 1992 researchers at Mobil Oil Research and Development Corporation discovered highly ordered inorganic mesoporous materials with high surface areas [Kresge et al., 1992]. These materials are designated as M41S family. The members of this family are MCM-41, MCM-48, and MCM-51.

MCM refers to Mobil Composition of Matter and the numbers are only sequence numbers.

MCM-41, MCM-48, and MCM-51 differ in sizes, molecular structures and surface areas. MCM-41 has one-dimensional, hexagonally-ordered pore structure, MCM-48 has three-dimensional, cubic-ordered pore structure, and MCM-51 has unstable lamellar structure. M41S family of materials can be used as adsorbents, catalysts, and, catalyst supports.

MCM-41 type catalytic materials have applications in many different fields. Cu-MCM-41 and Ni-MCM-41 type catalytic materials can be used in the steam reforming reaction of methanol or ethanol to form hydrogen which is the future scope of this study.

In this study, copper and nickel incorporated MCM-41 type catalytic materials were synthesized following three different methods, namely impregnation, high temperature and low temperature direct synthesis methods. The Cu-MCM-41, and Ni-MCM-41, as well as synthesized MCM-41 were characterized by using XRD, N_2 sorption, XRF, SEM, TEM, Energy Dispersive Spectroscopy (EDS), Atomic Absorption Spectroscopy (AAS) and Temperature Programmed Reduction (TPR).

CHAPTER 2

M41S MOLECULAR SIEVES MATERIALS

2.1 Historical Development of M41S Molecular Sieves Materials

Before the discovery of these materials in 1992 by Mobil Research and Development Corporation researchers (Kresge et al., 1992), a patent including the procedure for the preparation of low-density silica was already described by Chiola et al. in 1971. Di Renzo et al. (1997) reproduced the materials described in the patent and obtained MCM-41. However, the remarkable properties of these materials were actually discovered by Mobil researchers and patented in 1991 by Beck (Beck, 1991). These mesoporous molecular sieves were later designated as M41S family (Beck et al., 1992). The members of this family are MCM-41, MCM-48 and MCM-50.

2.2 M41S Family

Although MCM-41, MCM-48 and MCM-50 are synthesized from the same materials they show very different structural properties (Behrens et al, 1997). Detailed descriptions, properties and syntheses of these materials are given in the following sections.

2.2.1 MCM-41

Like other members of the M41S family, MCM-41 is synthesized by four main components (Øye et al., 2001):

- A source of silica
- Structure-directing surfactants
- A solvent
- Acid or base

Mobil researchers found that the relative concentrations of the species present in the synthesis solutions were of great importance for the final pore structures. In the M41S family, MCM-41 is formed with the highest concentration of silica, i.e., lowest surfactant/silica molar ratio. As the surfactant/silica molar ratio was varied, the products formed could be grouped into four main categories (Vartuli et al., 1994):

1. Surfactant/silica < 1 :hexagonal (MCM-41)
2. Surfactant/Silica = 1-1.5 : Cubic (MCM-48)
3. Surfactant/Silica = 1.2-2 : Lamellar (MCM-50)
4. Surfactant/Silica > 2 : Cubic octamer

The pore diameter of MCM-41 can be varied by changing the alkyl chain length of the cationic surfactants used in the synthesis procedure (Kresge et al., 1992). The experimental studies indicate that MCM-41 pore diameter increases with surfactant chain length (Beck et al., 1992).

MCM-41 mesoporous molecular sieves are formed by a liquid-crystal templating mechanism (LCT) in which surfactant liquid-crystal structures serve as templates (Kresge et al., 1992 and Beck et al., 1992). Two possible pathways were proposed by Beck et al. as can be seen in Figure 2.1 (1992):

(1) The liquid-crystal phase is intact before the silicate species are added

(2) The addition of silicate results in the ordering of the subsequent silicate encased surfactant micelles

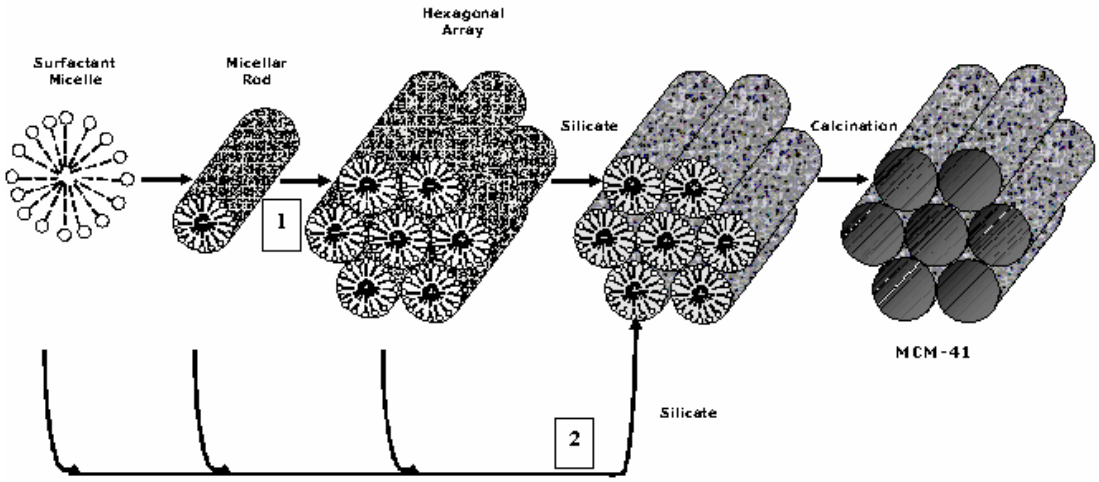

Figure 2.1 LCT Mechanism proposed by Beck et al. (1992)

For either pathway, the resultant composition would produce an inorganic material that mimics known liquid-crystal phases. For pathway (1) to be operative, it is required that the surfactant molecules exist in sufficient concentration for a liquid-crystal structure to form. This liquid-crystal structure serves as the templating agent and the inorganic silicate anions merely serve to counterbalance the charge of these fully ordered surfactant aggregates. For pathway (2), surfactant is only part of the template. The presence of a silicate anion species not only serves to charge balance the surfactant cations but also participates in the formation and ordering of the liquid-crystal phase. At

constant surfactant concentration, different types of M41S mesoporous materials are formed by varying silica concentration so pathway (1) is consistent with the synthesis data (Vartuli et al., 1994).

2.2.2 MCM-48

MCM-48 differs from MCM-41 and MCM-50 in its crystal and pore structures. It has a cubic Ia3d symmetrical structure, with a proposed three-dimensional pore system having two independent intertwined channel networks. Because of this three-dimensional pore structure, MCM-48 is an attractive candidate for use in various sorption and catalysis applications (Roth, 2000).

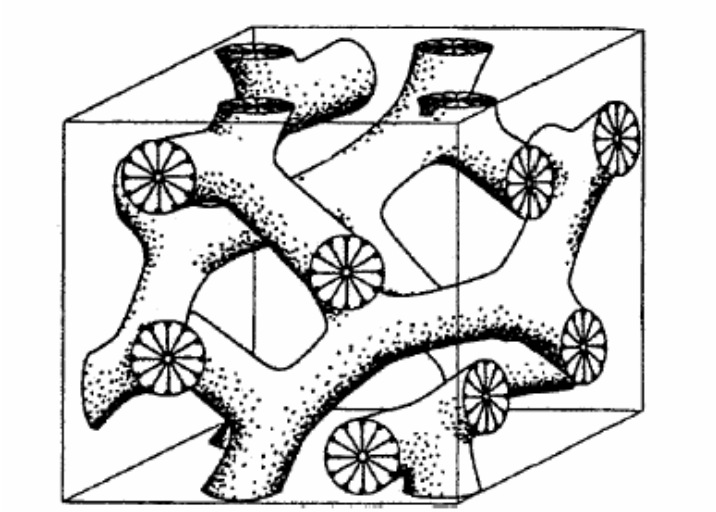

Figure 2.2 Structure of MCM-48 (Schumacher et al., 2000)

MCM-48 can be produced by reacting an inorganic silica reagent, an alkylammonium hydroxide, and a halide-containing surfactant in an aqueous medium. The process can be carried out in a single step or in multiple steps such that the inorganic silica reagent and the alkylammonium hydroxide are reacted first to form a first reaction mixture. The first reaction mixture then is

combined with a halide-containing surfactant to form a second reaction mixture that is maintained under sufficient conditions to form a crystalline MCM-48 product (Roth, 2000).

While attractive because of its possible three-dimensional pore structure, crystalline MCM-48 has not been widely used. Difficulties in synthesizing MCM-48, in the laboratory and particularly on a large scale commercial basis, have limited the availability of this material (Roth, 2000)

2.2.3 MCM-50

MCM-50 possesses a lamellar arrangement of surfactant and silica layers given in Figure 2.3.

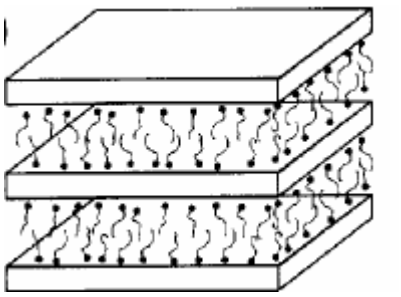

Figure 2.3 Structure of MCM-50 (Behrens et al, 1997)

This structure collapses upon calcination and does not give a mesoporous compound (Behrens et al., 1997).

2.3 Cu-MCM-41 and Ni-MCM-41 Type Catalytic Materials

Up to now Cu-MCM-41 type catalytic materials were synthesized by various methods. For example, while Ziolek et al. (2004) synthesized by room temperature method, Guo et al. (2004) synthesized at 273 K. Different types of impregnation techniques were employed by Tsoncheva and co-workers (2004). Cu-Al-MCM-41 type catalytic materials were studied by Wan et al.

(2004) by hydrothermal method. Also syntheses of Cu-MCM-48 type catalytic materials were studied by Hartmann et al. (1997) and Hadjiivanov et al. (2003).

Cu incorporated MCM-41 type catalytic materials have different applications. For example, Noreńa-Franco et al. (2002) studied the oxidation reaction of phenol, employing Cu-modified MCM-41 mesoporous catalysts. Velu et al. (2002) studied the catalytic performance of copper and zinc modified MCM-41 mesoporous catalysts for the selective oxidation of alcohols to aldehydes. Also copper is an attractive catalyst for H_2S removal at high temperatures from process gases in petroleum refining and other industrial processes (Yasyerli et al., 2004). So Cu-MCM-41 type catalytic materials can find applications in removal of H_2S.

Synthesis conditions of Ni-MCM-41 have great variety. Chang et al. (1999) synthesized Ni-MCM-41 type catalytic materials by hydrothermal synthesis method with a very high surface area (1151 m2/g). A novel synthesis method was followed by Jin and co-workers in 2004. In this method a coating process was applied to prepare nickel-silica composite hollow nanospheres (650 nm) with controllable shell thickness. Ion exchange synthesis method was performed by Brühwiller and Frei (2003). Incipient wetness technique was performed by Lensveld and co-workers (2001) to obtain high metal loading and high dispersion of the active phase.

Ni incorporated MCM-41 type catalytic materials find applications in the reduction of nitroarenes and carbonyl compounds to the corresponding amines and alcohols, respectively (Mohapatra et al., 2002). This type of materials also find applications in ethylene dimerization and butane isomerization (Hartmann et al., 1996). Nickel substituted MCM-41 molecular sieves are also used for the

oxidation of hydrocarbons (Parvulescu and Su, 2001) and for the gas phase hydrogenation of acetonitrile (Infantes-Molina et al., 2004).

Hydrogen production from steam reforming of ethanol might be attractive for countries with extensive plantations of sugar cane (Garcia et al., 1991). Ethanol has many good properties such as:

- Safe handling
- Cheap
- Easy transport
- Biodegradability
- Low toxicity

Recent studies have shown that copper-nickel supported catalysts are suitable for the production of hydrogen from ethanol (Mariño et al. 1998 and 2003) and catalytic behavior of catalysts were analyzed in the ethanol steam reforming reaction at 300 °C and atmospheric pressure (Mariño et al. 2003). The influence of the diffusional effects, the residence time and the water/ethanol molar ratio fed on the ethanol conversion and on the product distribution was analyzed and additional experiments were performed to postulate a mechanism and to clarify the role of each metal (Cu and Ni) by Mariño and co-workers (2004).

CHAPTER 3

CHARACTERIZATION OF M41S MOLECULAR SIEVES MATERIALS

In this study, XRD, TEM, N_2 sorption, SEM, XRF, EDS, AAS and TPR characterization techniques were studied. XRD and TEM techniques were used to determine pore architecture of the materials. N_2 sorption techniques were used to determine the porosity and specific surface area of materials. SEM is used to observe morphology. XRF, EDS, AAS, and TPR are used to determine metal content of Cu-MCM-41 and Ni-MCM-41 type catalytic materials. Detailed information of these techniques are given in the following sections.

3.1 X-ray Diffraction

XRD provides direct information of the pore architecture of the materials. For mesoporous materials, the diffraction patterns only have reflection peaks in the low-angle range, meaning 2θ less than 10. No reflections are seen at higher angles. It has thereby been concluded that the pore walls mainly are amorphous. The ordering lies in the pore structure, and the low-angle diffraction peaks can be indexed according to different lattices (Øye et al., 2001).

MCM-41 exhibits an XRD pattern containing typically 3-5 peaks which can be indexed to a hexagonal lattice as (100), (110), (200), (210), and (300) (Beck et al., 1992). Since the materials are not crystalline at the atomic level,

no reflections at higher angles are observed. By X-ray diffraction it is not possible to quantify the purity of the material (Ciesla and Schüth, 1999). In Figure 3.1 X-ray powder diffraction data for a sample of MCM-41 is given (Beck et al., 1992).

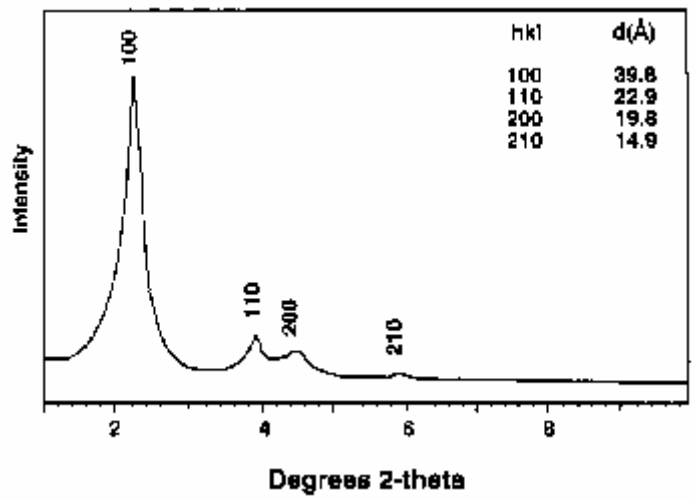

Figure 3.1 XRD of calcined MCM-41 (Beck et al., 1992)

A total of 8 peaks were used to index the X-ray diffraction pattern of MCM-48. The XRD powder pattern of MCM-48 could be indexed completely on the basis of a unit cell with a= 81.09 Å (Vartuli et al., 1994).In Figure 3.2 X-ray powder diffraction data for a sample of MCM-48 is given (Beck et al., 1992).

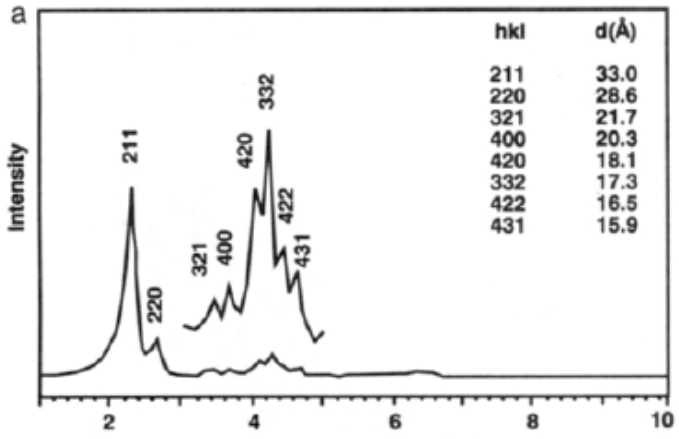

Figure 3.2 XRD of calcined MCM-48 (Beck et al., 1992)

3.2 Transmission Electron Microscopy

During the nineteenth and early twentieth century, it was realized that there was a need for a microscope with greater resolution than the optical microscope. As it was known that the very short wavelengths of electrons could theoretically provide subnanometer resolution, work was begun on the first electron microscope. After a sustained research effort toward this need, Ernst Ruska developed the first TEM in 1931. This was the first microscope to exceed the 500-nm resolution limit, of the best optical microscope of the time. By 1938, von Ardenne had improved the TEM resolution to between 50 and 100 nm. Due to the short mean free path of an electron in a solid, samples intended for TEM analysis need to be extremely thin, usually < 300 nm, or else the material will not transmit the electron beam. The absolute sample thickness depends on sample density and the electron accelerating voltage used. TEMs are typically capable of producing a beam between 100 and 300 kV, however, there are several instruments that produce 3000-kV beams. TEMs are most commonly used in the conventional or "parallel beam" operation mode in which a relatively defocused beam, measuring several microns in diameter, is used to illuminate the sample. More advanced TEMs may employ a scanned beam mode in which the beam is focused to a diameter of <10 nm and is scanned over the area of interest in much the same way as any other scanning. Due to the very small probe sizes obtainable in scanning TEM (STEM), they are better suited for microchemical analysis and crystallographic studies. Most TEMs are able to resolve details of <0.5 nm on almost any substance. With this resolution, lattice fringes and rows of atoms are visible (Wiley Interscience).

TEM is widely used by biologists as well as materials scientists, although the high cost of a TEM and the expertise required to utilize one limits usage.

The most significant drawback to TEM are the sample thickness requirement and the ultrahigh vacuum (UHV) environment. Special cutting devices called "ultramicrotomes" are commonly used to cut soft materials into <500-nm sections, but sample preparation can still be very time consuming and frustrating. With that said, the TEM is still one of the most generally useful microscopes. TEMs are applicable to the study of ultrafine particles (eg, pigments, abrasives and carbon blacks) as well as microtomed thin sections of plant and animal tissue, paper, polymers, composites, foods, industrial materials, minerals, etc. Even metals can be made thin enough for detailed examination (Wiley Interscience).

Transmission Electron Microscopy (TEM) is the pre-eminent method for determining dislocations' and other crystallographic defects character and for performing chemical and crystallographic analysis of micrometer and smaller precipitates and other microstructures (Cullity, 2001).

3.3 N_2 Sorption

In the literature, there are recorded tens of thousands of adsorption isotherms, measured on a wide variety of solids. Nevertheless, the majority of these isotherms which result from physical adsorption may conveniently be grouped into five classes- the five types I to V of the classification originally proposed by Brunauer, Deming, Deming and Teller, sometimes referred to as Brunauer, Emmett and Teller (BET) or simply Brunauer classification. The essential features of these types are indicated in Figure 3.3, including Type VI which is of particular theoretical interest (Gregg and Sing, 1982).

In the case of physical adsorption, Type I isotherms are encountered with microporous powders whose pore size does not exceed a few adsorbate

molecular diameters. Physical adsorption that produces Type I isotherm indicates that the pores are microporous and that the exposed surface resides almost exclusively within the micropores, which once filled with adsorbate; leave little or no external surface for additional adsorption. Type II isotherms are most frequently encountered when adsorption occurs on nonporous powders or on powders with pore diameters larger than micropores. Type III isotherms are characterized principally by heats of adsorption which are less than the adsorbate heat of liquefaction. Type IV isotherms occur on porous adsorbents possessing pores in the radius range of approximately 15-1000 Å. Type V isotherms result from small adsorbate-adsorbent interaction potentials similar to the Type III isotherms. However, Type V isotherms are also associated with pores in the same range as those of Type IV isotherms (Lowell and Shields, 1991).

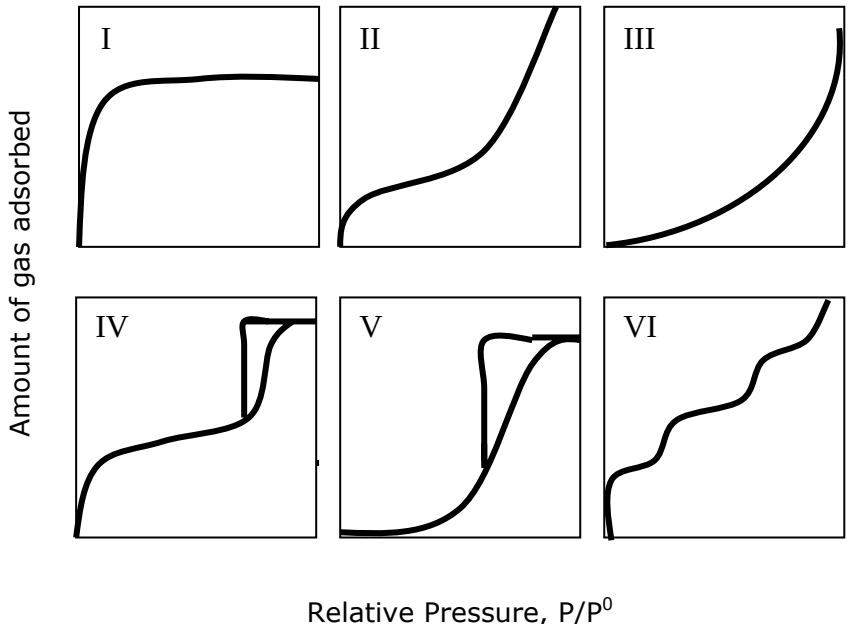

Figure 3.3 Types of Adsorption Isotherms (Adapted from Greg and Sing, 1982)

Adsorption techniques are used to determine the porosity and specific surface area of materials. The most common adsorbate is probably N_2 (at

77K). According to IUPAC definition, mesoporous materials exhibit a Type IV adsorption-desorption isotherm. At low relative pressures (P/P0) the adsorption only occurs a thin layer on the walls (monolayer coverage). Depending on the pore size, a sharp increase is seen at relative pressures from 0.25 to 0.5. This corresponds to capillary condensation of N2 in the mesopores. The sharpness of the inflection reflects the uniformity of the pore sizes and the height indicates the pore volume. A hysteresis effect is often observed for N2 adsorption-desorption isotherms when the pore diameter is larger than approximately 40 A° (Øye et al., 2001). Types of hysteresis are given in Figure 3.4. Type A hysteresis is due principally to cylindrical pores open at both ends. Type B hysteresis curve is associated with slit-shaped pores or the space between parallel plates. Type C hysteresis is produced by a mixture of tapered or wedge-shaped pores with open ends. Type d curves are also produced by tapered or wedge-shaped pores but with narrow necks at one or both open ends. Type E hysteresis result from bottle-neck pores (Lowell and Shields, 1991).

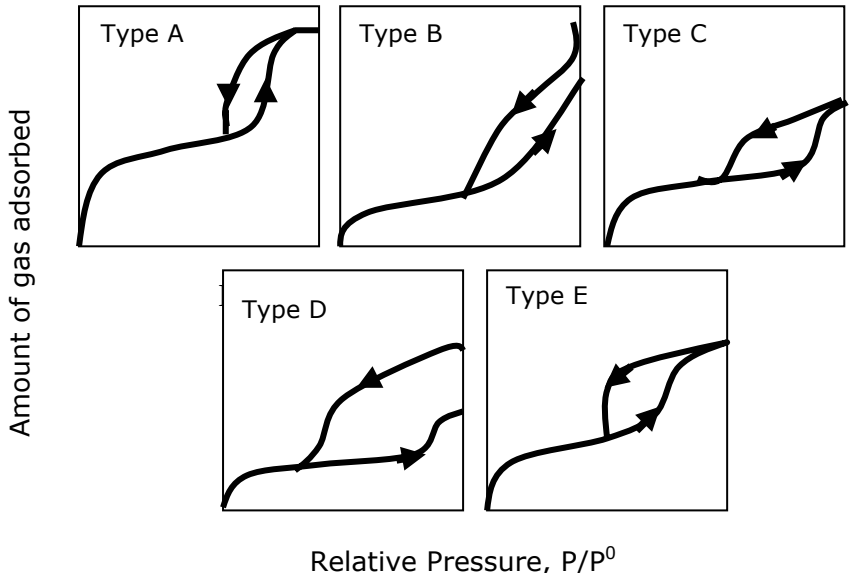

Figure 3.4 Types of Hysteresis (Adapted from Lowell and Shields, 1991)

The Barrett-Joyner-Halenda (BJH) method for calculating pore size distributions (Barrett et al., 1951) is based on a model of the adsorbent as a collection of cylindrical pores. The theory accounts for capillary condensation in the pores using the classical Kelvin equation, which in turn assumes a hemispherical liquid-vapor meniscus and a well-defined surface tension. The BJH theory also incorporates thinning of the adsorbed layer through the use of a reference isotherm; the Kelvin equation is only applied to the "core" fluid. (Gelb et al, 2005).

3.4 Scanning Electron Microscopy

The SEM consists of a column which houses the filament (ie, electron source), electromagnetic lens, and the beam scanning coils. At the base of the column is the sample chamber that contains the stage and detectors. Depending on the goal of a particular investigation, the SEM may be operated in a number of different modes. These include high depth of field; low voltage, surface sensitive; high beam current and high resolution modes. Like other scanning microscopes, the SEM acquires data from the sample one point at a time. At each location where the electron beam impacts the sample, a flux of secondary electrons, backscatter electrons, X-rays, and other signals are emitted from the sample A portion of each signal travels in a direction such that it enters a detector. The detector measures the intensity of electrons emitted at each point on the sample and converts this intensity value into a corresponding 8 bit (i.e., 2^8, or 256) grayscale value. This digitized value is then displayed on a monitor. The relative position of the output pixel on the monitor is synchronized with the movement and position of the beam on the sample. That is to say, when the beam is located at the position, row 1, column 1, the intensity measurement from that point will be displayed in row 1, column 1 of the monitor. This image formation process applies to all of the

collected signals and allows an image of each signal to be collected simultaneously. Given this image formation process, it is not difficult to understand that if the size of the raster is decreased then the magnification of the image will increase proportionally (Wiley Interscience).

3.5 X-ray Fluorescence

X-ray fluorescence is a nondestructive physical method used for chemical analyses of solids and liquids. The specimen is irradiated by an intense X-ray beam which causes the elements in the specimen to emit (that is, fluorescence) their characteristic X-ray line spectra. The lines of the spectra are diffracted at various angles by a single crystal plate which is analogous to the diffraction grating of optical spectroscopy. The elements may be identified by the wavelengths of their spectral lines, which vary in a regular manner with atomic number, and their concentrations may be determined from the intensities of the lines (McGraw-Hill Enc.).

The X-ray fluorescence method has proven particularly useful for mixtures of elements of similar chemical properties which are difficult to separate and analyze by conventional chemical methods (McGraw-Hill Enc.).

3.6 Energy Dispersive Spectroscopy

The Energy Dispersive Spectrometer first gained acceptance as an attachment for the Scanning Electron Microscope (SEM). The first use of EDS was for completely qualitative analysis that is the identification of elements present at the point on the sample surface (Russ, 1984). EDS identifies the elemental composition of materials imaged in a SEM.

CHAPTER 4

EXPERIMENTAL

In this study, synthesis and characterization of MCM-41, Cu-MCM-41 and Ni-MCM-41 type catalytic materials were investigated in detail. MCM-41 was synthesized by high temperature direct synthesis method. Three types of synthesis procedures were followed for Cu-MCM-41 type catalytic materials namely impregnation method, high temperature direct synthesis method and low temperature direct synthesis method. Ni-MCM-41 type catalytic materials were synthesized by high temperature direct synthesis method and impregnation.

The obtained catalytic materials as well as MCM-41 were characterized by XRD, TEM, N_2 sorption, SEM, XRF, EDS, AAS and TPR analysis techniques.

4.1 Chemicals

There are four main components in the synthesis of MCM-41 mesoporous materials. These are a source of silica, a source of surfactant, a source of solvent and stabilizers (acid or base).

For the synthesis of MCM-41 type catalytic materials, a source of metal was required.

4.1.1 Source of Silica

There were two silica sources used during experiments. These are:

- Sodium silicate solution (27 wt % SiO_2, 14 wt. % NaOH) from Aldrich
- Sodium metasilicate (44-47 wt % SiO_2) from Aldrich

Detailed information about these materials are given in Appendix A.

4.1.2 Source of Surfactant

The surfactant used during experiments was hexadecyltrimethyl ammonium bromide (CTMABr, 99 % pure powder) from Sigma. Information about this chemical is given in Appendix A.

4.1.3 Source of Solvent

Deionized water was used as solvent in the syntheses. It was obtained from Millipore Ultra-Pure Water System (Milli-QPlus).

4.1.4 Source of Acid

The acid used in experiments was sulfuric acid from Merck.

4.1.5 Source of Metal

Copper and nickel sources were found after a literature survey of ethanol steam reforming. Mariño et al (1998 and 2003) used $Cu(NO_3)_2 \cdot 3H_2O$ as copper source and $Ni(NO_3)_2 \cdot 6H_2O$ as nickel source. In the present study, the copper source was copper (II) nitrate trihydrate from Merck and the nickel source was nickel nitrate hexahydrate from Merck. Information about these chemicals were given in Appendix A.

4.2 Synthesis of MCM-41

MCM-41 was prepared by a modified procedure of Beck and co-workers (1992). This modified procedure was performed by Zhang and co-workers (2001). By using a similar recipe high specific surface areas of MCM-41 and V-MCM-41 mesoporous materials were synthesized and characterized by Güçbilmez et al. (in press). 13.2 g of hexadecyltrimethyl ammonium bromide was dissolved in 86 ml of deionized water. The solution was heated up to 30 °C for the complete dissolution of surfactant. Than 11.3 ml of sodium silicate was added dropwise to the clear solution with continuous stirring. After observing the formation of a gel, the pH of the mixture was adjusted to 11 by adding sufficient amount of 1 M H_2SO_4. The resulting gel was stirred for 1 hour before being transferred to a Teflon bottle and placed in a stainless-steel autoclave. The hydrothermal synthesis was carried out at 120 °C for 96 hours. The resultant solid was recovered by filtration, washed thoroughly with deionized water and dried at room temperature. Before calcination the solid was kept at 40 °C for 24 hours. The as-synthesized MCM-41 was finally calcined in a tubular furnace by heating from ambient temperature to 550 °C at a rate of 1 °C/min and kept at 550 °C for 6 hours in a flow of dry air. The calcination tube was 100 cm long made up of quartz glass. There is also a quartz filter in the calcination tube (40 cm from one end) to hold the solid during air flow. For calcination process, the solid sample was poured from the long end of the tube where air was introduced. The other end was connected to ventilation to remove the gas products.

The schematic representation of the synthesis of MCM-41 by high temperature synthesis method is given in Figure 4.1.

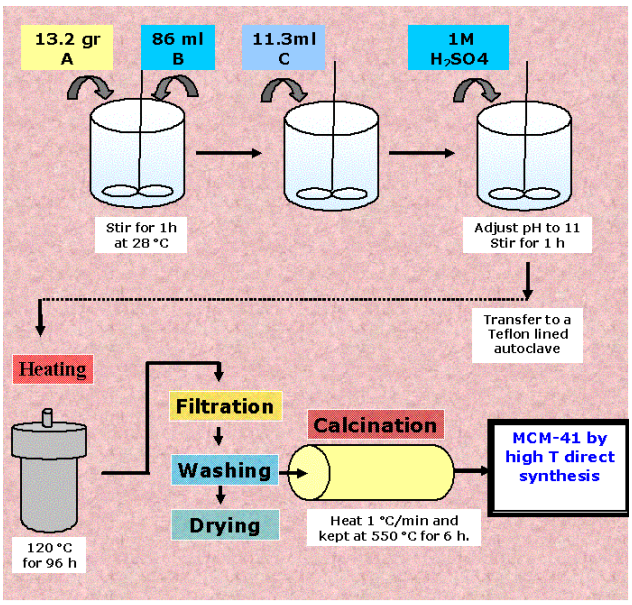

Figure 4.1 Schematic Representation of the Synthesis of MCM-41

Eight MCM-41 mesoporous materials were synthesized throughout the study. Some of the samples were eliminated due to their low surface area. Also some samples were lost during washing process or heating. As a result, only four of them were taken into consideration. These samples are named as MCM-41(I), MCM-41(II), MCM-41(III) and MCM-41 (IV). There are some differences in the synthesis of these samples which yield to different structural properties. These differences are summarized in Table 4.1.

Table 4.1 Synthesis differences of MCM-41 mesoporous materials

Sample ID	**Gel preparation**	**Washing**
MCM-41(I)	All surfactant was dissolved at once in 86 ml of water	Washed until pH of the filtrate is 7.4.
MCM-41(II)	Surfactant was added in small amounts into 55 ml of water.	Washed until pH of the filtrate is 7.3.
MCM-41(III)	Surfactant was added in small amounts into 55 ml of water.	Washed until pH of the filtrate is 8.0.
MCM-41(IV)	Surfactant was added in small amounts into 86 ml of water.	Washed until pH of the filtrate is 9.0.

4.3 Synthesis of Cu-MCM-41 Type Catalytic Materials

4.3.1 Impregnation Method

Cu-MCM-41 type catalytic materials obtained from the impregnation method were synthesized from a modified procedure of Tsoncheva et al. (2004). 2 grams of the uncalcined MCM-41 was shaken at room temperature with 11 ml of 1 M aqueous solution of copper (II) nitrate trihydrate. Then the liquid phase was removed by centrifugation and the obtained product was dried at room temperature and then under vacuum for one night. There was no washing treatment in this procedure. The obtained product was finally calcined by heating from ambient temperature to 550 °C at a rate of 1 °C/min and kept at 550 °C for 6 hours in a flow of dry air.

Two Cu-MCM-41 type catalytic materials obtained by impregnation method were taken into consideration. These are named as Cu-Imp(I) and Cu-Imp(II). These materials were obtained by incorporation of copper into as-synthesized MCM-41(I) and MCM-41(III) respectively. In the first sample, 2.66 g of copper nitrate trihydrate was added in 2 g of MCM-41(I). Excess amount of solution was removed by centrifugation. In the case of Cu-Imp(II), 0.67 g of copper nitrate trihydtrate was added in 0.5 g of MCM-41(III). Excess amount of solution was removed by centrifugation.

The schematic representation of impregnation method is given in Figure 4.2.

4.3.2 High Temperature Direct Synthesis Method

This is a modified method of MCM-41 synthesis. 13.2 grams of hexadecyltrimethyl ammonium bromide was dissolved in 86 ml of deionized water. The solution was heated up to 30 °C for the complete dissolution of surfactant. Than 11.3 ml of sodium silicate was added dropwise to the clear solution with continuous stirring. A certain amount of copper (II) nitrate trihydrate solution (1.7 g solid in 7 ml of water) was added to the gel mixture to obtain Cu/Si mole ratio of 0.05. After stirring for 1 hour, the pH of the mixture was adjusted to 11 by adding sufficient amount of 1 M H_2SO_4. The resulting gel is stirred for 1 hour before being transferred to a Teflon bottle and placed in a stainless-steel autoclave. The hydrothermal synthesis was carried out at 120 °C for 96 hours. The resultant solid was recovered by filtration, washed thoroughly with deionized water and dried at room temperature. Before calcination the solid was kept at 40 °C for 24 hours. The as-synthesized Cu/MCM-41 was finally calcined by heating from ambient temperature to 550 °C at a rate of 1 °C/min and kept at 550 °C for 6 hours in a flow of dry air.

Two Cu-MCM-41 type catalytic materials were taken into consideration and named as Cu-HT(I), and Cu-HT(II). There are some differences in the synthesis of these samples. The first sample was heated at 120 °C for 72 hours while the second one was heated for 96 hours as described in the procedure. No acid treatment was performed for both of the samples.

The schematic representation of the synthesis of Cu-MCM-41 type catalytic materials with high temperature synthesis method is given in Figure 4.2.

4.3.3 Low Temperature Direct Synthesis Method

This procedure was modified from Guo et al. (2004). The source of silica used in this synthesis procedure was different from the impregnation and high temperature direct synthesis. 9.3 grams of hexadecyltrimethylammonium bromide was dissolved in 250 ml of water. 12.2 g of sodium metasilicate was added to the clear solution. Then the mixture was cooled to 273 K in an ice-water bath. Than 50 ml of copperammonia solution composed of 1,2 g of copper (II) nitrate trihydrate and 25% aqueous ammonia was added at 273 K, resulting in a dark blue solution. With constant stirring, diluted sulfuric acid (1 M) was added to regulate pH to a value of 9. After further stirring for 3 hours, the solution was filtered to separate the solid phase from solution. The product was washed repeatedly with distilled water for a number of times and dried at room temperature. The as-synthesized Cu/MCM-41 was finally calcined by heating from ambient temperature to 550 °C at a rate of 1 °C/min and kept at 550 °C for 6 hours in a flow of dry air.

Two Cu-MCM-41 type catalytic materials synthesized by low temperature direct synthesis method and named as Cu-LT(I) and Cu-LT(II). For the first sample the pH of the solution was adjusted to 8.7 and the obtained product was washed with ethanol and deionized water for a number of times until the pH of the filtrate was 7.2. For Cu-LT(II), the pH of the solution was adjusted to 9 and the obtained product was washed with deionized water only for a number of times.

The schematic representation of the synthesis of Cu-MCM-41 type catalytic material by low temperature synthesis method is given in Figure 4.2.

Impregnation Method High Temperature Direct Synthesis Low Temperature Direct Synthesis

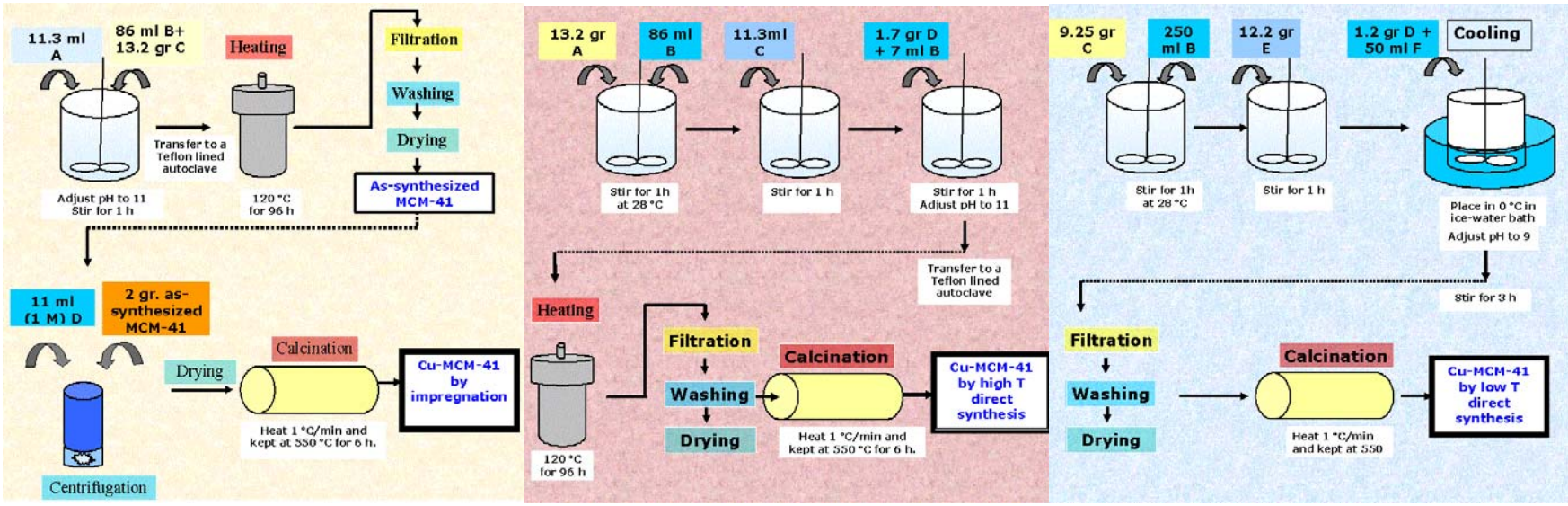

Figure 4.2 Schematic Representations of the Syntheses of Cu-MCM-41 Type Catalytic Materials

4.4 Synthesis of Ni-MCM-41 Type of Catalytic Materials

4.4.1 High Temperature Direct Synthesis Method

This is a modified method of MCM-41 synthesis. 13.2 grams of hexadecyltrimethyl ammonium bromide was dissolved in 86 ml of deionized water. The solution was heated up to 30 °C for the complete dissolution of surfactant. Than 11.3 ml of sodium silicate was added dropwise to the clear solution with continuous stirring. A certain amount of nickel (II) nitrate hexahydrate solution (1.7 g solid in 2 ml of water) was added to the gel mixture to obtain Ni/Si mole percent 0.05. The pH of the mixture was adjusted to 11 by dilute sulfuric acid. The resulting gel is stirred for 1 hour before being transferred to a Teflon bottle and placed in a stainless-steel autoclave. The hydrothermal synthesis was carried out at 120 °C for 96 hours. After heat treatment, the gel contained solid precipitates. The resultant solid was recovered by filtration, washed thoroughly with deionized water and dried at room temperature. Before calcination the solid was kept at 40 °C for 24 hours. The as-synthesized Ni/MCM-41 was finally calcined by heating from ambient temperature to 550 °C at a rate of 1 °C/min and kept at 550 °C for 6 hours in a flow of dry air.

Two Ni-MCM-41 type catalytic materials were synthesized and named as Ni-HT(I) and Ni-HT(II). There were some differences in the syntheses of these two samples. For the first sample, no acid treatment was done and the solution was kept at the pH of 11.1. For the second sample acid was added into the final solution to adjust pH at 11.

The schematic representation of the synthesis procedure is given in Figure 4.3.

4.4.2 Impregnation Method

2 grams of the uncalcined MCM-41 was stirred at room temperature with aqueous solution of nickel (II) nitrate hexahydrate (0.24 g of $Ni(NO_3)_2 \cdot 3H_2O$ with 20 ml of water). The solution was stirred for 10 hours at 40 °C and dried at room temperature and then under vacuum for one night. The obtained product was finally calcined by heating from ambient temperature to 550 °C at a rate of 1 °C/min and kept at 550 °C for 6 hours in a flow of dry air.

There was only one Ni-MCM-41 type catalytic material synthesized by this procedure. Nickel was incorporated into the as-synthesized MCM-41(IV).

The schematic representation of the synthesis of Ni-MCM-41 type catalytic material by impregnation method is given in Figure 4.3.

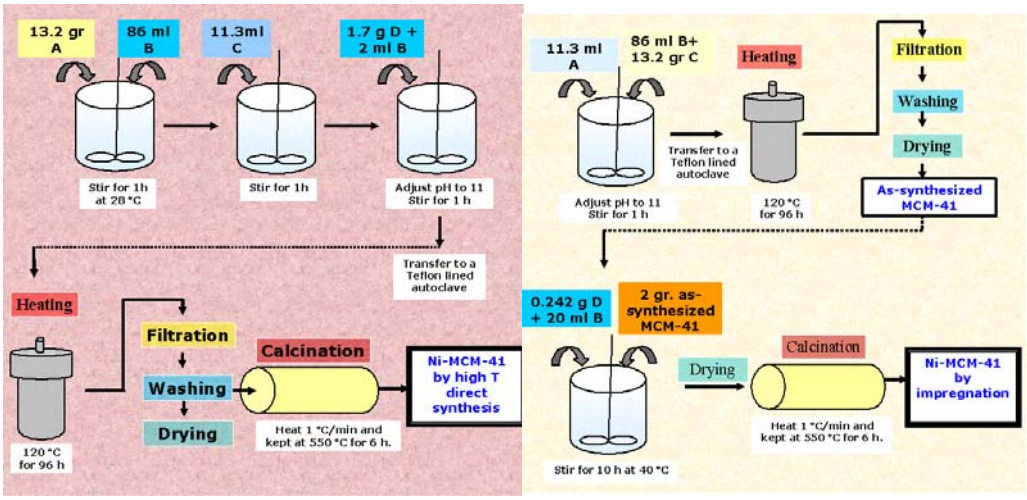

Figure 4.3 Schematic Representations of the Syntheses of Ni-MCM-41 Type Catalytic Materials

4.5 Characterization

4.5.1 X-ray Diffraction

The XRD patterns of all synthesized materials were by using a Philips PW3040 based X-Ray diffractometer with Cu Kα anode radiation source (wavelength 0.15406 nm). The diffraction patterns were collected at a diffraction angle 2θ from 1° to 25° at a step size of 0.02 and a scan speed of 0.025 (2θ/s). The samples for the XRD analysis were powder and outgassed in vacuum overnight at 110 °C before analysis.

4.5.2 Transmission Electron Microscopy

The Transmission Electron Microscope analyses were determined by TEM-100C (JEOL) .

4.5.3 N_2 Sorption

The BET surface area values and pore size distributions of all samples were determined from nitrogen adsorption data at 77 K by a computerized analyzer model ASAP 2000 of Micromeritics Co. Inc. except Cu-Imp(I) and Cu-HT(I). These two samples were characterized by Quantochrome Autosorb-1/C. Before measurements, calcined samples were outgassed in vacuum overnight at 110 °C. Pore size distributions and pore diameters were calculated by the BJH method from the adsorption and desorption branch of the nitrogen adsorption-desorption isotherms.

4.5.4 Scanning Electron Microscopy

The morphologies of the synthesized materials were determined by using a Scanning Electron Microscope, JSM-6335 F (JEOL) equipped with Oxford System.

4.5.5 X-ray Fluorescence

X-ray Fluorescence Analyses were obtained using ZIX3000 (Rigaku) X-ray Spectrometer.

4.5.6 Energy Dispersive Spectroscopy

Near surface compositions of the materials were determined from Energy Dispersive Spectroscopy by using JSM-6400 SEM (JEOL) equipped with NORAN System Six.

4.5.7 Atomic Absorption Spectroscopy

The copper and nickel content was determined by Atomic Absorption Spectroscopy on Philips PU9200X spectrometer. AAS analyses were carried out by a modified method suggested by Grubert et al. (1998).

The Cu-MCM-41 and Ni-MCM-41 type catalytic materials were dissolved in a mixture of nitric acid and hydrochloric acid (1:3, volume ratio). Digestion procedure was carried out on a hot plate, and repeated for three times. Than, the liquid phase was filtered and metal content was determined by atomic absorption spectrophotometer. The remaining solid phase that contained SiO_2 was determined from gravimetric titration method.

4.5.8 Temperature Programmed Reduction

TPR analyses were performed for Cu-MCM-41 type catalytic materials using a mass spectrometer connected to a tubular reactor. The weighted sample was placed to the quartz tubular reactor having an inside diameter of 4 mm and activated in a flow of 5 vol % O_2 in He with a flowrate of 17.6 ml/min up to a maximum temperature of 400 °C at a rate of 10 °C/min and kept at 400 °C for 30 minutes. After cooling the reactor to room temperature, the

reduction of the catalyst was done in a flow of 5 vol % H_2 in He up to a maximum temperature of 400 °C with a heating rate of 5 °C/min. Flowrates of H_2 and He were 2.9 ml/min and 55.1 ml/min respectively. TPR analyses were performed with a modified method suggested by Hartmann et al. (1999).

CHAPTER 5

RESULTS AND DISCUSSION

5.1 Synthesis Results

Synthesis of MCM-41, Cu-MCM-41 and Ni-MCM-41 were performed as described in the experimental section. 22 experiments were performed throughout the study. Out of them, 13 experiments were taken into consideration and are presented in the thesis. In Figure 5.1 the distribution of successful and unsuccessful experiments are given.

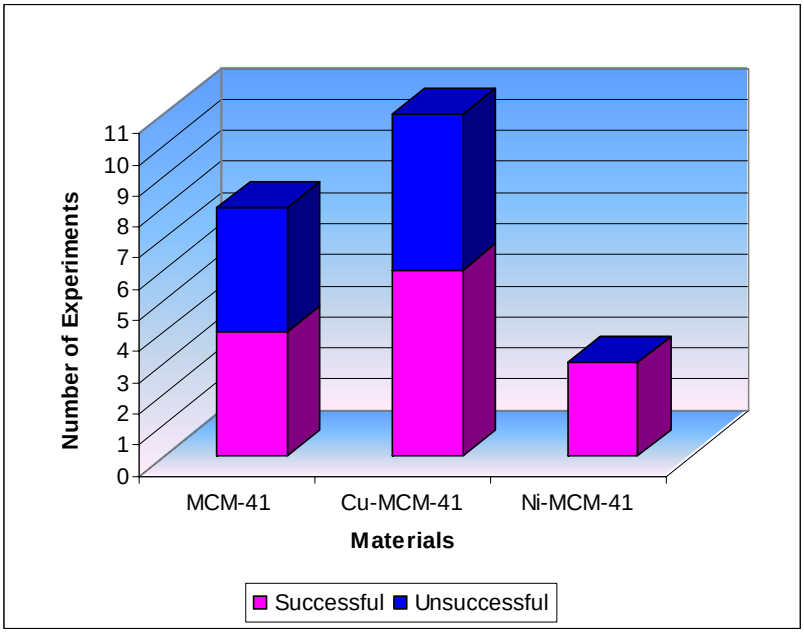

Figure 5.1 Success of experiments in terms of synthesized materials

The synthesized materials, their syntheses procedures and identification symbols are summarized in Table 5.1.

Table 5.1 Summary of the Synthesized Materials

Type of material	Type of synthesis	Sample ID
MCM-41	High temperature direct synthesis	MCM-41(I)
MCM-41	High temperature direct synthesis	MCM-41(II)
MCM-41	High temperature direct synthesis	MCM-41(III)
MCM-41	High temperature direct synthesis	MCM-41(IV)
MCM-41	High temperature direct synthesis	MCM-41(V)
Cu-MCM-41	Impregnation	Cu-Imp(I)
Cu-MCM-41	Impregnation	Cu-Imp(II)
Cu-MCM-41	High temperature direct synthesis	Cu-HT(I)
Cu-MCM-41	High temperature direct synthesis	Cu-HT(II)
Cu-MCM-41	Low temperature direct synthesis	Cu-LT(I)
Cu-MCM-41	Low temperature direct synthesis	Cu-LT(II)
Ni-MCM-41	High temperature direct synthesis	Ni-HT(I)
Ni-MCM-41	High temperature direct synthesis	Ni-HT(II)
Ni-MCM-41	Low temperature direct synthesis	Ni-LT(I)

5.2 Characterization Results

The synthesized materials were characterized by XRD, TEM, N_2 sorption, SEM, XRF, EDS,AAS and TPR techniques. Table 5.2 shows which techniques were performed to each sample.

Table 5.2 Summary of the Characterization Techniques

Sample ID	XRD	TEM	N_2 Sorption	SEM	XRF	EDS	AAS	TPR
MCM-41(I)	√	√	√	√	X	X	X	X
MCM-41(II)	√	X	√	X	X	X	X	X
MCM-41(III)	√	X	√	X	X	X	X	X
MCM-41(IV)	√	X	√	X	X	X	X	X
MCM-41(V)	√	X	√	X	X	X	X	X
Cu-Imp(I)	√	√	√	√	√	√	√	√
Cu-Imp(II)	√	X	√	X	√	√	√	X
Cu-HT(I)	√	√	√	√	√	√	√	√
Cu-HT(II)	√	X	√	X	√	√	√	X
Cu-LT(I)	√	√	√	√	√	√	√	X
Cu-LT(II)	√	X	√	X	√	√	√	√
Ni-HT(I)	√	X	√	X	√	√	√	X
Ni-HT(II)	√	X	√	X	√	√	√	X
Ni-LT(I)	√	X	√	X	√	√	√	X

5.2.1 X-ray Diffraction

XRD patterns of synthesized MCM-41 mesoporous materials, MCM-41(I), MCM-41(II), MCM-41(III) and MCM-41(IV) are given in Figure 5.2, Figure 5.3, Figure 5.4, and Figure 5.5 respectively. Raw data of these samples are given in Appendix B.1 from Table B.1 to Table B.4.

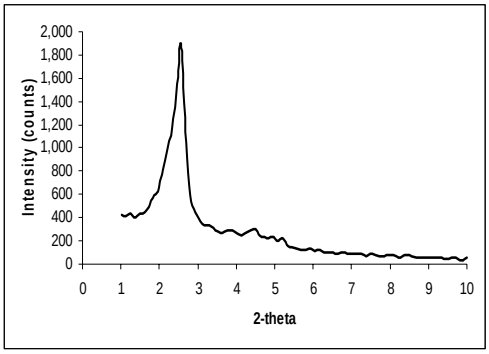

Figure 5.2 XRD plot of MCM-41(I)

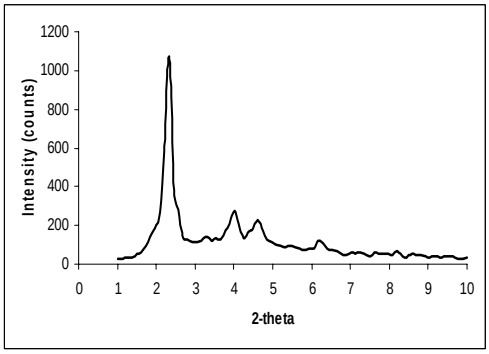

Figure 5.3 XRD plot of MCM-41(II)

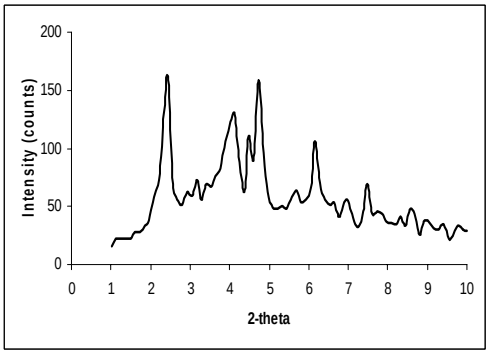

Figure 5.4 XRD plot of MCM-41(III)

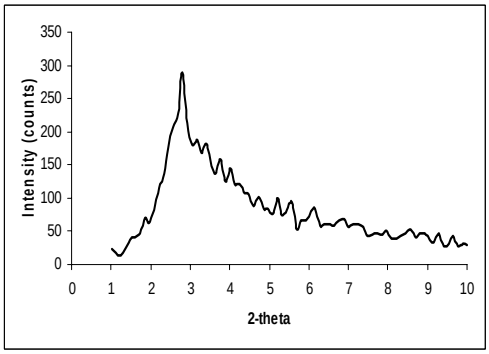

Figure 5.5 XRD plot of MCM-41(IV)

In the XRD patterns of MCM-41 materials, the characteristic sharp Bragg peak corresponding to $d_{(100)}$ were observed for MCM-41(I) and MCM-41(II) only. The major peaks were observed at 2θ values of 2.61 for MCM-41(I) and 2.42 for MCM-41(II). These peaks correspond to d values of 3.4 nm and 3.7 nm respectively. For instance, other reflections were observed for MCM-

41(II) at 2θ values of 4.14, 4.74 and 6.33 with d spacing of 2.1, 1.9, 1.4 nm respectively. There is only one measurable reflection for MCM-41(I) at 2θ value of 4.43 with d spacing of 2.0 nm. For MCM-41(III) and MCM-41(IV), the XRD patterns indicate some changes in MCM-41 structure although the same procedure was followed. These changes are due to the small differences in the synthesis procedure. As described in the experimental section, the amount of water added into the solution was 86 ml for MCM-41(I) and MCM-41(IV) while it was 55 ml for MCM-41(II) and MCM-41(III). If the reason was the amount of water than we expected to observe same XRD patterns for MCM-41 (I) and (IV) also for MCM-41 (II) and (II). However, the first two samples gave characteristic Bragg peaks although they contained different amounts of water. Than we came to a conclusion that washing process was the critical step in the syntheses of MCM-41 type mesoporous molecular sieves. The pH of the filtrate was about 7 for MCM-41(I) and MCM-41(II).

Figures 5.6, 5.7, 5.8, 5.9, 5.10 and 5.11 correspond to the XRD patterns of synthesized Cu-MCM-41 type catalytic materials, Cu-Imp(I), Cu-Imp(II), Cu-HT(I), Cu-HT(II), Cu-LT(I), and Cu-LT(II) respectively. Raw data of these samples are given in Appendix B.1 from Table b.5 to Table B.10.

The XRD patterns of Cu-Imp(II) and Cu-LT(I) gave the characteristic Bragg peaks at 2θ values of 2.48 for Cu-Imp(II) and 2.50 for Cu-LT(I). These peaks correspond to d values of 3.6 nm for both samples. Two reflections were observed for Cu-Imp(II) at 2θ 4.24 and 4.83 with d values of 2.1 and 1.8 nm respectively. There is only one measurable reflection for Cu-LT(I) at 2θ 3.87 with d spacing of 2.3 nm. In the case of Cu-Imp(I), a sharp peak was observed at a 2θ value less than 1° was observed indicating some changes in the MCM-41 structure by the incorporation of copper.

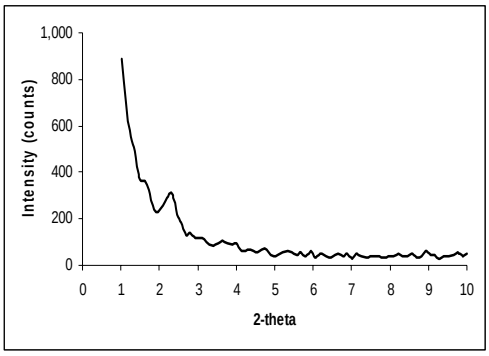

Figure 5.6 XRD plot of Cu-Imp(I)

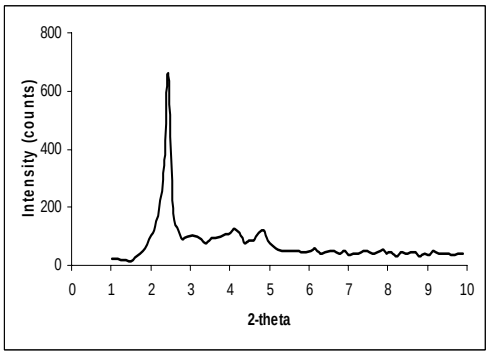

Figure 5.7 XRD plot of Cu-Imp(II)

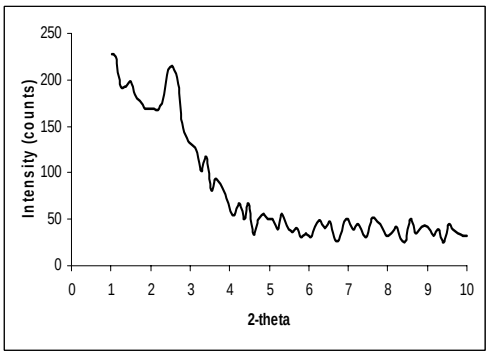

Figure 5.8 XRD plot of Cu-HT(I)

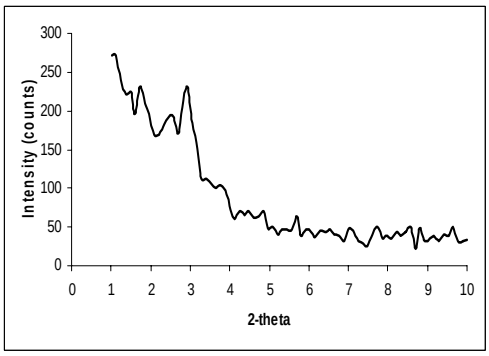

Figure 5.9 XRD plot of Cu-HT(II)

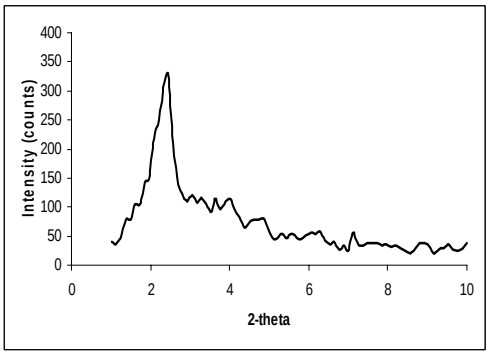

Figure 5.10 XRD plot of Cu-LT(I)

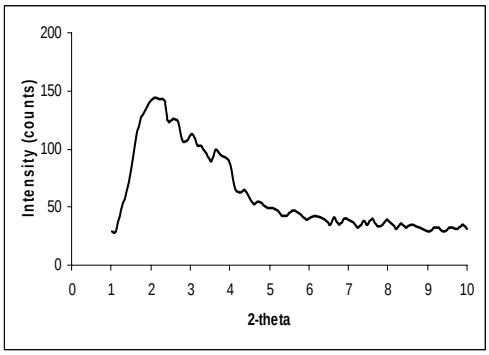

Figure 5.11 XRD plot of Cu-LT(II)

An interesting result was observed for impregnated copper samples. Copper was added into MCM-41(I) to obtain Cu-Imp(I), and into MCM-41(III) to obtain Cu-Imp(II). While the XRD pattern of MCM-41(I) was consistent with literature, copper addition led to some changes in the XRD pattern of Cu-Imp(I). However Cu-Imp(II) gave the characteristic Bragg peak and the two reflections, which were not seen in MCM-41(III) structure.

There were also some changes observed in the XRD patterns of Cu-MCM-41 type catalytic materials obtained by high temperature direct synthesis method which were due to the high metal loading. For Cu-LT(I) and Cu-LT(II), the XRD patterns indicated changes in the structure and wide bands observed. These may be an indication of the distribution of radii of the mesopores in a range.

When we compared the three synthesis methods, impregnation gives better XRD patterns than high temperature and low temperature synthesis methods. This is expected because; in the impregnation, copper is incorporated in synthesized MCM-41 mesoporous material which does not change the structure as much as the other two methods. However, in high and low temperature syntheses, copper is added to the solution mixture before gel formation which results in the changes of the crystal structure.

XRD patterns of synthesized Ni-MCM-41 type catalytic materials, Ni-HT(I), Ni-HT(II), and Ni-Imp(I) are given in Figure 5.12, Figure 5.13, and Figure 5.14 respectively. Raw data of these samples are given in Appendix B.1 from Table B.11 to Table B.13.

There were three Bragg peaks observed for Ni-HT(I) at 2θ values of 1.81, 2.18 and 3.94 with d spacing of 4.9 nm, 4.1 nm and 2.2 nm respectively.

The XRD pattern of Ni-HT(II) showed a pattern totally different from MCM-41. These differences were due to high metal loading. The wide spread distribution of XRD pattern shows that there is a pore dimension distribution in the synthesized materials.

The sample prepared by impregnation method was obtained by adding nickel into MCM-41(IV) which showed a XRD pattern different from MCM-41. However, after the impregnation, a sharp Bragg peak was observed at 2θ 2.45 with d spacing 3.6 nm. Also an additional peak was observed at 4.21° with a d spacing of 2.1 nm. The sample prepared by impregnation method gives XRD pattern similar to MCM-41 compared with the other two which were synthesized by high temperature direct synthesis.

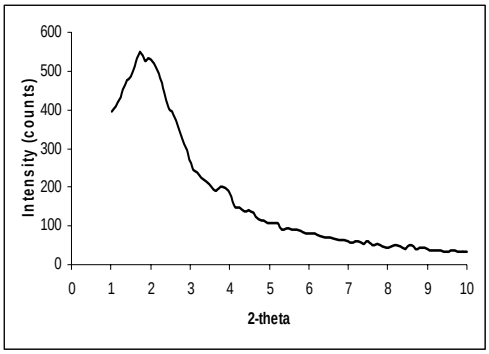

Figure 5.12 XRD plot of Ni-HT(I)

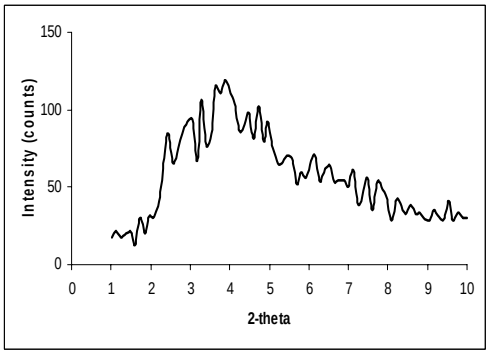

Figure 5.13 XRD plot of Ni-HT(II)

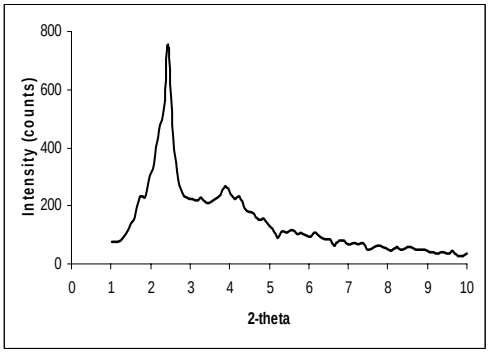

Figure 5.14 XRD plot of Ni-Imp(I)

5.2.2 Transmission Electron Microscopy

TEM images are required to understand the morphology of the samples. Obtaining TEM images in 100 nm scale is not easy for solid samples. In the literature there are not many TEM images for Cu-MCM-41 and Ni-MCM-41 type catalytic materials.

In Figure 5.16, 5.16, 5.17 and 5.18 TEM images of some samples are given. In all three copper samples hexagonality can be easily observed. The distribution of hexagonal cells are more regular in impregnated copper sample.

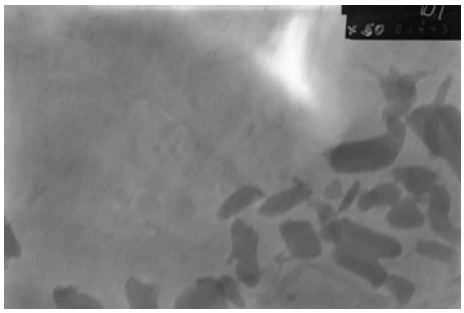

Figure 5.15 TEM of MCM-41(I)

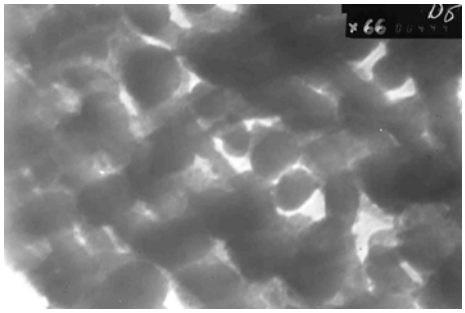

Figure 5.16 TEM of Cu-Imp(I)

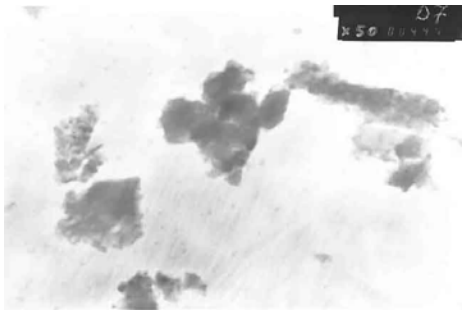

Figure 5.17 TEM of Cu-HT(I)

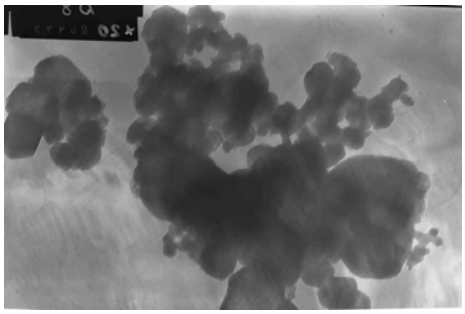

Figure 5.18 TEM of Cu-LT(I)

5.2.3 N_2 Sorption

N_2 adsorption-desorption isotherms of synthesized MCM-41 mesoporous materials are given in 5.19. For simplification adsorption-desorption isotherms were represented by "ADI" in the figures. The raw data of ADI in terms of relative pressure (P/P_0), pressure (mmHg), and volume adsorbed (cc/g STP) are given in Appendix B.

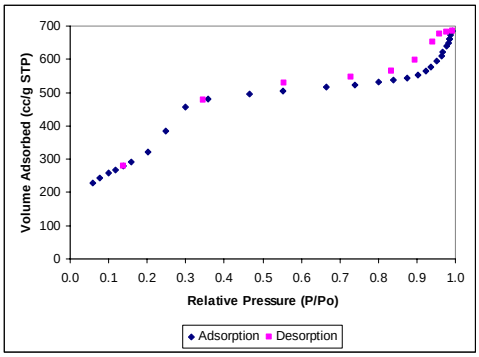

(a) ADI of MCM-41 (I)

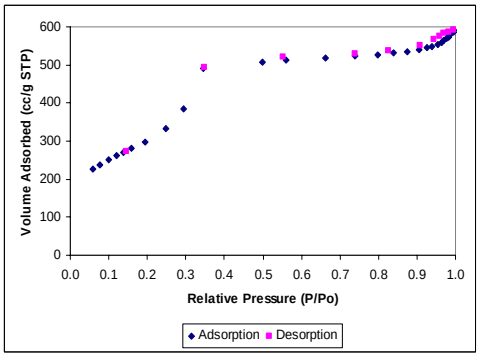

(**b**) ADI of MCM-41(II)

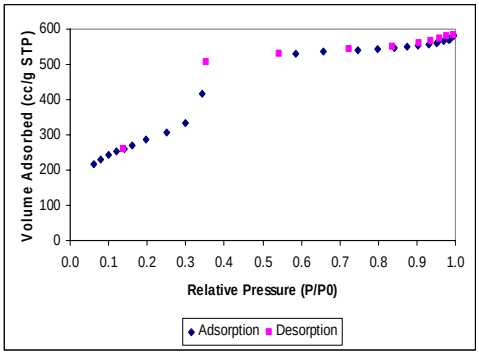

(c) ADI of MCM-41(III)

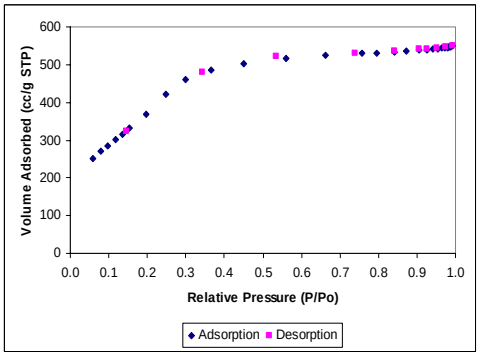

(d) ADI of MCM-41(IV)

Figure 5.19 N_2 Adsorption/Desorption Isotherms of Synthesized MCM-41 Mesoporous Materials

In the adsorption-desorption isotherms of MCM-41(I), MCM-41(II), and MCM-41(III), Type IV Isotherms were observed. However, MCM-41(IV) gave Type I isotherm which indicated the presence of micropores. This sample also has higher specific surface area when compared with other samples (Table 5.3). As reported in Table 5.3, the pore volumes of MCM-41(I), (II), (IIII) and (IV) were 1.17, 1.03, 1.00 and 1.05 cc/g, respectively.

Figure 5.20 indicated adsorption-desorption isotherms of Cu-MCM-41 type catalytic materials. All samples gave Type IV isotherms. For Cu-Imp(I), the volume adsorbed (1.09 cc/g) is less than MCM-41(I) and for Cu-Imp(II) again the volume adsorbed (0.53 cc/g) is less than MCM-41(III). The hystereses in these samples were much less than MCM-41(I) and MCM-41(III). As reported in Table 5.3, pore diameters of MCM-41(I) and MCM-41(III) are 3.0 nm, while pore diameters of Cu-Imp(I) and Cu-Imp(II) are 2.7 nm. The pore diameters are taken from the adsorption branch since the data points in the desorption branch are much less than the adsorption branch. When we analyze the samples obtained from high temperature direct synthesis, we observe that there is a decrease in volume adsorbed. The hysteresis observed for Cu-HT(II) is wider than Cu-HT(I). So average pore diameter of Cu-HT(II) is (4.0 nm) greater than Cu-HT(II) (2.5 nm). The volumes of Cu-HT(I) and Cu-HT(II) were 0.54, 0.42 cc/g, respectively. The hysteresis of the adsorption-desorption branches of Cu-LT(I) and Cu-LT(II) were wider which indicated larger pore diameters. Again from Table 5.3, the BJH adsorption pore diameters of these samples are 8.3 and 7.3 nm, respectively. Average pore volumes of these samples were found as 0.30 and 1.33 cc/g, respectively.

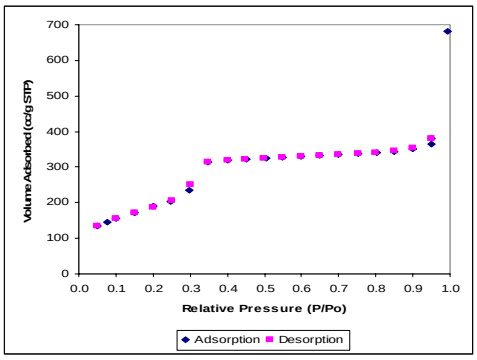

(a) ADI of Cu-Imp(I)

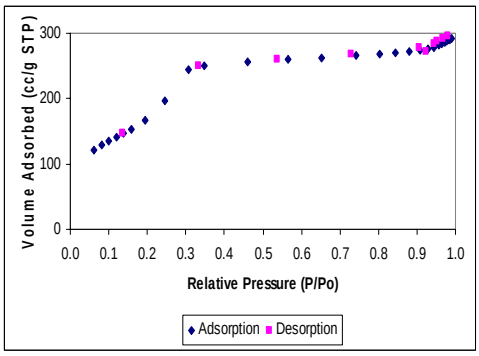

(b) ADI of Cu-Imp(II)

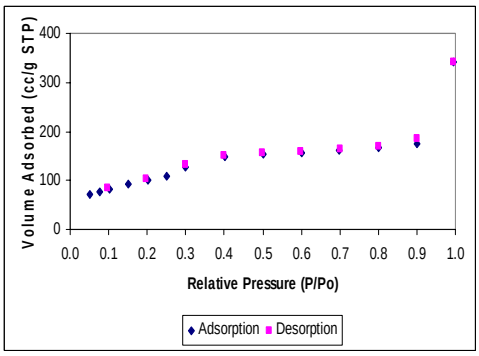

(c) ADI of Cu-HT(I)

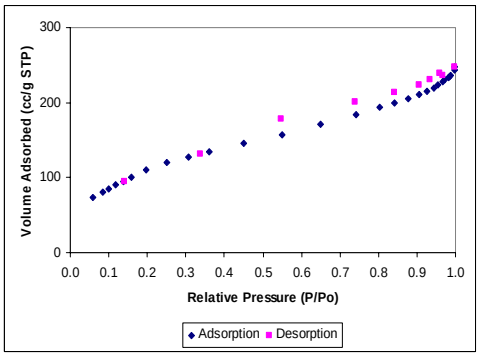

(d) ADI of Cu-HT(II)

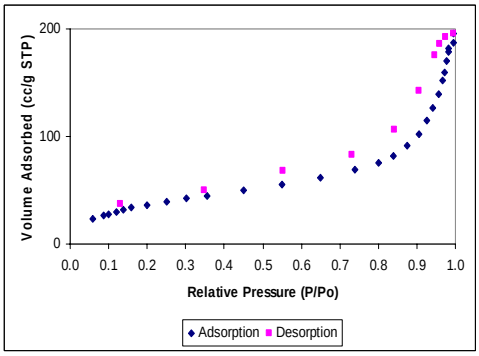

(e) ADI of Cu-LT(I)

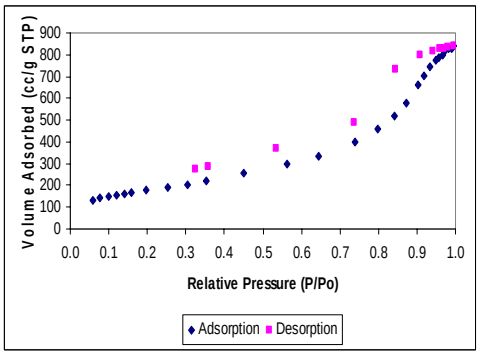

(f) ADI of Cu-LT(II)

Figure 5.20 N_2 Adsorption/Desorption Isotherms of Synthesized Cu-MCM-41 Type Catalytic Materials

Figure 5.21 shows the adsorption-desorption isotherms of Ni-MCM-41 type catalytic materials. Ni-HT(I)I Ni-HT(II) gave Type IV isotherms which means mesoporosity while Ni-Imp(I) gave a Type I isotherm. This is expected because Ni-Imp(I) is prepared by nickel incorporation into MCM-41(IV) which also shows microporosity. The pore volumes of these samples are 0.59 for Ni-HT(I), 0.91 for Ni-HT(II) and 1.39 cc/g for Ni-Imp(I).

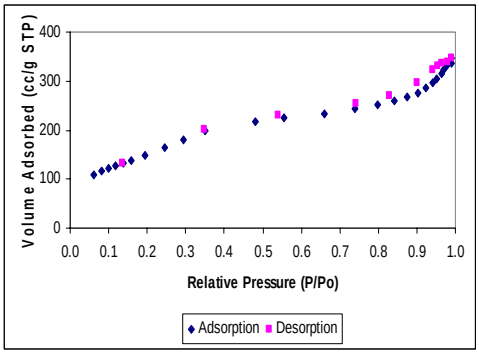

(a) ADI of Ni-HT(I)

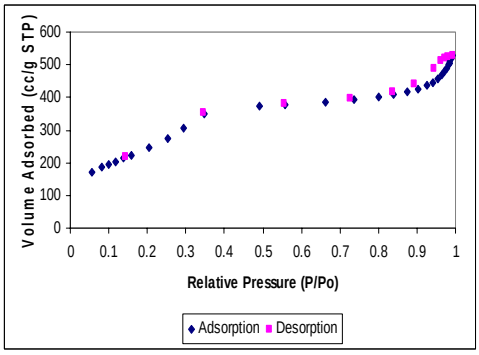

(b) ADI of Ni-HT(II) D11

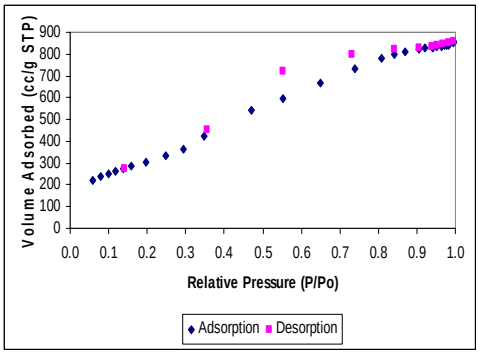

(c) ADI of Ni-Imp(I)

Figure 5.21 N_2 Adsorption/Desorption (ADI) Isotherms of Synthesized Ni-MCM-41 Type Catalytic Materials

Pore size distributions of synthesized materials in terms of adsorption and desorption isotherms are given in Figures 5.22, 5.23 and 5.24. For simplification adsorption pore size distribution is represented by "APSD", and desorption pore size distribution is represented by "DPSD". The raw data of BJH Adsorption Pore Distribution and BJH Desorption Pore Distribution in terms of average diameter, incremental pore volume, cumulative pore volume, incremental surface area, and cumulative surface area are given in Appendix B.

The desorption branch data points are much less than the adsorption branch data in N_2 sorption analyses. So the adsorption branches of pore sizes were considered. The pore diameters of MCM-41 mesoporous materials were 3.0, 2.8, 3.0 and 2.7 nm respectively. As reported in Figure 5.22, the pore size distribution was not completed for MCM-41(IV) which means that the obtained surface area was lower than the actual value. We know from adsorption-desorption isotherm that it is Type I isotherm which shows microporosity, so more data was required to analyze these micropores found in this sample.

For Cu-MCM-41 type catalytic materials, pore size distributions were given in Figure 5.23. The pore diameters of these materials were 2.7, 2.7, 2.5, 4.0, 8.3 and 7.3 nm, respectively. The pore diameters of Cu-MCM-41 synthesized by low temperature method gave somewhat larger pore diameters when compared to other samples.

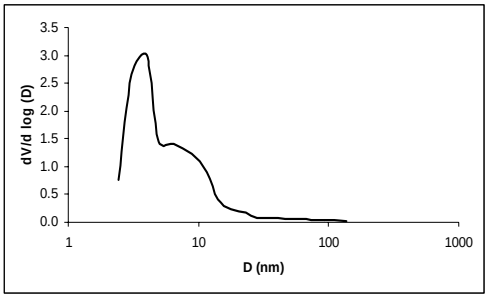

(a) APSD of MCM-41(I)

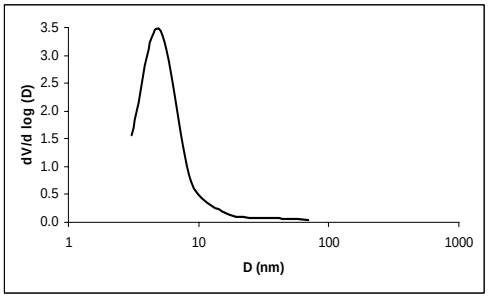

(b) DPSD of MCM-41(I)

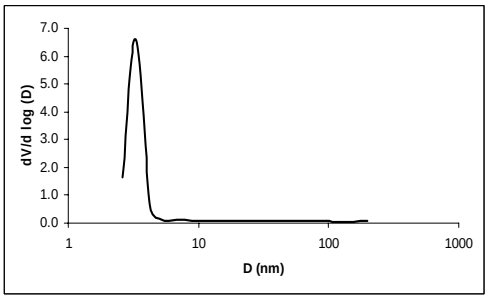

(c) APSD of MCM-41(II)

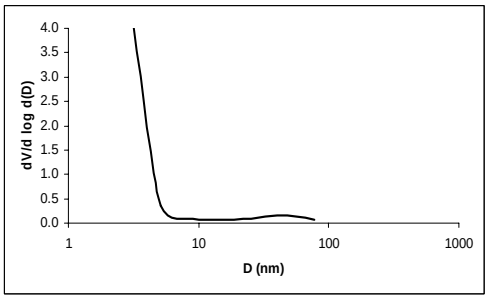

(d) DPSD of MCM-41(II)

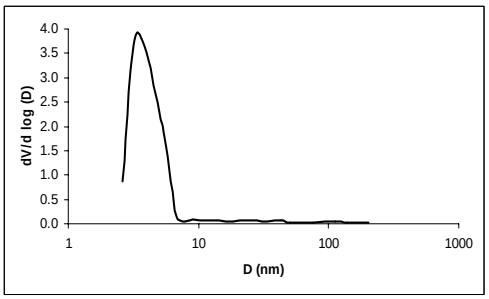

(e) APSD of MCM-41(III)

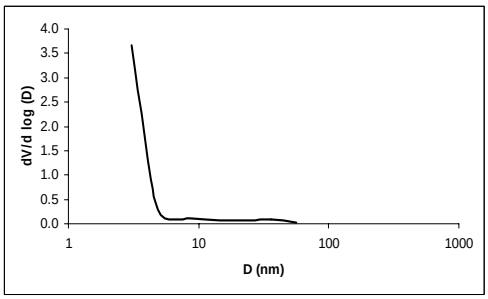

(f) DPSD of MCM-41(III)

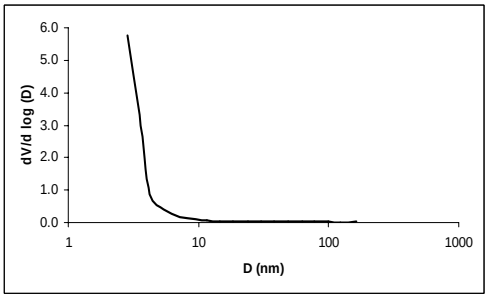

(g) APSD of MCM-41(IV)

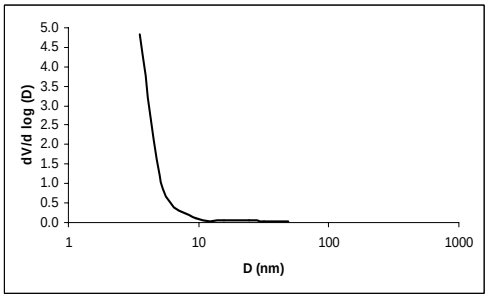

(h) DPSD of MCM-41(IV)

Figure 5.22 N_2 Adsorption Pore Size Distribution (APSD) and Desorption Pore Size Distribution (DPSD) of MCM-41 Mesoporous Materials

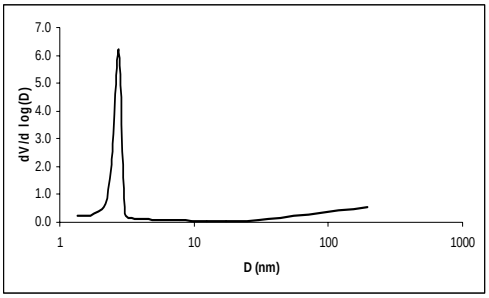

(a) APSD of Cu-Imp(I)

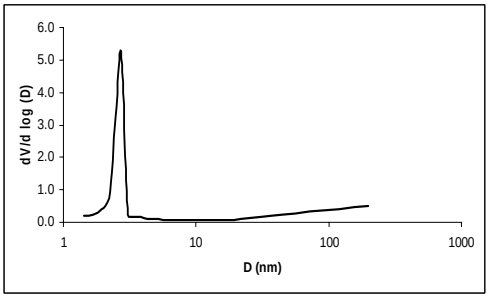

(b) DPSD of Cu-Imp(I)

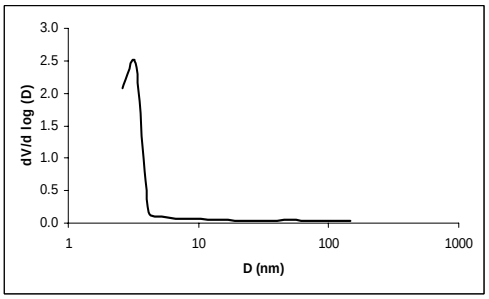

(c) APSD of Cu-Imp(II)

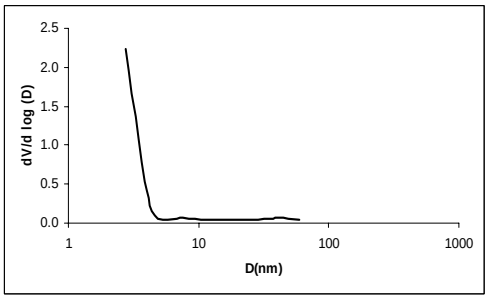

(d) DPSD of Cu-Imp(II)

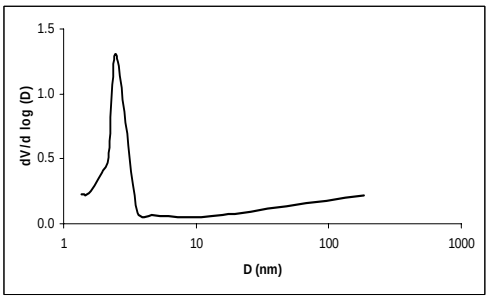

(e) APSD of Cu-HT(I)

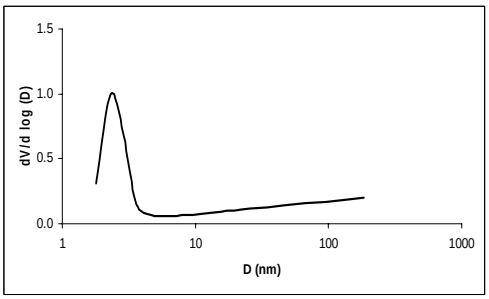

(f) DPSD of Cu-HT(I)

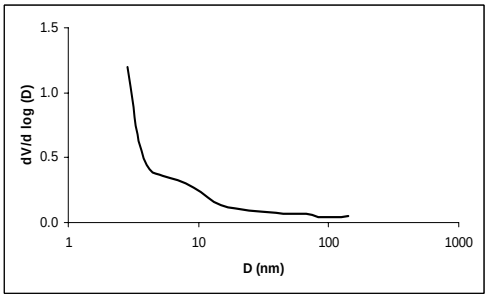

(g) APSD of Cu-HT(II)

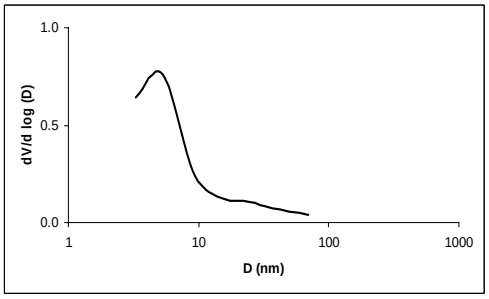

(h) DPSD of Cu-HT(II)

Figure 5.23 N_2 Adsorption Pore Size Distribution (APSD) and Desorption Pore Size Distribution (DPSD) of Cu-MCM-41 Type Catalytic Materials

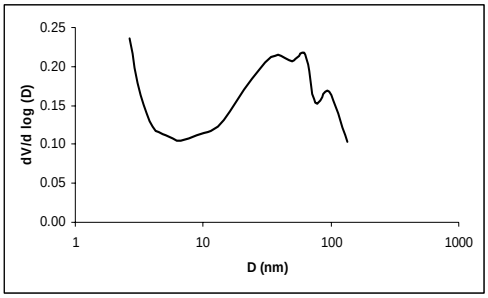

(i) APSD of Cu-LT(I)

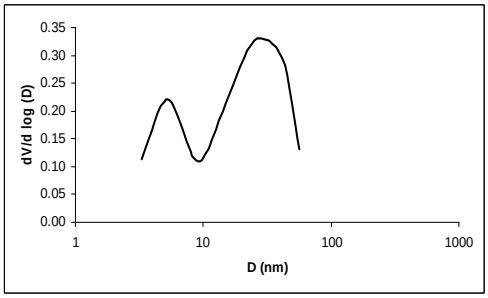

(j) DPSD of Cu-LT(I)

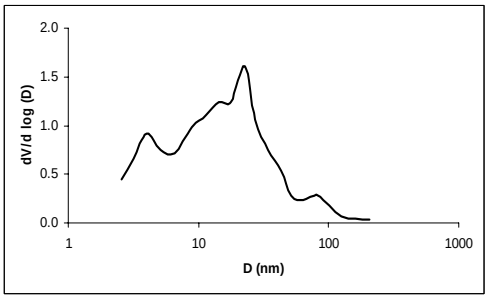

(k) APSD of Cu-LT(II)

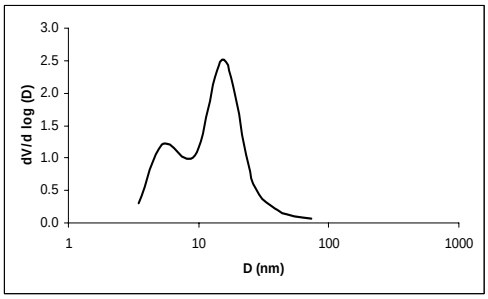

(l) DPSD of Cu-LT(II)

Figure 5.23 (continued) N_2 Adsorption Pore Size Distribution (APSD) and Desorption Pore Size Distribution (DPSD) of Cu-MCM-41 Type Catalytic Materials

Figure 5.24 correspond to the pore size distributions of Ni-MCM-41 type catalytic materials. Pore diameters of these samples were 3.8, 3.4 and 3.7 nm respectively. The graphs indicate that there may be micropores for Ni-HT(I) and Ni-HT(II).

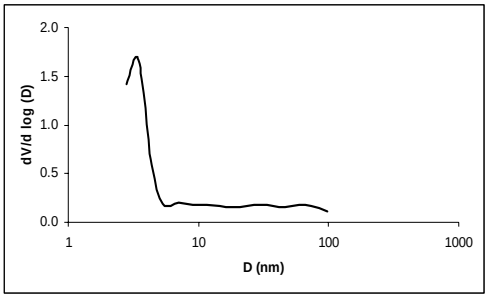

(a) APSD of Ni-HT(I)

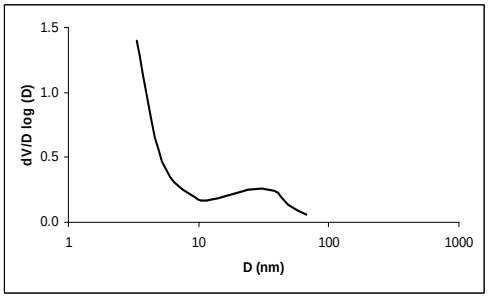

(b) DPSD of Ni-HT(I)

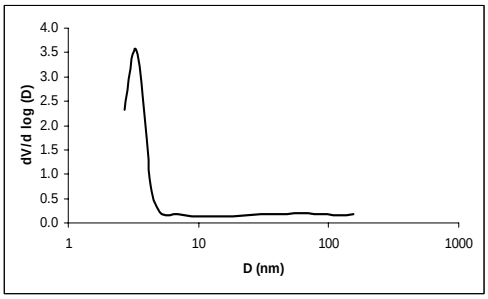

(c) APSD of Ni-HT(II)

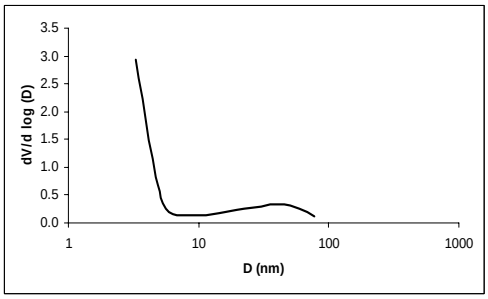

(d) DPSD of Ni-HT(II)

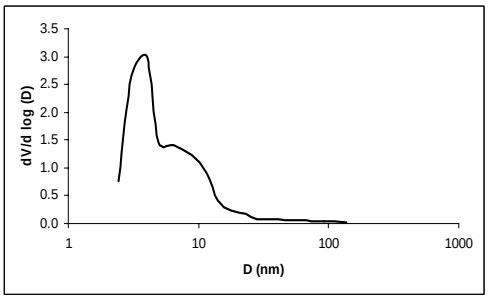

(e) APSD of Ni-Imp(I)

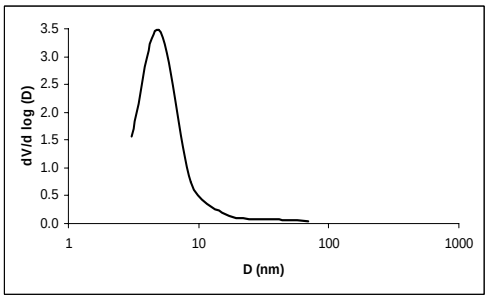

(f) DPSD of Ni-Imp(I)

Figure 5.24 N_2 Adsorption Pore Size Distribution (APSD) and Desorption Pore Size Distribution (DPSD) of Ni-MCM-41 Type Catalytic Materials

In Table 5.3, all physical properties obtained from XRD and N_2 sorption data of all samples are summarized. The specific surface areas of samples are given in terms of BET and BJH (adsorption and desorption) analyses.

By using the XRD data, characteristic lattice parameters of the synthesized materials were also calculated. Lattice parameter (a) is the repeating distance between two pore centers. It was calculated by using the following equation (Kresge et al., 1992):

$$a = \frac{2d_{(100)}}{\sqrt{3}}$$

The d spacing and lattice parameters of all synthesized materials are summarized in Table 5.3.

Pore wall thickness δ was estimated from the average pore diameter (d_p) and the lattice diameter (a) using the following equation (Schultz-Ekloff et al., 1999) :

$$\delta = a - 0.95\ d_p$$

From Table 5.3, the BET surface area values of all MCM-41 mesoporous materials are greater than 1000 m^2/g, pore volumes greater than 1.00 cc/g and have average pore diameter of about 3.0 nm. MCM-41(I) and MCM-41(II) gave the characteristic XRD pattern of MCM-41. These mesoporous materials have high surface areas up to 1200 m^2/g and pore volumes up to 1.17 cc/g.

High surface area values were obtained for Cu-Imp(I) and Cu-Imp(II) samples. These samples were synthesized by incorporation of copper into MCM-41(I) and MCM-41(III) respectively. From the Table 5.3, an increase was

observed in the pore wall thicknesses and decrease was observed in pore diameter which indicates thin layer formation of copper on the walls of MCM-41 structure. The surface area values and pore volumes of Cu-HT(I) and Cu-HT(II) are very close to each other while the pore diameter of Cu-HT(II) was larger than Cu-HT(I). Cu-MCM-41 type catalytic materials synthesized by low temperature direct synthesis method gave larger pore diameters. Although XRD pattern of Cu-LT(I) was in agreement with MCM-41 structure, its surface area and pore volume was lower than the others. When we compared Cu-HT(I) and Cu-HT(II), there were great differences between these two materials which showed the importance of titration and washing processes.

The acid treatment in the synthesis of Ni-MCM-41was very critical for obtaining high surface areas. As seen from the Figure Ni-HT(II) has higher surface area and higher pore volume than Ni-HT(I).

Table 5.3 Summary of Physical Properties

Sample ID	BET SA[a] (m^2/g)	BJH ASA[b] (m^2/g)	BJH DSA[c] (m^2/g)	BJH APV[d] (cc/g)	BJH DPV[e] (cc/g)	BJH APD[f] (nm)	BJH DPD[g] (nm)	d_{100} (nm)	a[h] (nm)	δ_{des} (nm)	δ_{ads} (nm)
MCM-41 (I)	1208	1119	1561	1.17	1.17	3.0	2.6	3.4	3.9	1.5	1.1
MCM-41 (II)	1097	1452	1812	1.02	1.03	2.8	2.3	3.7	4.3	2.1	1.6
MCM-41 (III)	1043	1314	1966	1.00	1.00	3.0	2.0	3.6	4.2	2.3	1.3
MCM-41 (IV)	1445	1566	1622	1.05	1.05	2.7	2.6	3.2	3.7	1.2	1.1
Cu-Imp(I)	729	867	878	1.09	1.09	2.7	2.7	3.8	4.4	1.8	1.8
Cu-Imp(II)	631	798	929	0.53	0.53	2.7	2.3	3.6	4.2	2.0	1.6
Cu-HT(I)	396	430	390	0.54	0.52	2.5	2.3	3.3	3.8	1.6	1.4
Cu-HT(II)	434	422	471	0.42	0.41	4.0	3.5	3.0	3.5		
Cu-LT(I)	145	145	173	0.30	0.31	8.3	7.1	3.5	4.0		
Cu-LT(II)	650	725	766	1.33	1.27	7.3	6.6	3.9	4.5		
Ni-HT(I)	562	613	720	0.59	0.59	3.8	3.3	4.1	4.7	1.6	1.1
Ni-HT(II)	929	1084	1262	0.91	0.92	3.4	2.9	3.5	4.0	1.3	0.8
Ni-Imp(I)	1130	1500	1950	1.39	1.38	3.7	2.8	3.6	4.2	1.5	0.6

[a]: Surface Area
[b]: Adsorption surface Area
[c]: Desorption Surface Area
[d]: Adsorption Pore Volume
[e]: Desorption Pore Volume
[f]: Adsorption Pore Diameter
[g]: Desorption Pore Diameter
[h]: Lattice Diameter

5.2.4 Scanning Electron Microscopy

SEM images of MCM-41(I), Cu-Imp(I), Cu-HT(I), and Cu-LT(I) are given in the following figures. In Appendix B, some other SEM images of these samples are also given.

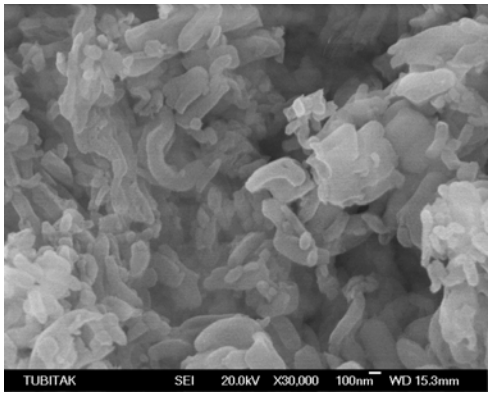

Figure 5.25 SEM of MCM-41(I)

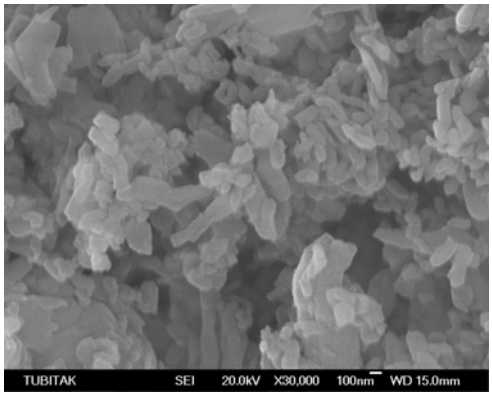

Figure 5.26 SEM of Cu-Imp(I)

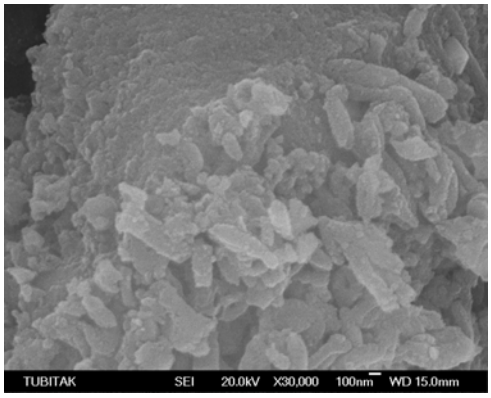

Figure 5.27 SEM of Cu-HT(I)

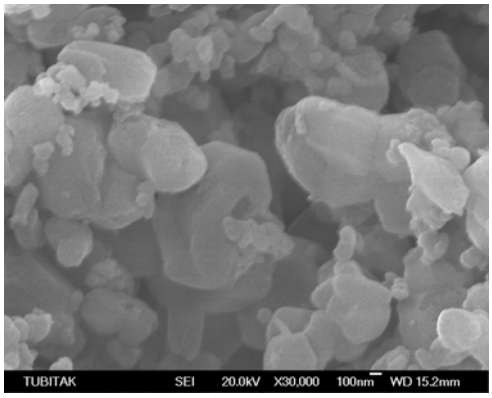

Figure 5.28 SEM of Cu-LT(I)

For the given samples, the average particle sizes were calculated using the SEM images. The particle sizes of MCM-41(I), Cu-Imp(I), Cu-HT(I) and Cu-LT(I) are 212 nm, 200 nm, 178 nm and 270 nm respectively.

5.2.5 X-ray Fluorescence

X-ray Fluorescence analyses of Cu-MCM-41 type catalytic materials are given in Table 5.2. The raw data of these samples were given in Appendix B.

Table 5.4 XRF results of Cu-MCM-41 type catalytic materials

Sample ID	Cu (mol)	Si (mol)	Cu/Si mol ratio
Cu-Imp(I)	0.223	1.337	0.167
Cu-Imp(II)	0.240	1.320	0.182
Cu-HT(I)	0.285	1.282	0.222
Cu-HT(II)	0.297	1.207	0.246
Cu-LT(II)	0.064	1.465	0.044

X-ray Fluorescence analyses of Ni-MCM-41 type catalytic materials are given in Table 5.2. The raw data of these samples are given in Appendix B.

Table 5.5 XRF results of Ni-MCM-41 type catalytic materials

Sample ID	Ni (mol)	Si (mol)	Ni/Si mol ratio
Ni-HT(I)	0.277	1.275	0.218
Ni-HT(II)	0.144	1.413	0.102
Ni-Imp(I)	0.077	1.513	0.051

5.2.6 Energy Dispersive Spectroscopy

Energy dispersive Spectroscopy results of Cu-MCM-41 and Ni-MCM-41 type catalytic materials are given in Table 5.4 and Table 5.5 respectively. Raw data of EDS analyses are given in Appendix B.

Table 5.6 EDS results of Cu-MCM-41 type catalytic materials

Sample ID	**Cu mol%**	**Si mol%**	**Cu/Si mol ratio**
Cu-Imp(I)	23.92	76.08	0.31
Cu-Imp(II)	16.07	83.93	0.19
Cu-HT(I)	20.80	79.20	0.26
Cu-HT(II)	17.23	82.77	0.21
Cu-LT(I)	1.80	98.20	0.02
Cu-LT(II)	5.09	94.91	0.05

Table 5.7 EDS results of Ni-MCM-41 type catalytic materials

Sample ID	**Ni mol%**	**Si mol%**	**Ni/Si mol ratio**
Ni-HT(I)	21.91	78.09	0.28
Ni-HT(II)	11.01	88.99	0.12
Ni-Imp(I)	5.79	94.21	0.06

5.2.7 Atomic Absorption Spectroscopy

Atomic Absorption Spectroscopy results of Cu-MCM-41 and Ni-MCM-41 type catalytic materials are given in Table 5.6 and Table 5.7 respectively. Raw data of AAS analyses are given in Appendix B.

Table 5.8 AAS results of Cu-MCM-41 type catalytic materials

Sample ID	Cu (mol)	Si (mol)	Cu/Si mol ratio
Cu-Imp(I)	0.260	0.974	0.266
Cu-Imp(II)	0.216	0.956	0.226
Cu-HT(I)	0.212	1.025	0.206
Cu-HT(II)	0.171	1.126	0.152
Cu-LT(I)	0.002	0.787	0.003
Cu-LT(II)	0.032	1.464	0.022

Table 5.9 AAS results of Ni-MCM-41 type catalytic materials

Sample ID	Ni (mol)	Si (mol)	Ni/Si mol ratio
Ni-HT(I)	0.236	0.898	0.263
Ni-HT(II)	0.180	1.082	0.167
Ni-Imp(I)	0.104	0.985	0.105

For comparison, the analysis results for determining metal content are summarized in Table 5.10. The Cu/Si and Ni/Si molar ratios obtained from different techniques gave the bulk composition of elements found in the solid samples. In order to obtain the metal content on the surface of the walls X-ray Photoelectron Spectroscopy (XPS) analyses are required. SEM and EDS gave similar results. However, when four methods are compared, the ratios are found to be rather close. This may be due to differences of sample sizes used in different techniques and heterogeneity of the samples.

Table 5.10 Summary of Metal Content

	Solution	**SEM**	**XRF**	**EDS**	**AAS**
Sample ID	**Cu/Si mol ratio**	**Cu/Si mol ratio**	**Cu/Si mol ratio**	**Cu/Si mol ratio**	**Cu/Si mol ratio**
Cu-Imp(I)	-	0.301	0.167	0.314	0.266
Cu-Imp(II)	-	-	0.182	0.191	0.226
Cu-HT(I)	0.05	0.214	0.222	0.263	0.206
Cu-HT(II)	0.05	-	0.246	0.208	0.152
Cu-LT(I)	0.05	0.045	0.004	0.018	-
Cu-LT(II)	0.05	-	0.044	0.054	0.022
Sample ID	**Ni/Si mol ratio**	**Ni/Si mol ratio**	**Ni/Si mol ratio**	**Ni/Si mol ratio**	**Ni/Si mol ratio**
Ni-HT(I)	0.05	-	0.218	0.281	0.263
Ni-HT(II)	0.05	-	0.102	0.124	0.167
Ni-Imp(I)	-	-	0.051	0.061	0.105

From Table 5.10, the copper samples obtained from impregnation and high temperature synthesis methods gave higher Cu/Si molar ratios when compared with the samples synthesized by low temperature method. In the case of impregnated samples, Cu/Si molar ratio was higher than 0.3 for Cu-Imp(I) and about 0.2 for Cu-Imp(II). For Cu-HT(I) and Cu-HT(II), EDS and XRF showed a Cu/Si molar ratio in the range of 0.20-0.25 while the initial ratio still being 0.05 in the original solution. These results showed that incorporation of Cu into the MCM-41 structure was highly successful. In the case of Cu-LT(II), the Cu/Si molar ratio evaluated from the EDS results was found to be about the same as that in the solution used in the synthesis while for Cu-LT(I), Cu/Si molar ratio was much lower than the prepared solution when XRF and EDS results are considered. More efficient incorporation of copper into MCM-41 structure is possible by impregnation, keeping the surface areas above 600 m^2/g and XRD patterns similar to MCM-41. For the case of high temperature synthesis, the Cu/Si molar ratios were as high as impregnated samples, however, surface areas are about 400 m^2/g and changes occur in the XRD patterns. In these three methods, low temperature synthesis is the least favorable in metal loading. For nickel samples obtained from high temperature direct synthesis method, high Ni/Si molar ratios were obtained. The small differences in the synthesis gave different Ni/Si molar ratios. For Ni-HT(I), no acid treatment was performed while acid was added into the solution mixture of Ni-HT(II). The Ni/Si molar ratio evaluated from EDS and AAS analysis was higher than 0.26 while the ratio was 0.05 in the original solution with a surface area of 560 m^2/g. While the Ni/Si molar ratio was about 0.16 Ni-HT(II), when AAS result was considered, the surface area was above 900 m^2/g. The sample obtained from impregnation gave Ni/Si molar ratio of about 0.06 but its specific surface area was 1130 m2/g and gave characteristic Bragg peak in its XRD pattern.

5.2.8 Temperature Programmed Reduction

TPR analyses were done with Cu-Imp(I), Cu-HT(I) and Cu-LT(II) samples. Because of density differences, 0.05 gr of Cu-Imp(I), 0.1 gr of Cu-HT(I) and 0.1 gr of Cu-LT(II) were used in the analyses. The graphs obtained for H_2 consumption and H_2O formation during analyses are given in Figures 5.29, 5.30 and 5.31, respectively. TPR data in terms of temperature are given in Appendix B for each sample.

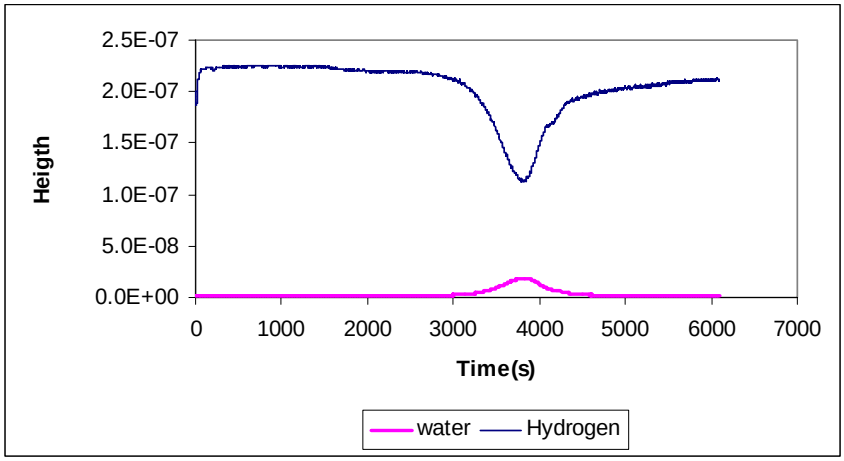

Figure 5.29 TPR of Cu-Imp(I)

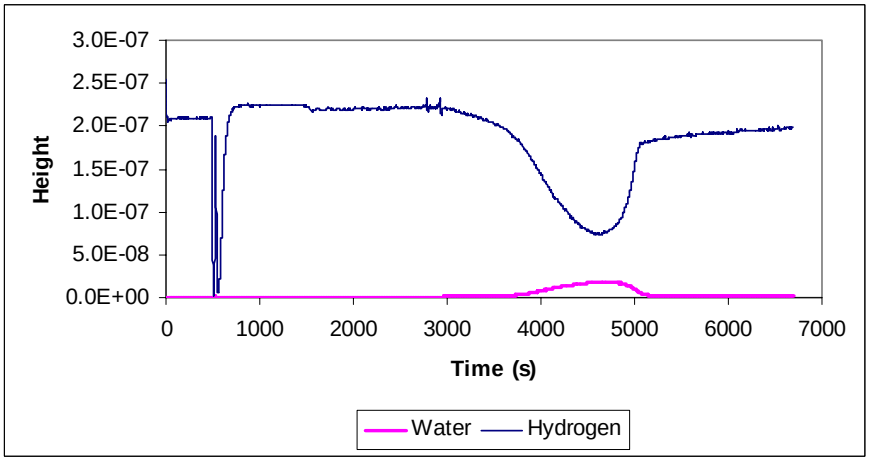

Figure 5.30 TPR of Cu-HT (I)

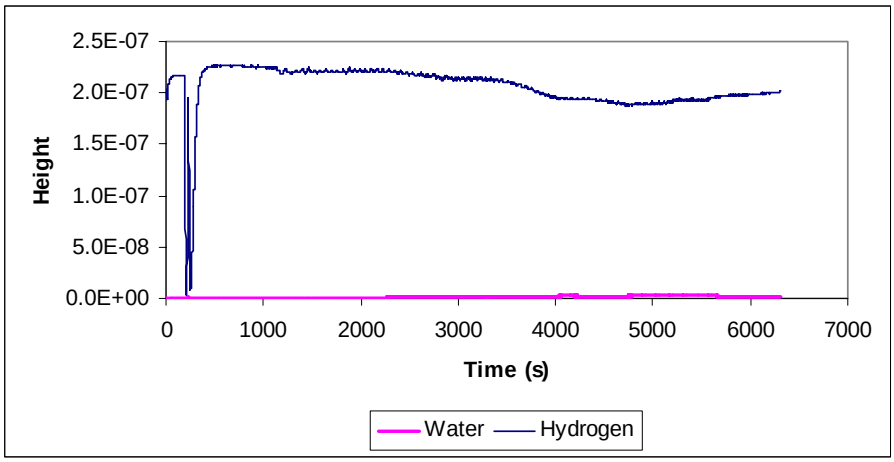

Figure 5.31 TPR of Cu-LT (I)

From the figures given above, combinations of two peaks were observed for hydrogen consumption. Hydrogen consumption started at a temperature of about 200 °C and gave a maximum of at 260 °C. The second hydrogen consumption peak gave a maximum at around 280 °C, for Cu-Imp(I). This TPR result also showed a long tail extending over 400 °C (Appendix B). These results indicated the presence of two kinds of reducible oxygen in the prepared sample. In the case of Cu-HT(I), the tail in the TPR curve is even longer. For Cu-LT(II), Cu/Si mole ratio was very low (0.05). TPR curve for this material was also very wide with a long tail extending to high temperatures. Presence of such long tails may be an indication of slow reduction of some of the copper oxide sites which are incorporated into MCM-41 structure. Further analysis is required for quantitative conclusions.

TPR result of impregnated sample (Figure 5.29) showed a rather symmetrical behavior indicating a first order reduction process. However for the sample obtained from high temperature direct synthesis method (Figure 5.30), the nonsymmetric TPR curve may be an indication of a second order reduction process.

5.3 Economics

Exxon Mobil had a materials synthesis effort attempting to identify new porous materials that could selectively convert bulky, high molecular weight petroleum molecules into more valuable fuel and lubricant products. Very recently, Exxon Mobil announced that they had scaled-up the synthesis and commercialized MCM-41 for an undisclosed application (Kresge et al., 2004). For this reason, economical analyses were done for the synthesized materials. For the economical analyses, cost of water, acid, electricity, instrumentation, labor and characterization were ignored.

The price of materials and their amounts are given in Table 5.11.

Table 5.11 Cost analyses of materials

Material	**Price (x 10^6 TL)**	**Amount**	**Cost, TL (Price x Amount)**
Sodium Silicate Solution	31 /2.5Lt	~11 ml	136,400 TL
Surfactant	46 /100 gr	~ 13 gr	5,980,000
$Cu(NO_3)_2$ $3{\cdot}H_2O$	28 /250 gr	~ 1.7 gr	190,400
$Ni(NO_3)_2$ $6{\cdot}H_2O$	21 / 100 gr	~ 2.3 gr	483,000

The approximate amount of solids obtained at the end of the syntheses and their costs were summarized in Table 5.11.

Table 5.12 Cost of synthesized materials

Material	**Amount (gr)**	**Cost (TL)**
MCM-41	~ 4-5	6,116,400
Cu-MCM-41	~ 6-7	6,306,800
Ni-MCM-41	~ 5-6	6,599,400

CHAPTER 6

CONCLUSIONS AND RECOMMENDATIONS

In this study, MCM-41 mesoporous molecular sieves, Cu-MCM-41 and Ni-MCM-41 type catalytic materials were synthesized and characterized.

High surface area values up to 1400 m^2/g of MCM-41 mesoporous materials were obtained with high pore volumes up to 1.17 cc/g. The pore volumes, average pore diameters and pore wall thicknesses of these samples were very close to each other showing the reproducibility of the synthesis procedure. The results also show the importance of washing process in the syntheses of these materials.

Cu-MCM-41 type catalytic materials were synthesized by three different methods. Impregnation and high temperature direct synthesis methods gave better results than those of low temperature direct synthesis methods. The surface area, pore volumes and Cu/Si molar ratio obtained by impregnation method were highest when compared with others. High temperature synthesis method gave Cu/Si molar ratio as high as 0.26 while initial ratio was 0.05 in the solution. The shifts and differences in the XRD patterns of these samples were the evidence of the incorporation of copper into the wall structure of the MCM-41 materials.

In the case of Ni-MCM-41 type catalytic materials high surface area values of 900 m^2/g with Ni/Si molar ratio of 0.12 was achieved by high temperature direct synthesis procedure while the initial molar ratio was 0.05 in the solution. It was observed that acid treatment was a critical step in the synthesis procedure. The impregnation method gave 1130 m^2/g with a Ni/Si molar ratio of 0.06.

Characterization of Cu-MCM-41 and Ni-MCM-41 type catalytic materials showed that, high metal content with high surface areas can be obtained by impregnation and high temperature direct synthesis methods. Their low cost is also an advantage for future catalytic applications.

For more accurate results, TEM analyses were required to calculate the pore diameters and pore wall thicknesses. Also XPS analyses were required to obtain the amount of copper and nickel on the surface of the walls.

REFERENCES

Barrett, E.P., Joyner, L.G., Halenda, P.P., 1951, "The Determination of Pore Volume and Area Distributions in Porous Substances. I. Computations from Nitrogen Isotherms", J. Am. Chem. Soc., 73, pp. 373-380

Beck, J.S., 1991, "Method For Synthesizing Mesoporous Crystalline Material", US Patent No. 5,057,296

Beck, J. S., Vartuli, J. C., Roth, W. J., Leonowicz, M. E., Kresge, C. T., Schmitt, K. D., Chu, C. T.-W., Olson, D. H., Sheppard, E. W., McCullen, S. B., Higgins, J. B., Schlenker, J. L., 1992, "A New Family Of Mesoporous Molecular Sieves Prepared With Liquid Crystal Templates" J. Am. Chem. Soc., 114, pp. 10834-10843

Behrens, P., Glaue, A., Haggenmüller, C., Scheshner, G., 1997," Structure-Directed Materials Syntheses: Synthesis Field Diagrams For The Preparation of Mesostructured Silicas", Solid state Ionics, 101-103, pp. 255-260

Brühwiler, D., Frei, H., 2003, "Structure Of Ni(II) And Ru(III) Ammine Complexes Grafted Onto Mesoporous Silicate Sieve", J. Phys. Chem. B., 107, pp. 8547-8556

Chang, Z., Zhu, Z., Kevan, L., 1999, "Electron Spin Resonance Of Ni(I) In Ni-Containing MCM-41 Molecular Sieves", J. Phys. Chem. B., 103, pp. 9442-9449

Chiola, V., Ritsko, J.E., Vanderpool, CD., 1971, US Patent No. 3 556 725

Ciesla, U., Schüth, F., 1999, "Ordered Mesoporous Materials", Mic. Meso. Mater. 27, pp. 131-149

Cullity, B.D., Stock, S.R., "Elements of X-Ray Dffraction", 3rd Edition, Prentice Hall Inc., 2001

DiRenzo, F., Cambon, H., Dutartre , R., 1997, Microporous Metarials, 10, p.283

García, E., Laborde, M., 1991, Int. J. Hydrogen energy, 16(5), 307

Gelb L.D., Gubbins, K.E., "Characterization of Porous Glasses by Adsorption : Models, Simulation and Data Inversion" from www.chemistry. wustl.edu/~gelb/papers/FOA6.ads.pdf at January 24, 2005

Gregg, S.J., Sing, K.S.W., 1982, "Adsorption, Surface Area And Porosity", 2nd Edition, Academic Press Inc.

Grubert, G., Rathouský, J., Schulz-Ekloff, G., Wark, M., Zukal, A., 1998, ”Reducibility of Vanadium Oxide Species in MCM-41”, Microporous and Mesoporous Materials, 22, pp. 225-236

Gucbilmez, Y., Dogu, T., Balci, S., “Vanadium Incorporated High Surface Area MCM-41 Catalysts”, Catalysis Today (in press).

Guo X., Lai M., Kong Y., Ding W., Yan Q., 2004, “Novel Coassembly Route To Cu-Sio2 MCM-41-Like Mesoporous Materials”, Langmuir, 20, pp. 2879-2882

Hadjiivanov K., Tsoncheva T., Dimitrov M., Minchev C., Knözinger H., 2003, “Characterization Of Cu/MCM-41 And Cu/MCM-48 Mesoporous Catalysts By FTIR Spectroscopy Of Adsorbed CO” Applied Catalysis A: General, 241, pp. 331-340

Hartmann, M., Pöppl, A., Kevan, L., 1996, “ Ethylene Dimerization And Butene Isomerization In Nickel-Containing MCM-41 And AlMCM-41 Mesoporous Molecular Sieves: An Electron Spin Rsonance And Gas Chromatography Study”, J. Phys. Chem., 100, pp. 9906-9910

Hartmann M., Racouchot S., Bischof C., 1997, “Synthesis And Redox Properties Of MCM-48 Containing Copper And Zinc”, Chem. Commun., 24, pp. 2367-2368

Infantes-Molina, A., Merida-Robles, J., Braos-García, P., Rodríguez-Castellón, E., Finocchio, E., Busca, G., Maireles-Torres, P., Jiménez-López, A., 2004, “Nickel Supported On Porous Silica As Catalysts For The Gas-Phase Hydrogenation Of Acetonitrile”, Journal Of Catalysis, 225, pp 479-488

IUPAC Manual Of Symbols And Terminology, 1978, Pure Appl. Chem., 31, 578

JEOL Scanning Electron Microscopes, http://www.jeol.com/sem/sem.html
JSM-6700F, http://www.jeol.com/sem/semprods/jsm6700f.html at January 24, 2005

Jin, P., Chen, Q., Hao, L., Tian, R., Zhang, L., Wang, L., 2004, “Synthesis And Catalytic Properties Of Nickel-Silica Composite Hallow Nanospheres”, J. Phys. Chem. B., 108, pp. 6311-6314

Kresge, C. T., Leonowicz, M. E., Roth, W. J., Vartuli, J. C., Beck, J. S., 1992, ”Ordered Mesoporous Molecular Sieves Synthesized By A Liquid-Crystal Template Mechanism” Nature, 359, pp. 710-712

Kresge, C.T., Vartuli, J.C., Roth, W.J., Leonowicz, M.E., 2004, “The Discovery Of ExxonMobil’s M41S Family Of Mesoporous Materials”, Studies in Surface Science and Catalysis, Vol 148, pp 53-72

Lensveld, D.J., Mesu, J.G., Dillen, A.J., Jong, K.P., 2001, “Synthesis And Characterization Of MCM-41 Supported Nickel Oxide Catalysts”, Mic. Meso Materials, 44-45, pp. 401-407

Lowell, S., Shields, J.E., 1991, "Powder Surface Area And Porosity", 3rd Edition, Chapman and Hall Publication

Mariño, F.J., Cerrella, E.G., Duhalde, S., Jobbagy M., Laborde M.A., 1998, "Hydrogen From Steam Reforming Of Ethanol. Characterization And Performance Of Copper-Nickel Supported Catalysts" Int. J. Hydrogen Energy, Vol. 23, No. 12, pp. 1095-1101

Mariño, F., Baronetti, G., Jobbagy, M., Laborde M., 2003, "Cu-Ni-K/γ-Al_2O_3 Supported Catalysts For Ethanol Steam Reforming. Formation Of Hydrotalcite-Type Compounds As A Result Of Metal-Support Interaction" Applied Catalysis A: General, 238, pp. 41-54

Mariño, F., Boveri, M., Baronetti, G., Laborde, M., 2004, "Hydrogen Production Via Catalytic Gasification Of Ethanol. A Mechanism Proposal Over Copper-Nickel Catalysts", Int. J. Hyrogen Energy, 29, pp. 67-71

McGraw-Hill Encyclopedia of Science and Technology, 1960, Volume 14, McGraw-Hill Book company, Inc.

Mohapatra, S.K., Sonavane, S.U., Jayaram, R.V., Selvam, P., 2002, "Regio- And Chemoselective Catalytic Transfer Hydrogenation Of Aromatic Nitro And Carbonyl As Well As Reductive Cleavage Of Azo Compounds Over Novel Mesoporous Nimcm-41 Molecular Sieves", Organic Letters, Vol.4, No.24, pp. 4297-4300

Noreńa-Franco, L., Hernandez-Perez, I., Aguliar-Pliego, J., Maubert-Franco, A., 2002, "Selective Hydroxylation Of Phenol Employing Cu-MCM-41 Catalysts", Catalysis Today, 75, pp.189-195

Parvulescu, V., Su, B.L., 2001, "Iron, Cobalt Or Nickel Substituted MCM-41 Molecular Sieves For Oxidation Of Hydrocarbons", Catalysis Today, 69, pp. 315-322

Peña M.L., Kan Q., Corma A., Rey F., 2001, "Synthesis Of Cubic Mesoporous MCM-48 Materials From The System Sio_2:CTAOH/Br:H_2O" Microporous And Mesoporous Materials, 44-45, pp. 9-16

Øye G., Sjöblom J., Stöcker M., 2001, "Synthesis, Characterization And Potential Applications Of New Materials In The Mesoporous Range" Advances In Colloid And Interface Science, 89-90, pp. 439-466

Roth, W.J., 2000, " Synthesis Of The Cubic Mesoporous Molecular Sieve MCM-48", US Patent No. 6,096,288

Russ, J.C., 1982, "Fundamentals of Energy Dispersive X-ray analysis", Buttorworths Monographs in Materials

Schultz-Ekloff, G., Rathouský J., Zukal, A., 1999,"Mesoporous Silica With Controlled Porous structure and Regular Morphology", Int. J. Inorganic Mater., 1, pp. 97-102

Schumacher K., Ravikovitch P.I., Chesne A., Neimark A.V., Unger K.K., 2000 "Characterization Of MCM-48 Materials" Langmuir , 16, pp. 4648-4654

Tsoncheva T., Venkov Tz., Dimitrov M., Minchev C., Hadjiivanov K., 2004, "Copper-Modified Mesoporous MCM-41 Silica: FTIR And Catalytic Study", Journal Of Molecular Catalysis A: Chemical 209, pp. 125–134

Vartuli, J. C., Schmitt, K. D., Kresge, C. T., Roth, W. J., Leonowicz, M. E., Mccullen, S. B., Hellring, S. D., Beck, J. S., Schlenker, J. L., Olson, D. H., Sheppard, E. W., 1994, "Effect Of Surfactant/Silica Molar Ratios On The Formation Of Mesoporous Molecular Sieves: Inorganic Mimicry Of Surfactant Liquid-Crystal Phases And Mechanistic Implications" *Chem. Mater.*, *6*, pp. 2317-2326

Velu, S., Wang, L., Okazaki, M., Suzuki, K., Tomura, S., 2002, "Characterization Of MCM-41 Mesoporous Molecular Sieves Containing Copper and Zinc And Their Catalytic Performance In The Selective Oxidation Of Alcohols To Aldehydes", Mic. Meso. Mater., 54, pp. 113-126

Wan, Y., Ma, J., Wang, Z., Zhou, W., Kaliaguine, S., 2004, "Selective Catalytic Reduction Of NO over Cu-Al-MCM-41", Journal of Catalysis, 227, pp. 242-252

Wiley Interscience, Kirk-Othmer Encyclopedia of Chemical Technology,, http://www3.interscience.wiley.com/cgi-bin/mrwhome/104554789/HOME ,Weaver, R., 2003, McCrone Research Institute, "Microscopy", http://www.mrw.interscience.wiley.com/kirk/articles/micrmccr.a01/abstract-fs.html , at December 22, 2004

Yasyerli, S, Dogu, G., Ar, I., Dogu, T., 2004," Dynamic Analysis of Removal and Selective Oxidation of H_2S to Elemental Sulfur Over Cu-V and Cu-V-Mo Mixed Oxides in a Fixed Bed Reactor", Chemical Engineering Science, 59, pp. 4001-4009

Zhang Q., Wang Y., Ohishi Y., Shishido T., Takehira K., 2001, "Vanadium-Containing MCM-41 For Partial Oxidation Of Lower Alkanes" Journal Of Catalysis, 202, pp. 308-318

Ziolek M., Nowak I., Kilos B., Sobczak I., Decyk P., Trejda M., Volta J.C., 2004, "Template Synthesis And Characterisation Of MCM-41 Mesoporous Molecular Sieves Containing Various Transition Metal Elements—TME (Cu, Fe, Nb, V, Mo)", Journal Of Physics And Chemistry Of Solids, 65, pp. 571–581

APPENDIX A

MSDS of CHEMICALS

Table A.1 MSDS of Sodium Silicate Solution

Product Name	Sodium Silicate solution extra pure
Company/ Catalog Number	Aldrich / 33.844-3
CAS Number	1344-09-8
Molecular Weight	242.23 g/mol
Formula	$SiO_2 \cdot NaOH$
Hazards Identification	No hazardous product as specified in Directive 67/548/AAC.
First Aid Measures	After inhalation: fresh air. After skin contact: wash off with plenty of water. After eye contact: rinse out with plenty of water. After swallowing: make victim drink plenty of water
Handling and Storage	Tightly closed. Dry. At 5 °C to 30 °C.
Personal Protection	Eye and hand protection are required.
Stability and Reactivity	Avoid strong heating. Avoid fluorine.
Disposable considerations	Chemicals must be disposed of in compliance with the respective national regulations.

Table A.2 Physical and Chemical Properties of Sodium Silicate Solution

Form	Liquid
Color	Colorless
Odor	Odorless
pH value at 50g/l H_2O (20 °C)	~11-11.5
Viscosity dynamic (20 °C)	~130 MPa*s
Melting point	0 °C
Boiling point	> 100 °C
Ignition temperature	Not available
Flash point	Not available
Explosion limits	Not available
Density (20 °C)	1.35 g/cm^3
Bulk density	~1050 kg/m^3
Solubility in water (20 °C)	Soluble

TableA.3 MSDS of Sodium Metasilicate

Product Name	Sodium Metasilicate
Company/ Catalog Number	Aldrich / 30.781-5
CAS Number	6834-92-0
Molecular Weight	122.06 g/mol
Formula	Na_2O_3Si
Hazards Identification	Harmful if swallowed. Irritating to eyes and skin. Corrosive. Causes burns to mouth and stomach. No known chronic hazards.
First Aid Measures	After inhalation: fresh air. After skin contact: wash off with plenty of water. After eye contact: rinse out with plenty of water. After swallowing: make victim drink plenty of water
Handling and Storage	Tightly closed. Away from acids, reactive metals, ammonium salts.
Personal Protection	Eye and hand protection are required.
Stability and Reactivity	Reacts with acids and some organics. Generates heat when mixed with acid. May react with ammonium salt solutions resulting in evolution of ammonia gas. Flammable hydrogen gas may be produced on contact with aluminum, tin, lead, and zinc. Carbon monoxide gas may be produced on contact with reducing sugars.
Disposable considerations	Chemicals must be disposed of in compliance with the respective national regulations.

Table A.4 Physical and Chemical Properties of Sodium Metasilicate

Form	Granular powder
Color	White
Odor	Odorless or musty odor
pH value at 50g/l H_2O (20 °C)	~14
Melting point	~114 °C
Boiling point	Not available
Ignition temperature	Not available
Flash point	Not available
Explosion limits	Not available
Density (20 °C)	Not available
Bulk density	Not available
Solubility in water (20 °C)	Soluble

Table A.5 MSDS of Hexadecyltrimethyl ammonium bromide

Product Name	Hexadecyltrimethyl ammonium bromide
Company/ Catalog Number	Sigma / H-5882
CAS Number	57-09-0
Molecular Weight	364.45 g/mol
Formula	C19H42BrN
Hazards Identification	Harmful if swallowed. Irritating to eyes and skin. Very toxic to aquatic organisms, may cause long term adverse effects in the aquatic environment.
First Aid Measures	After inhalation: fresh air. After skin contact: wash off with plenty of water. After eye contact: rinse out with plenty of water. After swallowing: make victim drink plenty of water
Handling and Storage	Tightly closed. Dry. At 15 °C to 25 °C.
Personal Protection	Eye and hand protection are required.
Stability and Reactivity	Avoid heating. Avoid strong oxidizing agents.
Disposable considerations	Chemicals must be disposed of in compliance with the respective national regulations. Do not allow to enter sewerage system.

Table A.6 Physical and Chemical Properties of Hexadecyltrimethyl ammonium bromide

Form	Solid
Color	White
Odor	Weak
pH value at 50g/l H_2O (20 °C)	5-7
Melting point	248-251 °C
Boiling point	Not available
Ignition temperature	Not available
Flash point	Not applicable
Explosion limits	Not available
Density (20 °C)	Not available
Bulk density	~390 kg/m^3
Solubility in water (20 °C)	50 mg/ml
Thermal decomposition	> 230 °C

Table A.7 MSDS of Copper (II) nitrate trihydrate

Product Name	Cupper (II) nitrate trihydrate extra pure
Company/ Catalog Number	Merck KGaA / 102752
CAS Number	10031-43-3
Molecular Weight	241.60 g/mol
Formula	$Cu(NO_3)_2 \cdot 3H_2O$
Hazards Identification	Harmful if swallowed. Irritating to eyes and skin. Very toxic to aquatic organisms, may cause long term adverse effects in the aquatic environment.
First Aid Measures	After inhalation: fresh air. After skin contact: wash off with plenty of water. After eye contact: rinse out with plenty of water. After swallowing: make victim drink plenty of water
Handling and Storage	Tightly closed. Away from combustible materials and sources of ignition and heat. Dry.
Personal Protection	Eye and hand protection are required.
Stability and Reactivity	Avoid strong heating. Risk of explosion with ammonia/amides, cyanide complexes, metals in powder form, oxidizable substances
Disposable considerations	Chemicals must be disposed of in compliance with the respective national regulations. Do not allow to enter sewerage system.

Table A.8 Physical and Chemical Properties of Copper (II) nitrate trihydrate

Form	Solid
Color	Blue
Odor	Of nitric acid
pH value at 50g/l H_2O (20 °C)	~3-4
Melting point	~114 °C
Boiling point	Not available
Ignition temperature	Not applicable
Flash point	Not flammable
Explosion limits	Not applicable
Density (20 °C)	2.05 g/cm^3
Bulk density	~1050 kg/m^3
Solubility in water (20 °C)	2670 g/l
Thermal decomposition	> 170 °C

Table A.9 MSDS of Nickel (II) nitrate hexahydrate

Product Name	Nickel (II) nitrate hexahydrate GR for analysis
Company/ Catalog Number	Merck KGaA / 106721
CAS Number	13478-00-7
Molecular Weight	290.81 g/mol
Formula	$Ni(NO_3)_2 \cdot 6H_2O$
Hazards Identification	Contact with combustible material may cause fire. Harmful if swallowed. May cause sensitization by skin contact.
First Aid Measures	After inhalation: fresh air. After skin contact: wash off with plenty of water. After eye contact: rinse out with plenty of water. After swallowing: make victim drink plenty of water
Handling and Storage	Tightly closed. Away from combustible materials and sources of ignition and heat. Dry.
Personal Protection	Eye and hand protection are required.
Stability and Reactivity	Avoid heating. Avoid reducing agents and combustible substances.
Disposable considerations	Chemicals must be disposed of in compliance with the respective national regulations.

Table A.10 Physical and Chemical Properties of Nickel (II) nitrate hexahydrate

Form	Solid
Color	Green
Odor	Of nitric acid
pH value at 50g/l H_2O (20 °C)	~5
Melting point	~56.7 °C
Boiling point	Not available
Ignition temperature	Not available
Flash point	Not available
Explosion limits	Not available
Density	Not available
Bulk density	~800 kg/m^3
Solubility in water (0° C)	2380 g/l

APPENDIX B

CHARACTERIZATION DATA

B.1 X-ray Diffraction

Table B.1 XRD data of MCM-41(I)

Angle [2θ]	Intensity [counts]	Intensity [counts]	Intensity [counts]	Intensity [counts]	Intensity [counts]	Intensity [counts]
1.01	424	428	424	424	408	384
1.13	396	412	396	376	369	376
1.25	353	433	420	388	365	400
1.49	384	437	404	428	454	462
1.61	424	445	454	458	475	562
1.73	543	488	552	484	543	548
1.85	562	595	605	635	640	610
1.97	620	630	702	666	751	773
2.09	729	818	790	818	906	847
2.21	888	967	1,018	961	1,076	1,082
2.33	1,149	1,170	1,225	1,225	1,267	1,391
2.45	1,521	1,552	1,656	1,681	1,756	1,772
2.57	1,747	1,884	1,731	1,689	1,537	1,362
2.69	1,296	1,050	955	930	784	708
2.81	692	595	610	548	502	529
2.93	471	445	458	454	384	424
3.05	380	369	396	404	328	365
3.17	372	331	331	353	331	313
3.53	262	282	289	266	250	276
3.89	289	289	299	253	276	262
4.25	282	269	276	286	259	276
4.97	202	237	210	237	216	199
5.57	154	137	121	130	112	135
5.93	112	130	130	128	94	110
6.53	119	104	121	119	98	85
6.89	92	88	94	104	104	90
7.97	66	79	77	71	76	86
8.57	61	67	59	76	67	67
9.29	66	56	56	59	42	66
10.01	44	58	49	52	42	58

Table B.2 XRD data of MCM-41(II)

Angle [2θ]	Intensity [counts]	Intensity [counts]	Intensity [counts]	Intensity [counts]	Intensity [counts]	Intensity [counts]
1.01	18	28	31	26	24	16
1.13	26	26	35	29	25	30
1.25	22	36	22	27	30	26
1.37	25	50	36	36	35	40
1.49	48	40	52	44	52	67
1.61	62	56	53	64	59	77
1.73	69	79	88	72	96	98
1.85	98	123	110	125	142	142
1.97	159	174	180	202	188	199
2.09	246	250	256	256	269	342
2.21	369	428	493	520	581	645
2.33	751	847	900	1109	1076	1005
2.45	829	655	471	400	353	384
2.57	346	320	342	266	279	240
2.69	216	193	166	164	137	144
2.81	161	159	139	139	125	137
2.93	137	123	100	98	114	119
3.05	119	110	112	114	114	130
3.17	123	114	123	128	119	108
3.29	117	119	114	130	139	125
3.53	119	142	137	130	135	135
3.65	132	149	182	156	130	169
3.77	159	151	142	166	177	169
3.89	204	202	199	204	207	225
4.01	246	279	259	282	276	313
4.13	276	282	266	225	207	193
4.37	161	169	142	169	169	199
4.49	164	188	154	180	182	196
4.61	177	196	193	210	231	222
4.73	213	237	199	219	177	159
4.85	137	144	137	132	130	137
5.21	108	114	104	83	94	110
5.93	100	85	104	86	79	86
6.17	108	102	92	96	119	94
6.89	72	71	58	72	48	50
7.25	62	62	71	55	59	62
8.45	42	38	58	40	32	56
9.65	48	46	42	34	38	31
10.01	27	31	34	28	32	35

Table B.3 XRD data of MCM-41(III)

Angle [2θ]	Intensity [counts]	Intensity [counts]	Intensity [counts]	Intensity [counts]	Intensity [counts]	Intensity [counts]
1.01	16	24	26	27	22	23
1.13	22	17	27	27	25	21
1.25	22	18	22	22	24	19
1.37	22	26	29	22	34	25
1.49	22	15	35	24	38	28
1.61	28	27	27	21	41	36
1.73	28	36	30	35	36	30
1.85	34	29	48	46	38	38
1.97	38	48	45	53	48	53
2.09	58	55	67	62	66	79
2.21	72	83	90	86	98	130
2.33	132	156	149	180	164	154
2.45	161	135	108	86	86	77
2.57	66	71	53	53	56	64
2.69	55	56	42	50	56	37
2.81	52	62	52	59	50	45
2.93	62	66	49	69	62	59
3.05	59	72	53	55	66	53
3.17	72	66	56	58	56	67
3.29	56	56	64	69	76	76
3.41	69	59	74	81	64	71
3.53	67	71	85	59	76	53
3.65	76	67	67	96	79	98
3.77	83	110	112	100	85	102
3.89	106	114	106	110	130	123
4.01	123	132	123	149	135	119
4.13	130	144	128	119	92	92
4.25	88	83	53	85	66	81
4.49	110	69	86	85	96	92
4.61	90	88	106	114	144	137
4.73	159	149	112	121	98	85
4.85	96	85	71	67	55	66
5.21	48	61	50	58	56	56
6.29	71	50	53	62	59	74
7.25	32	42	45	41	44	52
8.33	41	38	29	37	32	36
9.29	30	41	28	37	32	20
10.01	29	35	44	32	31	31

Table B.4 XRD data of MCM-41(IV)

Angle [2θ]	Intensity [counts]	Intensity [counts]	Intensity [counts]	Intensity [counts]	Intensity [counts]	Intensity [counts]
1.01	24	26	27	30	34	32
1.13	18	29	25	28	27	22
1.25	14	28	21	35	23	27
1.37	26	29	30	34	31	37
1.49	38	30	44	36	44	52
1.61	41	50	56	44	48	50
1.73	46	42	55	62	53	61
1.85	71	56	67	59	72	79
1.97	62	85	71	128	90	98
2.09	83	90	85	92	92	117
2.21	114	92	106	121	121	130
2.33	137	144	130	182	164	159
2.45	177	196	180	174	193	146
2.57	207	182	196	202	243	193
2.69	228	240	259	246	276	231
2.81	289	266	243	259	240	243
2.93	213	222	234	246	216	199
3.05	180	190	196	196	172	207
3.17	188	166	199	180	188	174
3.29	169	144	159	154	166	149
3.41	182	130	161	159	193	128
3.53	149	137	169	164	135	125
3.65	137	149	188	154	169	161
3.77	159	161	132	130	144	149
3.89	125	137	166	149	146	144
4.13	121	112	123	121	106	110
4.25	121	108	104	106	121	119
4.49	106	108	94	123	106	110
4.73	102	98	117	106	114	110
4.97	85	98	90	106	110	100
5.21	100	104	98	81	88	90
5.45	83	79	83	62	72	88
5.93	66	81	86	83	69	72
6.17	85	83	59	67	61	62
6.89	69	66	50	53	49	50
7.73	46	48	58	58	38	52
8.93	46	32	36	31	41	46
9.77	28	36	32	34	38	30
10.01	29	30	37	34	32	36

Table B.5 XRD data of Cu-Imp(I)

Angle [2θ]	Intensity [counts]	Intensity [counts]	Intensity [counts]	Intensity [counts]	Intensity [counts]	Intensity [counts]
1.01	888	858	756	756	767	686
1.13	702	671	650	610	576	615
1.25	552	571	562	548	557	502
1.37	493	416	441	428	416	400
1.49	369	396	380	372	357	328
1.61	361	357	303	306	324	272
1.73	324	296	266	279	262	266
1.85	240	259	243	240	228	262
1.97	231	266	246	262	240	259
2.09	259	256	272	262	299	299
2.21	289	279	279	303	331	286
2.33	310	262	250	250	225	225
2.45	216	177	169	193	174	193
2.57	182	149	182	159	159	164
2.69	130	137	130	112	137	144
2.81	139	142	119	125	117	121
2.93	119	123	102	110	117	104
3.05	119	114	135	90	130	110
3.17	110	96	94	92	121	110
3.29	88	92	90	130	108	81
3.41	83	94	94	102	85	117
3.53	96	96	92	104	102	102
3.65	106	92	92	92	114	96
3.77	96	100	100	94	108	90
3.89	92	96	92	114	102	88
4.01	94	83	81	77	67	77
4.13	61	62	79	62	67	76
4.25	64	59	59	72	76	74
4.37	69	71	67	64	56	77
4.61	64	66	66	62	59	50
4.85	56	46	61	56	59	64
5.09	46	66	52	50	46	55
5.57	46	40	53	50	52	52
5.81	40	56	52	41	36	58
6.29	44	45	34	50	44	56
6.65	50	42	41	36	44	44
6.89	48	44	45	44	50	37
7.37	34	38	48	40	32	49
7.61	38	35	38	38	36	49
7.85	32	36	41	37	38	40
8.33	41	52	44	48	44	44
8.57	49	48	38	40	45	38
8.81	38	38	38	42	40	40
9.29	30	46	46	36	38	55
9.53	37	44	42	44	36	38
9.77	56	42	44	53	40	38
10.01	50	37	40	42	42	34

Table B.6 XRD data of Cu-Imp(II)

Angle [2θ]	Intensity [counts]	Intensity [counts]	Intensity [counts]	Intensity [counts]	Intensity [counts]	Intensity [counts]
1.01	28	21	30	25	26	28
1.13	27	20	22	19	29	15
1.25	15	19	34	22	22	19
1.37	21	16	22	22	30	29
1.49	25	15	31	15	27	34
1.61	28	26	35	36	37	42
1.73	44	41	50	50	58	56
1.85	49	59	56	69	83	79
1.97	94	88	104	102	110	90
2.09	121	121	121	137	166	169
2.21	180	199	234	234	276	303
2.33	361	342	404	484	520	595
2.45	640	660	625	480	357	276
2.57	199	180	151	151	142	121
2.69	135	119	106	106	102	98
2.81	96	90	112	81	83	90
2.93	92	98	104	90	96	106
3.05	104	104	86	94	98	110
3.17	88	100	88	90	106	88
3.29	94	90	85	98	90	94
3.41	102	77	92	112	100	85
3.53	83	92	88	94	88	102
3.65	96	96	86	90	108	117
3.77	86	100	86	112	108	98
3.89	100	106	114	102	102	92
4.01	125	110	112	128	117	123
4.13	112	123	130	108	146	130
4.25	110	112	130	98	90	71
4.37	94	76	88	77	83	79
4.49	96	83	90	110	88	100
4.61	112	83	92	79	94	92
4.73	85	112	110	114	117	100
4.85	117	119	106	94	100	77
4.97	86	83	81	53	59	48
5.21	66	55	48	53	58	40
5.45	56	48	50	50	48	55
5.93	41	45	35	48	50	53
6.17	48	56	50	37	50	48
6.41	45	45	55	44	49	38
6.89	42	48	41	44	35	53
7.13	42	41	46	44	48	42
7.37	46	48	45	35	45	48
7.61	38	41	49	48	41	48
8.33	42	46	42	41	37	32
8.57	32	44	58	34	45	35
9.05	37	37	38	32	36	52
9.53	35	40	40	38	45	48
10.01	44	42	45	44	40	35

Table B.7 XRD data of Cu-HT(I)

Angle [2θ]	Intensity [counts]	Intensity [counts]	Intensity [counts]	Intensity [counts]	Intensity [counts]	Intensity [counts]
1.01	272	237	222	250	228	231
1.13	237	219	204	222	225	188
1.25	207	207	231	210	193	182
1.37	219	196	213	210	193	188
1.49	180	174	193	199	199	177
1.61	172	202	154	174	185	196
1.73	164	172	164	185	177	174
1.85	169	177	177	182	169	169
1.97	190	177	202	185	169	177
2.09	190	196	196	193	169	169
2.21	177	185	174	177	169	177
2.33	207	177	196	188	185	188
2.45	199	199	185	169	210	202
2.57	190	213	216	190	213	196
2.69	202	210	216	196	196	188
2.81	202	196	180	185	154	161
2.93	159	149	156	137	137	135
3.05	142	135	142	137	130	142
3.17	125	100	121	125	121	104
3.29	119	112	112	110	102	114
3.41	92	88	98	96	117	88
3.53	114	90	85	94	81	98
3.65	106	86	106	104	94	96
3.77	83	90	100	92	88	90
3.89	88	104	94	98	77	77
4.01	79	71	64	85	59	66
4.13	62	53	72	58	55	66
4.25	44	59	52	61	67	69
4.37	62	56	41	59	50	56
4.49	53	50	56	62	67	76
4.61	50	50	53	44	34	40
4.73	59	56	48	50	50	50
4.85	49	50	50	50	56	50
4.97	41	48	58	55	50	45
5.21	53	52	59	34	38	46
5.57	38	38	48	41	36	38
5.93	32	46	38	38	35	38
6.05	44	44	46	41	31	44
6.29	46	37	37	38	49	50
6.77	44	37	38	49	28	44
7.25	38	46	46	38	45	42
7.49	35	31	27	59	32	34
7.97	38	48	34	35	32	36
8.33	34	34	38	38	29	29
8.81	32	45	44	35	38	37
9.77	36	46	52	35	35	32
10.01	38	28	48	31	32	32

Table B.8 XRD data of Cu-HT(II)

Angle [2θ]	Intensity [counts]	Intensity [counts]	Intensity [counts]	Intensity [counts]	Intensity [counts]	Intensity [counts]
1.01	266	276	272	250	266	292
1.13	303	282	272	262	262	237
1.25	193	246	240	262	237	253
1.37	250	216	222	234	243	243
1.49	231	210	225	231	231	237
1.61	228	216	196	216	225	237
1.73	234	219	231	207	213	202
1.85	210	219	210	196	204	177
1.97	188	199	196	196	199	180
2.09	202	204	169	199	182	204
2.21	169	188	169	196	188	213
2.33	204	164	182	213	169	182
2.45	185	204	190	180	193	219
2.57	210	225	193	193	204	213
2.69	190	222	172	213	210	219
2.81	190	210	204	213	213	193
2.93	196	204	231	199	213	216
3.05	199	188	185	182	169	154
3.17	154	169	151	142	121	139
3.29	128	144	112	108	130	144
3.41	119	130	112	112	106	106
3.53	110	117	106	96	98	112
3.65	92	88	100	112	106	100
3.77	102	102	104	88	92	100
3.89	112	98	98	108	86	98
4.01	96	72	72	76	71	72
4.13	76	71	61	62	62	56
4.25	58	71	71	76	58	71
4.37	49	56	66	45	55	45
4.49	58	56	71	56	64	59
4.61	66	53	62	52	69	58
4.73	40	67	64	48	64	53
4.85	61	67	71	62	53	50
4.97	67	48	49	48	49	44
5.09	55	58	50	52	48	59
5.33	44	48	48	52	53	67
5.69	44	48	64	49	48	35
5.93	48	40	48	35	44	52
6.29	44	38	45	40	49	38
6.53	46	50	48	35	29	42
6.89	44	37	32	35	49	41
7.37	30	45	29	36	29	38
7.85	41	50	36	30	41	37
8.33	44	36	38	34	38	44
8.81	38	34	49	48	42	41
9.29	42	28	32	45	41	40
9.53	41	32	38	36	40	42
10.01	29	30	34	44	34	37

Table B.9 XRD data of Cu-LT(I)

Angle [2θ]	Intensity [counts]	Intensity [counts]	Intensity [counts]	Intensity [counts]	Intensity [counts]	Intensity [counts]
1.01	25	41	38	38	30	37
1.13	46	35	44	38	38	38
1.25	55	48	55	58	59	69
1.37	59	79	76	53	59	72
1.49	71	79	86	77	76	83
1.61	86	104	86	102	92	117
1.73	98	106	110	151	121	135
1.85	123	144	130	132	156	164
1.97	146	146	166	174	188	182
2.09	202	216	222	213	231	262
2.21	219	250	279	279	306	313
2.33	303	313	331	320	361	310
2.45	339	328	339	317	276	240
2.57	219	210	210	172	177	156
2.69	166	139	149	149	135	149
2.81	151	123	164	125	112	142
2.93	130	110	108	98	121	114
3.05	114	121	121	108	90	104
3.17	123	108	108	106	96	114
3.29	108	117	108	121	102	110
3.41	90	104	98	121	94	117
3.53	88	92	96	94	88	106
3.65	94	114	96	96	119	132
3.77	119	96	117	106	90	110
3.89	119	110	123	106	112	108
4.01	108	114	96	98	88	90
4.13	88	96	92	106	90	102
4.25	88	83	102	76	85	102
4.37	72	66	83	90	72	85
4.49	83	72	67	72	79	67
4.61	90	77	79	76	77	66
4.73	88	79	56	86	83	85
4.85	64	81	90	74	62	71
4.97	72	66	72	55	72	64
5.09	59	48	64	59	53	59
5.33	48	53	44	45	62	53
5.57	41	53	61	50	59	59
5.81	62	45	41	50	44	38
6.05	56	55	41	42	38	56
6.29	48	58	49	34	45	50
6.77	48	27	40	41	40	32
7.25	44	35	41	38	38	45
7.97	37	35	27	36	28	40
8.33	38	28	32	36	36	45
8.81	31	38	32	29	32	29
9.29	35	26	29	30	20	18
9.53	31	36	32	27	26	23
10.01	32	38	26	26	23	19

Table B.10 XRD data of Cu-LT(II)

Angle [2θ]	Intensity [counts]	Intensity [counts]	Intensity [counts]	Intensity [counts]	Intensity [counts]	Intensity [counts]
1.01	25	32	27	25	31	30
1.13	21	30	27	22	41	36
1.25	38	45	49	44	48	61
1.37	50	59	59	56	66	77
1.49	76	81	77	81	85	86
1.61	123	102	98	112	104	86
1.73	108	123	108	130	142	130
1.85	114	119	132	137	144	149
1.97	130	139	149	139	142	139
2.09	130	144	154	149	144	144
2.21	156	135	144	132	139	151
2.33	139	149	156	142	125	137
2.45	132	135	121	128	110	121
2.57	119	125	135	112	130	135
2.69	125	146	119	119	117	108
2.81	94	117	104	110	98	119
2.93	130	100	100	90	119	104
3.05	102	121	130	100	110	114
3.17	100	94	121	100	94	106
3.29	106	110	102	110	88	102
3.41	112	98	83	83	96	102
3.53	96	86	79	100	81	90
3.65	81	104	96	100	104	112
3.77	102	88	79	100	106	92
3.89	94	83	90	94	96	102
4.01	88	92	94	85	88	67
4.13	76	64	69	76	59	59
4.25	67	66	56	71	66	53
4.37	69	76	69	67	50	59
4.49	66	56	53	62	66	53
4.61	56	58	46	58	53	44
4.73	50	50	52	62	59	56
4.85	56	41	62	48	53	49
5.21	50	49	49	49	48	38
5.57	50	44	53	46	49	38
5.69	59	53	48	32	38	44
6.05	42	46	40	40	42	38
6.17	40	34	46	41	49	46
6.89	26	44	31	44	48	52
7.25	31	28	27	35	40	31
7.61	42	45	38	36	37	44
7.73	20	38	30	27	35	50
8.21	28	27	32	48	32	22
8.81	29	37	27	29	34	36
9.29	36	31	35	31	36	23
10.01	36	38	21	34	26	32

Table B.11 XRD data of Ni-HT(I)

Angle [2θ]	Intensity [counts]	Intensity [counts]	Intensity [counts]	Intensity [counts]	Intensity [counts]	Intensity [counts]
1.01	388	380	445	369	388	396
1.13	424	396	404	376	437	416
1.25	412	416	437	441	458	424
1.37	484	454	484	449	480	462
1.49	497	488	488	493	480	462
1.61	493	506	480	520	520	562
1.73	562	520	581	543	548	538
1.85	529	538	502	520	538	538
1.97	543	548	529	529	524	515
2.09	484	493	557	529	524	529
2.21	484	475	529	529	484	462
2.33	445	437	458	471	437	424
2.45	412	416	396	388	424	420
2.57	408	428	361	380	384	376
2.69	350	372	372	346	350	335
2.81	320	361	365	324	286	303
2.93	289	299	286	296	310	289
3.05	246	289	228	253	250	243
3.17	279	228	240	234	213	243
3.29	234	237	225	234	193	231
3.41	228	219	231	207	216	188
3.53	225	185	193	204	196	204
3.65	202	182	185	196	202	177
3.77	213	207	210	196	193	185
3.89	182	225	210	199	202	177
4.01	207	154	196	182	180	159
4.13	154	132	161	164	144	144
4.25	154	144	144	161	144	137
4.37	146	117	149	139	121	149
4.49	154	151	137	132	135	135
4.61	137	142	119	132	149	135
4.97	108	96	88	117	117	121
5.21	102	108	117	114	106	94
5.45	96	100	92	94	90	85
5.93	86	79	79	85	88	66
6.17	61	86	86	90	76	85
6.53	71	59	76	77	69	67
6.77	59	71	53	66	71	69
7.25	74	52	49	62	56	59
7.61	44	50	61	53	49	49
7.97	34	44	44	37	50	56
8.21	53	41	45	46	62	49
8.69	50	45	32	38	34	46
8.93	50	32	53	45	38	44
9.17	38	36	30	42	40	40
9.77	35	28	28	35	36	32
10.01	44	37	32	32	31	34

Table B.12 XRD data of Ni-HT(II)

Angle [2θ]	Intensity [counts]	Intensity [counts]	Intensity [counts]	Intensity [counts]	Intensity [counts]	Intensity [counts]
1.01	29	19	32	23	20	18
1.13	26	13	25	17	20	22
1.25	17	18	20	18	17	18
1.37	32	23	25	18	18	20
1.49	19	19	18	12	20	21
1.61	19	27	19	20	28	13
1.73	18	29	21	32	27	30
1.85	23	26	30	30	38	20
1.97	26	29	32	20	32	31
2.09	36	29	32	34	27	31
2.21	41	42	37	40	38	41
2.33	46	42	50	49	71	69
2.45	69	77	72	72	90	85
2.57	83	88	94	85	88	66
2.69	71	83	86	92	72	76
2.81	85	79	86	86	92	85
2.93	81	90	79	83	81	92
3.05	81	94	79	85	88	94
3.17	85	88	100	72	86	67
3.29	83	108	71	71	96	106
3.41	96	110	83	81	90	77
3.53	79	83	96	100	86	85
3.65	90	86	77	92	106	114
3.77	81	98	114	94	104	110
3.89	96	106	121	98	102	119
4.01	114	106	86	90	119	110
4.13	98	104	104	102	112	104
4.25	110	86	130	108	96	86
4.37	98	88	85	92	77	90
4.49	85	112	90	86	98	98
4.61	79	88	90	76	79	81
4.73	85	94	76	108	88	102
4.85	98	112	104	96	102	79
4.97	81	90	88	74	76	92
5.09	77	96	85	92	85	76
5.33	71	79	66	79	71	66
5.81	72	67	62	58	77	59
6.05	53	72	56	61	44	67
6.29	55	62	56	74	67	53
6.89	53	62	50	50	45	55
7.13	55	52	48	50	41	61
7.85	44	52	41	42	30	49
8.33	34	38	50	37	34	40
8.81	35	37	32	48	38	34
9.29	36	35	34	30	44	31
9.53	35	32	32	35	30	41
10.01	22	26	29	30	41	30

Table B.13 XRD data of Ni-Imp(I)

Angle [2θ]	Intensity [counts]	Intensity [counts]	Intensity [counts]	Intensity [counts]	Intensity [counts]	Intensity [counts]
1.01	76	85	66	81	83	72
1.13	76	86	88	119	88	112
1.25	79	117	114	90	92	114
1.37	102	121	128	137	130	154
1.49	137	156	149	142	139	154
1.61	159	199	199	207	213	190
1.73	231	228	216	216	196	231
1.85	228	272	259	279	246	282
1.97	292	328	286	339	350	335
2.09	342	361	380	380	420	428
2.21	462	441	467	493	497	543
2.33	543	595	610	595	660	702
2.45	756	635	686	645	615	538
2.57	441	428	404	369	331	342
2.69	289	296	272	282	259	243
2.81	246	279	222	228	243	240
2.93	228	259	256	228	240	228
3.05	222	246	240	204	234	243
3.17	219	240	250	237	210	243
3.29	228	213	225	216	202	231
3.41	210	253	204	199	213	237
3.53	216	188	234	202	225	246
3.65	225	231	228	213	243	231
3.77	237	222	237	243	216	237
3.89	269	228	250	240	240	231
4.01	243	234	250	246	234	240
4.13	222	243	286	266	246	231
4.25	234	225	213	216	164	185
4.37	190	174	196	174	228	180
4.49	180	161	164	161	156	182
4.61	174	188	166	188	161	137
4.73	151	142	164	151	144	156
4.85	156	139	164	159	164	144
5.21	90	108	108	110	135	112
6.29	94	112	110	106	98	79
7.37	72	62	55	58	50	45
8.33	50	56	46	37	42	50
9.29	37	44	32	40	40	46
10.01	34	38	38	38	30	44

B.2 Transmission Electron Microscopy

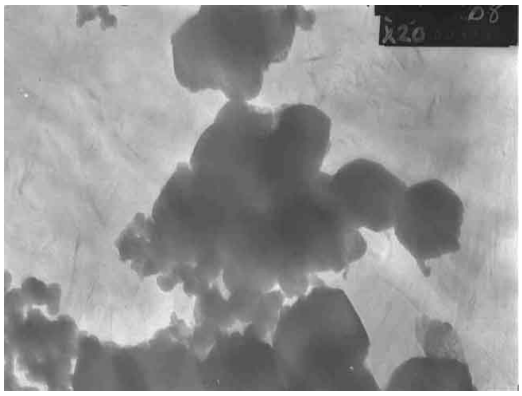

Figure B.1 TEM of Cu-LT (I)

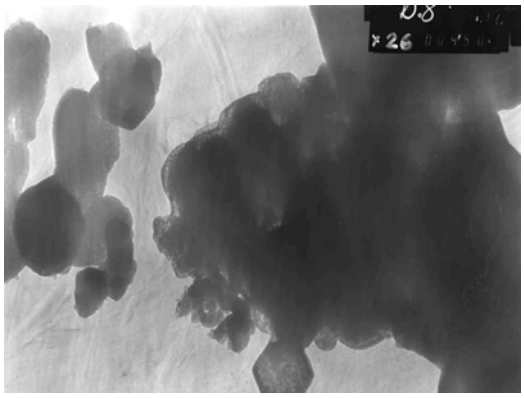

Figure B.2 TEM of Cu-LT (I)

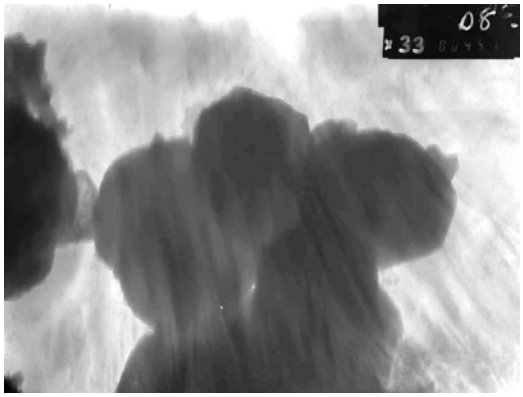

Figure B.3 TEM of Cu-LT (I)

B.3 N_2 Sorption

Table B.14 N_2 Sorption Data of MCM-41(I)

Relative Pressure (P/P_0)	Pressure (mmHg)	Volume Adsorbed (cc/g STP)
0.0589	40.803	228.8951
0.0774	53.623	242.7974
0.0990	68.574	256.8961
0.1188	82.279	268.7957
0.1384	95.828	280.2105
0.1579	109.269	291.6037
0.2010	139.005	321.8332
0.2491	172.144	385.4736
0.2983	206.084	455.7818
0.3590	248.072	480.0744
0.4653	321.517	496.1538
0.5526	381.807	504.8549
0.6654	459.746	515.5568
0.7379	509.869	523.0518
0.7993	552.306	530.3334
0.8383	579.198	536.8646
0.8759	605.221	544.4396
0.9023	623.419	552.7889
0.9240	638.417	563.5003
0.9373	647.611	576.5142
0.9526	658.218	594.2390
0.9641	666.136	609.4467
0.9660	667.382	623.1053
0.9773	675.155	639.6318
0.9813	677.844	650.0634
0.9858	680.890	660.6472
0.9850	680.342	661.4651
0.9873	681.847	672.4582
0.9925	685.363	686.1833
0.9764	674.208	681.2368
0.9580	661.430	674.5521
0.9412	649.737	650.9924
0.8942	617.110	597.2867
0.8337	575.221	564.1829
0.7301	503.704	546.0987
0.5553	383.058	528.3945
0.3456	238.360	478.0417
0.1373	94.737	279.9366

Table B.14 Continued (BJH Adsorption Pore Distribution)

Average Diameter (Å)	Incremental Pore Volume (cc/g)	Cumulative Pore Volume (cc/g)	Incremental Pore Area (m^2/g)	Cumulative Pore Area (m^2/g)
1408.3	0.018232	0.018232	0.518	0.518
1155.1	0.018990	0.037223	0.658	1.175
946.1	0.017487	0.054710	0.739	1.915
674.2	0.028005	0.082714	1.661	3.576
570.9	0.023913	0.106627	1.675	5.252
472.8	0.026177	0.132804	2.215	7.466
360.2	0.031237	0.164041	3.469	10.935
290.7	0.023341	0.187382	3.212	14.147
232.1	0.018868	0.206250	3.252	17.399
183.4	0.014678	0.220928	3.202	20.601
142.7	0.013242	0.234169	3.712	24.313
113.8	0.011953	0.246122	4.201	28.514
88.7	0.013509	0.259631	6.095	34.609
68.8	0.015038	0.274669	8.745	43.354
51.2	0.023995	0.298665	18.730	62.084
40.7	0.021707	0.320372	21.353	83.437
32.7	0.048464	0.368836	59.316	142.753
26.1	0.377298	0.746134	579.071	721.823
20.4	0.428090	1.174224	839.219	1561.042

Table B.14 Continued (BJH Desorption Pore Distribution)

Average Diameter (Å)	Incremental Pore Volume (cc/g)	Cumulative Pore Volume (cc/g)	Incremental Pore Area (m^2/g)	Cumulative Pore Area (m^2/g)
561.8	0.011644	0.011644	0.829	0.829
387.7	0.042320	0.053963	4.366	5.195
227.7	0.101056	0.155020	17.752	22.947
143.2	0.063045	0.218065	17.613	40.560
88.4	0.031645	0.249709	14.325	54.885
51.9	0.032814	0.282523	25.307	80.192
31.8	0.142949	0.425472	179.981	260.173
19.5	0.747731	1.173203	1530.058	1790.230

Table B.15 N_2 Sorption Data of MCM-41(II)

Relative Pressure (P/P_0)	Pressure (mmHg)	Volume Adsorbed (cc/g STP)
0.0598	41.269	226.0036
0.0763	52.646	237.3304
0.0985	67.943	250.4652
0.1191	82.175	261.4077
0.1393	96.086	271.3247
0.1593	109.827	280.8965
0.1945	134.097	297.6532
0.2488	171.487	332.5031
0.2939	202.619	385.8789
0.3457	238.458	491.2985
0.4979	343.486	508.5721
0.5589	385.587	512.3963
0.6621	456.855	518.5742
0.7388	509.827	522.9396
0.7969	549.927	526.8251
0.8391	579.042	530.6038
0.8743	603.354	534.9913
0.9043	624.138	540.2222
0.9258	638.960	544.9543
0.9392	648.284	549.2227
0.9532	657.965	554.6429
0.9635	665.101	559.7551
0.9704	669.859	564.5270
0.9775	674.772	569.9650
0.9816	677.622	573.6622
0.9831	678.702	576.2067
0.9881	682.219	580.8591
0.9942	686.408	585.8624
0.9944	686.615	592.8211
0.9812	677.466	587.3076
0.9703	669.968	582.4025
0.9600	662.929	576.5742
0.9435	651.547	566.4155
0.9069	626.372	550.2765
0.8262	570.675	536.4792
0.7383	509.987	529.8223
0.5519	381.238	519.5681
0.3491	241.194	493.3863
0.1468	101.413	273.3908

Table B.15 Continued (BJH Adsorption Pore Distribution)

Average Diameter (Å)	Incremental Pore Volume (cc/g)	Cumulative Pore Volume (cc/g)	Incremental Pore Area (m^2/g)	Cumulative Pore Area (m^2/g)
1975.9	0.008165	0.008165	0.165	0.165
1238.0	0.011924	0.020089	0.385	0.551
954.2	0.006171	0.026260	0.259	0.809
747.4	0.009180	0.035440	0.491	1.301
597.5	0.008159	0.043599	0.546	1.847
474.9	0.008819	0.052417	0.743	2.589
369.6	0.009503	0.061920	1.029	3.618
298.4	0.007604	0.069524	1.019	4.637
237.2	0.008521	0.078045	1.437	6.074
182.8	0.009695	0.087740	2.121	8.195
142.7	0.008282	0.096021	2.322	10.517
113.1	0.007239	0.103261	2.561	13.078
88.6	0.007641	0.110902	3.449	16.527
68.4	0.009157	0.120059	5.357	21.885
51.8	0.014680	0.134739	11.344	33.229
42.9	0.009754	0.144492	9.087	42.316
32.6	0.054973	0.199465	67.459	109.775
25.9	0.659350	0.858815	1019.209	1128.984
20.5	0.165298	1.024113	323.076	1452.060

Table B.15 Continued (BJH Desorption Pore Distribution)

Average Diameter (Å)	Incremental Pore Volume (cc/g)	Cumulative Pore Volume (cc/g)	Incremental Pore Area (m^2/g)	Cumulative Pore Area (m^2/g)
775.1	0.008352	0.008352	0.431	0.431
559.4	0.010080	0.018432	0.721	1.152
403.7	0.017962	0.036394	1.780	2.931
255.1	0.029524	0.065918	4.630	7.562
139.4	0.025916	0.091834	7.435	14.996
89.8	0.012045	0.103879	5.366	20.363
51.2	0.021247	0.125126	16.597	36.960
31.6	0.074003	0.199129	93.714	130.674
19.7	0.826089	1.025218	1681.416	1812.090

Table B.16 N_2 Sorption Data of MCM-41(III)

Relative Pressure (P/P_0)	Pressure (mmHg)	Volume Adsorbed (cc/g STP)
0.0609	42.303	218.2606
0.0781	54.249	229.7080
0.0998	69.283	241.7346
0.1195	82.997	251.7463
0.1399	97.121	261.0818
0.1605	111.389	269.8277
0.1968	136.528	285.2770
0.2513	174.228	308.2898
0.2999	207.837	333.4574
0.3433	237.811	417.8730
0.5846	404.887	530.4541
0.6583	455.966	535.5040
0.7477	517.874	540.7870
0.7976	552.389	544.2021
0.8412	582.569	547.3132
0.8753	606.157	549.9893
0.9017	624.407	554.2075
0.9318	645.284	557.7048
0.9525	659.584	561.1552
0.9547	661.068	562.0093
0.9693	671.147	565.3677
0.9811	679.323	569.8198
0.9842	681.490	571.6097
0.9847	681.811	572.5692
0.9883	684.288	574.6489
0.9955	689.257	580.5817
0.9960	689.511	582.6710
0.9763	675.910	578.3694
0.9586	663.664	572.3517
0.9354	647.596	565.9734
0.9052	626.682	559.5426
0.8370	579.467	551.0844
0.7246	501.630	542.6718
0.5416	374.980	530.4153
0.3519	243.629	507.3553
0.1374	95.104	260.5357

Table B.16 Continued (BJH Adsorption Pore Distribution)

Average Diameter (Å)	Incremental Pore Volume (cc/g)	Cumulative Pore Volume (cc/g)	Incremental Pore Area (m^2/g)	Cumulative Pore Area (m^2/g)
2011.1	0.009677	0.009677	0.192	0.192
1398.5	0.004987	0.014664	0.143	0.335
1127.0	0.002952	0.017616	0.105	0.440
756.0	0.007471	0.025087	0.395	0.835
507.9	0.005727	0.030815	0.451	1.286
433.8	0.001507	0.032322	0.139	1.425
339.4	0.006058	0.038380	0.714	2.139
237.9	0.006329	0.044708	1.064	3.203
182.6	0.008156	0.052864	1.787	4.990
144.5	0.005069	0.057933	1.403	6.394
114.0	0.006203	0.064136	2.177	8.571
91.0	0.007214	0.071350	3.169	11.740
68.6	0.011939	0.083290	6.967	18.707
54.2	0.012580	0.095869	9.276	27.984
33.5	0.390896	0.486765	466.860	494.843
26.1	0.423381	0.910146	649.053	1143.896
20.7	0.088119	0.998266	170.485	1314.381

Table B.16 Continued (BJH Desorption Pore Distribution)

Average Diameter (Å)	Incremental Pore Volume (cc/g)	Cumulative Pore Volume (cc/g)	Incremental Pore Area (m^2/g)	Cumulative Pore Area (m^2/g)
568.0	0.010419	0.010419	0.734	0.734
360.6	0.011276	0.021696	1.251	1.984
244.3	0.011649	0.033345	1.907	3.891
146.4	0.015909	0.049254	4.346	8.237
85.5	0.016561	0.065815	7.747	15.985
48.7	0.027099	0.092914	22.252	38.237
30.6	0.060441	0.153355	79.050	117.287
18.1	0.838082	0.991437	1848.404	1965.691

Table B.17 N_2 Sorption Data of MCM-41(IV)

Relative Pressure (P/P_0)	Pressure (mmHg)	Volume Adsorbed (cc/g STP)
0.0601	41.527	251.6213
0.0794	54.870	269.5260
0.0974	67.276	284.4630
0.1168	80.675	300.6594
0.1361	94.018	316.3301
0.1547	106.843	332.2144
0.1957	135.126	368.8206
0.2486	171.539	421.3115
0.3004	207.274	460.8995
0.3645	251.490	484.7643
0.4513	311.324	503.6163
0.5608	386.839	516.7349
0.6613	456.121	523.9078
0.7570	522.109	529.1091
0.7962	549.110	531.4931
0.8424	580.961	533.6726
0.8733	602.247	535.4746
0.9063	624.976	537.4060
0.9248	637.744	538.8187
0.9408	648.759	540.2388
0.9532	657.329	541.7175
0.9653	665.665	543.1369
0.9710	669.539	544.1165
0.9784	674.669	545.3317
0.9820	677.104	546.2153
0.9848	679.070	547.1131
0.9871	680.662	547.6878
0.9891	682.007	548.3757
0.9932	684.846	550.4069
0.9736	671.307	547.4017
0.9512	655.798	544.6080
0.9264	638.722	542.0887
0.9059	624.526	540.4929
0.8423	580.703	536.3626
0.7399	510.060	531.3437
0.5337	367.911	520.5395
0.3437	236.855	479.8199
0.1459	100.581	322.9615

Table B.17 Continued (BJH Adsorption Pore Distribution)

Average Diameter (Å)	Incremental Pore Volume (cc/g)	Cumulative Pore Volume (cc/g)	Incremental Pore Area (m^2/g)	Cumulative Pore Area (m^2/g)
1640.0	0.001137	0.001137	0.028	0.028
1240.1	0.002456	0.003592	0.079	0.107
991.2	0.001485	0.005077	0.060	0.167
769.7	0.002060	0.007137	0.107	0.274
623.6	0.001688	0.008825	0.108	0.382
484.4	0.002476	0.011301	0.204	0.587
378.4	0.002651	0.013953	0.280	0.867
300.7	0.002590	0.016542	0.344	1.211
241.9	0.002644	0.019186	0.437	1.649
185.3	0.003739	0.022925	0.807	2.456
146.8	0.003674	0.026599	1.001	3.457
115.9	0.004632	0.031231	1.598	5.055
95.4	0.005498	0.036729	2.305	7.360
71.9	0.013050	0.049779	7.261	14.621
54.4	0.020574	0.070353	15.141	29.762
42.5	0.044043	0.114396	41.475	71.237
35.1	0.072790	0.187187	82.945	154.182
28.6	0.295239	0.482426	413.202	567.385
22.8	0.568345	1.050770	998.442	1565.826

Table B.17 Continued (BJH Desorption Pore Distribution)

Average Diameter (Å)	Incremental Pore Volume (cc/g)	Cumulative Pore Volume (cc/g)	Incremental Pore Area (m^2/g)	Cumulative Pore Area (m^2/g)
490.8	0.004996	0.004996	0.407	0.407
320.3	0.004646	0.009642	0.580	0.987
242.6	0.003010	0.012652	0.496	1.484
156.0	0.008418	0.021070	2.158	3.642
95.6	0.011328	0.032398	4.738	8.380
53.1	0.030837	0.063235	23.228	31.609
35.1	0.157336	0.220571	179.158	210.767
23.6	0.834289	1.054860	1411.605	1622.372

Table B.18 N_2 Sorption Data of Cu-Imp(I)

Relative Pressure (P/P_0)	Volume Adsorbed (cc/g STP)
0.00505	134.9022
0.00753	146.1988
0.00997	155.2956
0.14988	171.4126
0.19916	189.5811
0.24913	203.8409
0.29921	235.4958
0.34931	313.2960
0.40096	318.3750
0.45159	321.5421
0.50376	324.4318
0.54926	326.7824
0.59915	329.3054
0.64906	331.7712
0.69908	334.3405
0.75287	337.3736
0.80168	340.4892
0.85021	344.3618
0.89984	350.4561
0.94921	365.2124
0.99457	680.5536
0.95086	380.8252
0.90093	353.6804
0.84981	345.9129
0.79885	341.4916
0.75097	338.3270
0.70030	335.4690
0.64979	332.8607
0.59961	330.3325
0.54972	327.7928
0.49973	325.1922
0.44712	321.8158
0.40032	318.9293
0.34927	314.8165
0.30096	251.6382
0.25080	206.9843
0.20086	188.8092
0.15008	172.6929
0.10014	156.5021
0.04999	135.7817

Table B.18 Continued (BJH Adsorption Pore Distribution)

Average Diameter (Å)	Cumulative Pore Volume (cc/g)	Cumulative Pore Area (m^2/g)
13.61	0.0113	33.34
14.99	0.0197	55.54
16.88	0.0357	93.51
19.35	0.0563	136.20
21.83	0.0903	198.30
24.47	0.1903	361.90
27.33	0.4855	793.80
30.56	0.5003	813.20
34.23	0.5082	822.40
38.50	0.5148	829.30
43.24	0.5199	834.00
48.85	0.5250	838.20
56.05	0.5297	841.50
65.29	0.5343	844.40
78.32	0.5395	847.00
96.62	0.5445	849.10
123.97	0.5505	851.00
174.10	0.5602	853.20
302.57	0.5846	856.50
1973.12	1.0890	866.70

Table B.18 Continued (BJH Desorption Pore Distribution)

Average Diameter (Å)	Cumulative Pore Volume (cc/g)	Cumulative Pore Area (m^2/g)
14.25	0.017740	49.81
16.90	0.033230	86.52
19.39	0.055980	133.50
21.92	0.093560	202.10
24.57	0.250500	457.90
27.38	0.489500	807.20
30.54	0.500600	821.70
34.02	0.507500	829.80
38.12	0.515500	838.30
43.08	0.520900	843.30
48.91	0.525900	847.30
56.15	0.530400	850.60
65.50	0.534800	853.30
78.14	0.539300	855.60
95.55	0.544100	857.60
123.04	0.550800	859.70
175.01	0.563300	862.60
310.05	0.610600	868.70
1979.50	1.089000	878.40

Table B.19 N_2 Sorption Data of Cu-Imp(II)

Relative Pressure (P/P_0)	Pressure (mmHg)	Volume Adsorbed (cc/g STP)
0.0611	42.975	120.8299
0.0831	58.386	129.3334
0.0995	69.919	134.9420
0.1191	83.623	141.2665
0.1389	97.534	147.4136
0.1582	111.084	153.7059
0.1942	136.290	166.0730
0.2443	171.384	196.6582
0.3068	215.010	245.3939
0.3488	244.405	250.3128
0.4610	323.002	255.7939
0.5647	395.568	259.7121
0.6510	455.966	262.7227
0.7422	519.839	266.1000
0.8035	562.695	268.5565
0.8431	590.378	270.6626
0.8798	615.977	272.7214
0.9083	635.893	274.9265
0.9296	650.766	277.0829
0.9445	661.119	279.1386
0.9572	669.963	281.7806
0.9650	675.388	283.5706
0.9708	679.483	285.1837
0.9768	683.662	287.2368
0.9818	687.189	289.4814
0.9847	689.206	290.5734
0.9849	689.356	291.3781
0.9891	692.252	292.9450
0.9956	696.860	302.4792
0.9783	684.748	296.3373
0.9665	676.479	291.5323
0.9520	666.348	287.4452
0.9427	659.775	284.4970
0.9053	633.607	278.2266
0.8230	576.059	271.5911
0.7283	509.755	267.3205
0.5372	375.963	260.3040
0.3326	232.769	249.9647
0.1344	94.070	147.6197

Table B.19 Continued (BJH Adsorption Pore Distribution)

Average Diameter (Å)	Incremental Pore Volume (cc/g)	Cumulative Pore Volume (cc/g)	Incremental Pore Area (m^2/g)	Cumulative Pore Area (m^2/g)
1469.4	0.002592	0.002592	0.071	0.071
1173.6	0.003166	0.005758	0.108	0.178
941.2	0.003770	0.009528	0.160	0.339
748.5	0.003477	0.013005	0.186	0.524
616.5	0.002754	0.015759	0.179	0.703
510.1	0.003087	0.018846	0.242	0.945
403.6	0.004647	0.023493	0.461	1.406
318.4	0.003646	0.027139	0.458	1.864
248.4	0.003892	0.031031	0.627	2.491
191.3	0.004087	0.035118	0.854	3.345
147.6	0.003911	0.039029	1.060	4.405
117.1	0.004227	0.043256	1.444	5.850
90.8	0.005103	0.048360	2.249	8.098
67.4	0.007682	0.056041	4.559	12.657
52.4	0.007386	0.063427	5.644	18.301
41.3	0.010695	0.074122	10.363	28.664
32.6	0.017181	0.091303	21.059	49.723
26.3	0.229814	0.321117	350.145	399.869
20.9	0.208016	0.529133	398.049	797.918

Table B.19 Continued (BJH Desorption Pore Distribution)

Average Diameter (Å)	Incremental Pore Volume (cc/g)	Cumulative Pore Volume (cc/g)	Incremental Pore Area (m^2/g)	Cumulative Pore Area (m^2/g)
688.3	0.008270	0.008270	0.481	0.481
476.6	0.007136	0.015405	0.599	1.079
379.7	0.005244	0.020649	0.552	1.632
251.7	0.011443	0.032092	1.818	3.450
137.9	0.012750	0.044842	3.698	7.148
87.6	0.008422	0.053264	3.843	10.992
50.3	0.016261	0.069525	12.934	23.925
31.4	0.029656	0.099181	37.743	61.669
20.0	0.432588	0.531769	867.057	928.726

Table B.20 N_2 Sorption Data of Cu-HT(I)

Relative Pressure (P/P_0)	Volume Adsorbed (cc/g STP)
0.051080	70.9654
0.102640	82.6204
0.152040	91.7299
0.201240	100.6321
0.299910	127.4763
0.401080	149.5486
0.500030	153.2714
0.601130	156.8343
0.699450	160.6186
0.801020	165.7971
0.994460	340.6843
0.799510	170.3829
0.700890	164.4671
0.599340	160.2514
0.498890	156.6586
0.398280	150.7986
0.299890	131.4560
0.097878	83.8237

Table B.20 Continued (BJH Adsorption Pore Distribution)

Average Diameter (Å)	Cumulative Pore Volume (cc/g)	Cumulative Pore Area (m^2/g)
13.67	0.0111	32.40
15.11	0.0199	55.85
19.45	0.0382	98.89
21.91	0.0596	142.90
29.09	0.0849	189.00
36.38	0.1480	292.00
46.40	0.2228	394.80
61.47	0.2314	404.30
88.69	0.2388	410.70
157.96	0.2462	415.50
1843.22	0.2559	419.80

Table B.20 Continued (BJH Desorption Pore Distribution)

Average Diameter (Å)	Cumulative Pore Volume (cc/g)	Cumulative Pore Area (m^2/g)
18.02	0.0372	82.61
28.99	0.1376	255.80
36.23	0.2018	344.30
46.22	0.2169	361.00
61.51	0.2241	367.20
157.58	0.2321	372.40
1843.24	0.2432	377.50

Table B.21 N_2 Sorption Data of Cu-HT(II)

Relative Pressure (P/P_0)	Pressure (mmHg)	Volume Adsorbed (cc/g STP)
0.0581	40.751	73.5749
0.0840	58.903	81.0411
0.0991	69.453	85.1019
0.1182	82.842	90.1616
0.1378	96.552	95.2789
0.1574	110.308	100.4172
0.1964	137.614	109.8714
0.2502	175.257	119.8878
0.3062	214.462	127.8506
0.3609	252.726	134.7851
0.4496	314.789	145.2735
0.5490	384.341	157.2594
0.6490	454.321	170.8152
0.7419	519.239	184.4963
0.8030	561.971	193.6266
0.8415	588.817	199.6383
0.8772	613.748	205.2612
0.9061	633.912	210.4575
0.9265	648.144	215.1876
0.9431	659.723	219.4091
0.9544	667.532	223.3807
0.9679	676.944	228.1212
0.9730	680.404	230.3539
0.9808	685.803	233.4510
0.9839	687.965	235.0691
0.9877	690.602	236.4529
0.9963	696.580	242.9282
0.9968	696.932	248.0071
0.9852	688.787	239.5700
0.9655	674.933	236.6272
0.9340	652.881	230.8242
0.9051	632.681	224.2822
0.8424	588.801	213.2692
0.7386	516.250	201.2107
0.5464	381.910	178.3163
0.3374	235.820	132.0240
0.1395	97.529	95.4781

Table B.21 Continued (BJH Adsorption Pore Distribution)

Average Diameter (Å)	Incremental Pore Volume (cc/g)	Cumulative Pore Volume (cc/g)	Incremental Pore Area (m^2/g)	Cumulative Pore Area (m^2/g)
1423.5	0.013049	0.013049	0.367	0.367
1108.8	0.002675	0.015724	0.096	0.463
834.7	0.005190	0.020914	0.249	0.712
671.4	0.003814	0.024728	0.227	0.939
503.3	0.008262	0.032990	0.657	1.596
391.8	0.007103	0.040093	0.725	2.321
309.2	0.007673	0.047766	0.993	3.314
243.4	0.008882	0.056648	1.460	4.773
189.3	0.010055	0.066702	2.124	6.898
147.6	0.011384	0.078086	3.085	9.983
118.5	0.012869	0.090955	4.346	14.328
92.6	0.020930	0.111885	9.042	23.370
69.0	0.034655	0.146540	20.078	43.448
52.8	0.037513	0.184053	28.430	71.878
42.1	0.035540	0.219593	33.789	105.667
34.9	0.033503	0.253095	38.375	144.042
28.6	0.054483	0.307579	76.149	220.191
22.9	0.115529	0.423107	202.003	422.194

Table B.21 Continued (BJH Desorption Pore Distribution)

Average Diameter (Å)	Incremental Pore Volume (cc/g)	Cumulative Pore Volume (cc/g)	Incremental Pore Area (m^2/g)	Cumulative Pore Area (m^2/g)
693.8	0.005075	0.005075	0.293	0.293
365.6	0.010494	0.015568	1.148	1.441
246.5	0.012341	0.027909	2.003	3.443
154.2	0.022107	0.050016	5.736	9.180
93.5	0.026118	0.076135	11.177	20.356
52.8	0.059862	0.135997	45.308	65.664
33.1	0.153543	0.289540	185.395	251.059
21.6	0.118785	0.408325	220.426	471.485

Table B.22 N_2 Sorption Data of Cu-LT(I)

Relative Pressure (P/P_0)	Pressure (mmHg)	Volume Adsorbed (cc/g STP)
0.0577	39.924	23.1381
0.0879	60.817	26.6978
0.0995	68.827	27.9733
0.1191	82.377	29.9734
0.1393	96.304	31.7904
0.1592	110.050	33.5746
0.1997	138.027	36.4600
0.2514	173.814	39.5846
0.3028	209.285	42.4081
0.3543	244.865	45.1258
0.4490	310.290	49.9104
0.5494	379.640	55.2715
0.6495	448.798	61.4420
0.7389	510.525	68.6893
0.8009	553.299	75.5593
0.8400	580.263	82.3512
0.8756	604.807	91.4292
0.9054	625.312	102.6573
0.9264	639.714	114.4298
0.9423	650.559	126.8525
0.9553	659.418	139.8282
0.9662	666.906	152.3461
0.9710	670.170	159.3389
0.9773	674.508	169.6920
0.9824	678.030	178.3315
0.9829	678.397	181.7009
0.9944	686.320	187.6102
0.9947	686.517	195.8259
0.9741	672.285	192.4166
0.9589	661.849	186.2677
0.9452	652.369	176.0524
0.9046	624.324	142.6717
0.8408	580.341	106.5324
0.7327	505.669	82.4471
0.5518	380.829	67.8704
0.3474	239.792	49.7999
0.1313	90.641	36.8986

Table B.22 Continued (BJH Adsorption Pore Distribution)

Average Diameter (Å)	Incremental Pore Volume (cc/g)	Cumulative Pore Volume (cc/g)	Incremental Pore Area (m^2/g)	Cumulative Pore Area (m^2/g)
1332.2	0.015399	0.015399	0.462	0.462
964.1	0.014524	0.029923	0.603	1.065
756.7	0.017606	0.047529	0.931	1.996
632.1	0.011990	0.059519	0.759	2.754
501.2	0.021727	0.081246	1.734	4.489
388.1	0.022963	0.104209	2.367	6.855
305.5	0.022355	0.126564	2.927	9.783
240.1	0.021500	0.148064	3.582	13.365
185.2	0.020808	0.168872	4.493	17.858
144.1	0.017037	0.185909	4.730	22.589
115.2	0.012781	0.198690	4.439	27.027
89.5	0.012813	0.211503	5.727	32.754
66.9	0.014134	0.225637	8.457	41.211
50.8	0.012534	0.238171	9.878	51.089
40.0	0.011623	0.249794	11.631	62.720
32.5	0.011126	0.260921	13.680	76.401
26.5	0.014429	0.275350	21.782	98.183
20.9	0.024339	0.299689	46.634	144.816

Table B.22 Continued (BJH Desorption Pore Distribution)

Average Diameter (Å)	Incremental Pore Volume (cc/g)	Cumulative Pore Volume (cc/g)	Incremental Pore Area (m^2/g)	Cumulative Pore Area (m^2/g)
566.6	0.010757	0.010757	0.759	0.759
411.5	0.018302	0.029059	1.779	2.539
252.2	0.062844	0.091903	9.968	12.507
152.0	0.716020	0.163505	18.843	31.349
90.7	0.048072	0.211577	21.191	52.540
52.6	0.026125	0.237702	19.855	72.395
33.0	0.044750	0.282452	54.236	126.631
20.4	0.023873	0.306325	46.792	173.423

Table B.23 N_2 Sorption Data of Cu-LT(II)

Relative Pressure (P/P_0)	Pressure (mmHg)	Volume Adsorbed (cc/g STP)
0.0581	40.027	132.2080
0.0773	53.261	140.4977
0.0992	68.362	148.4651
0.1191	82.072	155.0062
0.1395	96.086	161.0244
0.1596	109.931	166.7637
0.1969	135.648	176.6886
0.2524	173.814	190.9858
0.3046	209.704	205.0008
0.3536	243.417	220.8378
0.4505	310.031	257.6810
0.5626	387.190	297.6599
0.6452	444.087	335.4595
0.7381	508.074	396.7620
0.7989	549.937	456.4626
0.8405	578.691	515.8816
0.8716	600.101	578.0209
0.9028	621.832	661.7502
0.9174	632.035	705.8564
0.9345	644.007	747.3854
0.9500	654.810	776.6026
0.9571	659.832	789.0206
0.9660	666.032	801.5262
0.9723	670.464	819.4543
0.9817	676.991	827.2866
0.9887	681.904	831.3764
0.9935	685.229	835.9843
0.9948	686.217	839.1736
0.9792	675.450	835.1030
0.9691	668.520	831.3520
0.9590	661.595	826.7202
0.9424	650.202	818.9410
0.9086	626.941	799.5978
0.8451	583.242	735.0515
0.7378	509.444	491.4977
0.5352	369.571	370.0070
0.3587	247.710	283.9286
0.3260	225.167	272.5699

Table B.23 Continued (BJH Adsorption Pore Distribution)

Average Diameter (Å)	Incremental Pore Volume (cc/g)	Cumulative Pore Volume (cc/g)	Incremental Pore Area (m^2/g)	Cumulative Pore Area (m^2/g)
2047.6	0.007510	0.007510	0.147	0.147
1255.3	0.006740	0.014251	0.215	0.362
825.0	0.013226	0.027477	0.641	1.003
639.0	0.031017	0.058494	1.941	2.944
514.2	0.021670	0.080164	1.686	4.630
430.6	0.021922	0.102086	2.036	6.666
344.0	0.052730	0.154816	6.131	12.797
271.4	0.077173	0.231989	11.376	24.173
226.3	0.084037	0.316026	14.854	39.026
179.1	0.163766	0.479791	36.579	75.606
142.3	0.123527	0.603318	34.715	110.320
113.9	0.119733	0.723051	42.064	152.384
88.4	0.122129	0.845180	55.275	207.659
65.5	0.127857	0.973036	78.093	285.752
51.1	0.077160	1.050197	60.391	346.143
39.7	0.082259	1.132456	82.789	428.932
31.9	0.086987	1.219443	109.227	538.159
25.8	0.060281	1.279724	93.293	631.452
20.2	0.047134	1.326858	93.264	724.716

Table B.23 Continued (BJH Desorption Pore Distribution)

Average Diameter (Å)	Incremental Pore Volume (cc/g)	Cumulative Pore Volume (cc/g)	Incremental Pore Area (m^2/g)	Cumulative Pore Area (m^2/g)
740.2	0.006453	0.006453	0.349	0.349
546.3	0.008107	0.014560	0.594	0.942
398.4	0.013950	0.028509	1.401	2.343
260.6	0.036427	0.064936	5.590	7.933
157.4	0.132511	0.197448	33.684	41.617
93.6	0.566249	0.763697	241.985	283.603
51.7	0.269594	1.033291	208.620	492.222
34.5	0.211538	1.244829	245.469	737.692
29.5	0.020566	1.265395	27.849	765.541

Table B.24 N_2 Sorption Data of Ni-HT(I)

Relative Pressure (P/P_0)	Pressure (mmHg)	Volume Adsorbed (cc/g STP)
0.0620	43.172	108.8545
0.0827	57.605	115.8532
0.0990	68.977	120.9582
0.1188	82.744	126.6409
0.1382	96.288	132.2350
0.1577	109.843	137.8791
0.1944	135.390	148.4363
0.2444	170.246	163.5023
0.2937	204.595	179.8286
0.3506	244.250	199.8400
0.4817	335.579	217.7374
0.5543	386.171	223.9504
0.6604	460.057	233.8383
0.7380	514.094	242.7015
0.7989	556.614	251.7895
0.8406	585.719	259.6987
0.8751	609.880	267.6575
0.9026	629.108	276.5684
0.9240	644.121	286.3588
0.9408	655.901	295.5955
0.9515	663.452	303.6570
0.9630	671.566	314.6144
0.9703	676.737	323.3002
0.9758	680.621	331.5161
0.9892	690.002	337.2416
0.9900	690.545	346.6374
0.9807	684.127	340.1983
0.9648	673.019	336.5063
0.9541	665.619	331.8718
0.9414	656.832	323.7912
0.8999	628.079	298.0047
0.8286	578.463	269.7023
0.7416	517.874	253.0416
0.5401	377.209	231.3095
0.3477	242.854	201.1764
0.1353	94.483	131.6338

Table B.24 Continued (BJH Adsorption Pore Distribution)

Average Diameter (Å)	Incremental Pore Volume (cc/g)	Cumulative Pore Volume (cc/g)	Incremental Pore Area (m^2/g)	Cumulative Pore Area (m^2/g)
984.7	0.009683	0.009683	0.393	0.393
732.3	0.014170	0.023853	0.774	1.167
594.2	0.015126	0.038979	1.018	2.186
463.9	0.019375	0.058354	1.671	3.856
373.8	0.014448	0.072802	1.546	5.402
298.4	0.016809	0.089611	2.253	7.655
234.7	0.018308	0.107919	3.120	10.755
184.8	0.016997	0.124915	3.679	14.454
145.9	0.015506	0.140421	4.252	18.706
116.2	0.016080	0.156501	5.537	24.244
90.6	0.019394	0.175895	8.560	32.804
70.0	0.019909	0.195804	11.370	44.174
53.2	0.024066	0.219870	18.078	62.251
43.8	0.016162	0.236032	14.775	77.026
34.6	0.060476	0.296508	69.934	146.960
27.8	0.158819	0.455327	228.744	375.704
22.4	0.132741	0.588068	237.380	613.084

Table B.24 Continued (BJH Desorption Pore Distribution)

Average Diameter (Å)	Incremental Pore Volume (cc/g)	Cumulative Pore Volume (cc/g)	Incremental Pore Area (m^2/g)	Cumulative Pore Area (m^2/g)
671.4	0.006377	0.006377	0.380	0.380
485.8	0.008182	0.014559	0.674	1.054
380.6	0.014589	0.029147	1.533	2.587
240.4	0.048884	0.078031	8.133	10.719
142.1	0.056779	0.134811	15.985	26.705
92.9	0.033654	0.168464	14.496	41.201
51.7	0.048934	0.217398	37.854	79.055
33.3	0.088930	0.306329	106.934	185.989
21.0	0.280021	0.586350	534.248	720.237

Table B.25 N_2 Sorption Data of Ni-HT(II)

Relative Pressure (P/P_0)	Pressure (mmHg)	Volume Adsorbed (cc/g STP)
0.0573	39.614	171.0447
0.0824	56.918	186.1052
0.0989	68.310	194.8497
0.1183	81.658	204.4052
0.1378	95.099	213.7955
0.1574	108.602	223.1181
0.2041	140.768	246.5204
0.2522	173.866	273.9011
0.2938	202.444	305.7901
0.3468	238.975	350.6137
0.4918	338.837	372.4891
0.5563	383.229	378.1429
0.6612	455.506	386.9330
0.7374	507.997	394.2240
0.7995	550.708	401.4791
0.8397	578.375	407.8914
0.8748	602.588	415.5363
0.9038	622.483	424.9059
0.9252	637.227	435.2154
0.9413	648.242	445.7616
0.9539	656.879	456.7405
0.9640	663.814	469.0140
0.9718	669.135	480.2787
0.9778	673.283	490.5661
0.9822	676.272	499.0657
0.9839	677.466	503.6953
0.9859	678.858	510.7042
0.9892	681.133	519.6069
0.9923	683.346	530.3144
0.9787	673.924	525.1478
0.9715	669.027	519.2567
0.9629	663.079	511.6745
0.9437	649.892	488.8043
0.8919	614.297	442.4172
0.8351	575.221	416.3506
0.7269	500.736	396.8193
0.5562	383.151	380.6087
0.3457	238.179	353.5422
0.1427	98.310	217.0848

Table B.25 Continued (BJH Adsorption Pore Distribution)

Average Diameter (Å)	Incremental Pore Volume (cc/g)	Cumulative Pore Volume (cc/g)	Incremental Pore Area (m^2/g)	Cumulative Pore Area (m^2/g)
1544.3	0.014712	0.014712	0.381	0.381
1215.6	0.019386	0.034098	0.638	1.019
977.0	0.014216	0.048314	0.582	1.601
777.1	0.017390	0.065704	0.895	2.496
613.0	0.019290	0.084994	1.259	3.755
482.2	0.021340	0.106334	1.770	5.525
380.7	0.019314	0.125648	2.029	7.555
301.2	0.018849	0.144497	2.503	10.058
236.7	0.018751	0.163248	3.169	13.227
184.1	0.017280	0.180529	3.755	16.981
144.2	0.014251	0.194780	3.954	20.936
115.1	0.012186	0.206966	4.234	25.169
89.5	0.014222	0.221188	6.355	31.524
69.1	0.015259	0.236447	8.835	40.359
52.4	0.020256	0.256702	15.456	55.815
43.4	0.014390	0.271093	13.261	69.076
33.5	0.071679	0.342771	85.551	154.626
27.0	0.330368	0.673140	489.923	644.549
21.4	0.235210	0.908350	439.904	1084.453

Table B.25 Continued (BJH Desorption Pore Distribution)

Average Diameter (Å)	Incremental Pore Volume (cc/g)	Cumulative Pore Volume (cc/g)	Incremental Pore Area (m^2/g)	Cumulative Pore Area (m^2/g)
779.6	0.010079	0.010079	0.517	0.517
597.4	0.013136	0.023215	0.880	1.397
412.7	0.040808	0.064023	3.955	5.352
225.1	0.087768	0.151791	15.596	20.948
144.7	0.050059	0.201851	13.837	34.785
88.6	0.036949	0.238800	16.686	51.471
53.0	0.031518	0.270318	23.800	75.271
32.8	0.074092	0.344410	90.219	165.490
20.9	0.572394	0.916803	1096.957	1262.447

Table B.26 N_2 Sorption Data of Ni-Imp(I)

Relative Pressure (P/P_0)	Pressure (mmHg)	Volume Adsorbed (cc/g STP)
0.0595	41.574	222.9397
0.0781	54.508	237.2182
0.0997	69.551	250.8617
0.1188	82.899	262.4347
0.1388	96.810	273.6031
0.1593	111.084	284.1267
0.1961	136.678	303.1659
0.2477	172.573	331.2125
0.2940	204.791	362.5294
0.3474	241.819	425.9056
0.4713	328.080	541.6578
0.5531	385.018	596.3774
0.6494	452.087	665.5525
0.7396	514.869	735.2752
0.8072	561.982	782.7491
0.8413	585.693	799.8655
0.8708	606.250	812.0263
0.9058	630.659	822.2783
0.9203	640.697	826.0476
0.9400	654.448	830.3437
0.9510	662.102	833.1711
0.9642	671.312	836.6638
0.9707	675.806	838.4742
0.9759	679.489	840.6536
0.9830	684.443	843.3041
0.9827	684.215	844.0232
0.9949	692.754	850.1935
0.9955	693.286	858.9395
0.9818	683.714	849.9347
0.9665	673.102	844.3924
0.9517	662.872	839.7358
0.9398	654.552	836.5126
0.9045	629.992	829.5714
0.8427	587.017	819.7928
0.7307	509.088	797.0579
0.5520	384.656	720.7115
0.3559	248.185	450.4016
0.1400	97.633	274.2692

Table B.26 Continued (BJH Adsorption Pore Distribution)

Average Diameter (Å)	Incremental Pore Volume (cc/g)	Cumulative Pore Volume (cc/g)	Incremental Pore Area (m^2/g)	Cumulative Pore Area (m^2/g)
1375.5	0.011386	0.011386	0.331	0.331
933.6	0.004330	0.015766	0.188	0.519
735.2	0.003661	0.019427	0.199	0.718
605.2	0.003049	0.022476	0.201	0.919
460.8	0.006012	0.028488	0.522	1.441
365.7	0.004965	0.033453	0.543	1.984
284.1	0.007701	0.041153	1.084	3.069
232.6	0.006972	0.048126	1.199	4.268
178.6	0.019725	0.067850	4.417	8.684
141.3	0.024466	0.092316	6.926	15.610
116.1	0.035692	0.128008	12.295	27.905
88.5	0.105175	0.233183	47.510	75.415
65.0	0.163857	0.397039	100.809	176.225
49.2	0.169306	0.566346	137.566	313.790
39.6	0.137259	0.703604	138.660	452.450
30.8	0.328820	1.032425	427.499	879.949
24.4	0.269578	1.302003	442.423	1322.372
18.9	0.084059	1.386062	177.457	1499.829

Table B.26 Continued (BJH Desorption Pore Distribution)

Average Diameter (Å)	Incremental Pore Volume (cc/g)	Cumulative Pore Volume (cc/g)	Incremental Pore Area (m^2/g)	Cumulative Pore Area (m^2/g)
701.9	0.009448	0.009448	0.538	0.538
471.7	0.008049	0.017496	0.682	1.221
364.8	0.005636	0.023133	0.618	1.839
245.6	0.012482	0.035614	2.033	3.872
150.5	0.018467	0.054081	4.909	8.780
87.2	0.047376	0.101458	21.720	30.500
49.6	0.181735	0.283193	146.529	177.029
30.5	0.734346	1.017538	962.618	1139.648
17.9	0.361710	1.379248	810.254	1949.902

Table B.27 Summary of N_2 Sorption Data

	MCM-41 (I)	MCM-41 (II)	MCM-41 (III)	MCM-41 (IV)	Cu-Imp (I)	Cu-Imp (II)	Cu-HT (I)	Cu-HT (II)	Cu-LT (I)	Cu-LT (II)	Ni-HT (I)	Ni-HT (II)	Ni-Imp (I)
AREA													
BET Surface Area m^2/g	1207.80	1096.86	1042.65	1445.30	728.50	630.91	396.00	433.55	145.17	649.57	562.33	928.85	1129.54
Single Point Surface Area (P/P0 0.2010) m^2/g	1119.46	1043.72	997.42	1291.32	-	582.56	-	384.33	127.03	617.68	520.57	854.12	1060.98
BJH Cumulative Ads. Sur. Area m^2/g (Pores Between 17 and 3000 A Diameter)	1561.04	1452.06	1314.38	1565.83	866.70	797.92	430.20	422.19	144.82	724.72	613.08	1084.45	1499.83
BJH Cumulative Des. Surface Area m^2/g (Pores Between 17 and 3000 A Diameter)	1790.23	1812.09	1965.69	1622.37	878.40	928.73	389.60	471.49	173.42	765.54	720.24	1262.45	1949.90
VOLUME													
Single Point Total Pore Volume cc/g (Pores < 1382.3854 A Diameter at P/P0 0.9858)	1.02	0.89	0.89	0.85	-	0.45	-	0.37	0.28	1.29	0.52	0.78	1.31
BJH Cumulative Ads. Pore Volume cc/g (Pores Between 17 and 3000 A Diameter)	1.17	1.02	1.00	1.05	1.09	0.53	0.54	0.42	0.30	1.33	0.59	0.91	1.39
BJH Cumulative Des. Pore Volume cc/g (Pores Between 17 and 3000 A Diameter)	1.17	1.03	0.99	1.05	1.09	0.53	0.52	0.41	0.31	1.27	0.59	0.92	1.38
PORE SIZE													
Average Pore Diameter Å (4V/A by BET)	33.84	32.50	33.98	23.42	-	28.50	-	33.74	77.44	79.19	37.11	33.55	46.23
BJH Adsorption Pore Diameter Å (4V/A)	30.09	28.21	30.38	26.84	27.33	26.53	24.51	40.09	82.78	73.23	38.37	33.50	36.97
BJH Desorption Pore Diameter Å (4V/A)	26.21	22.63	20.17	26.01	27.38	22.90	23.19	34.64	70.65	66.12	32.56	29.05	28.29

B.4 Scanning Electron Microscopy

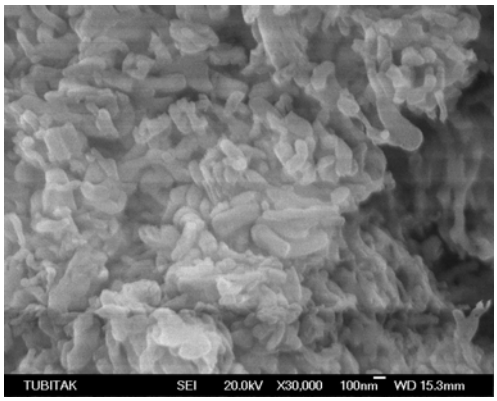

Figure B.4 SEM of MCM-41(I)

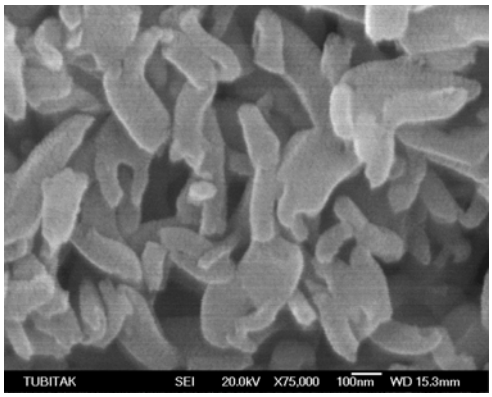

Figure B.5 SEM of MCM-41(I)

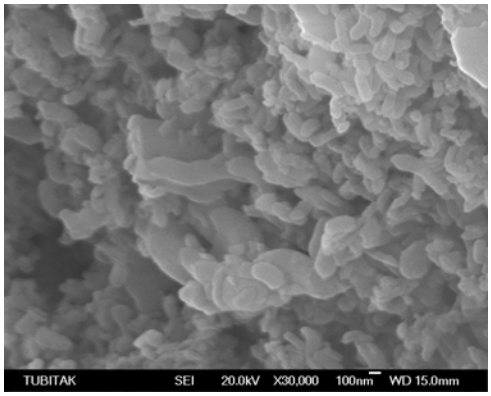

Figure B.6 SEM of Cu-Imp(I)

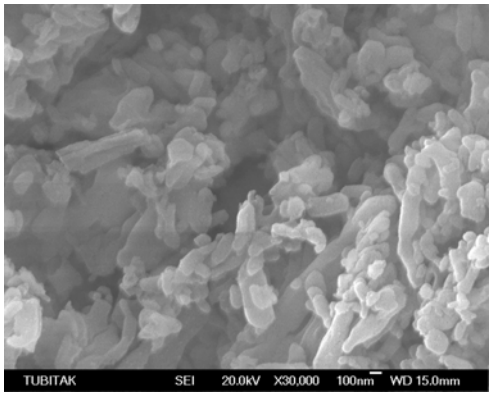

Figure B.7 SEM of Cu-Imp(I)

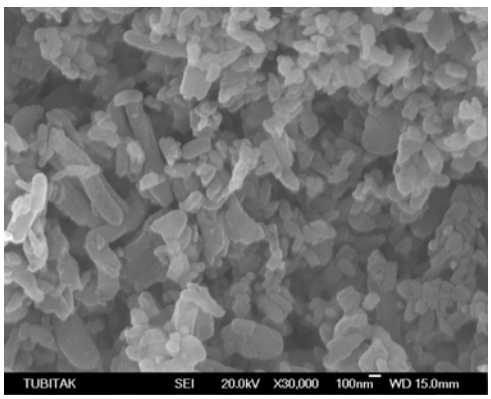

Figure B.8 SEM of Cu-Imp(I)

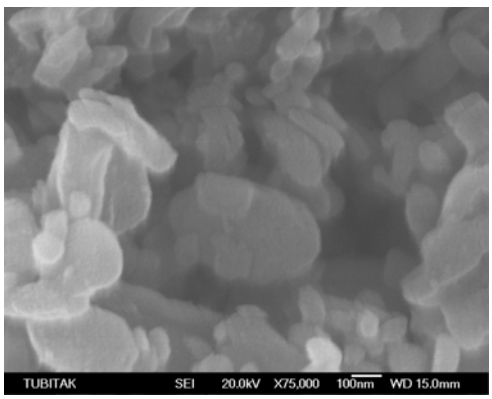

Figure B.9 SEM of Cu-Imp(I)

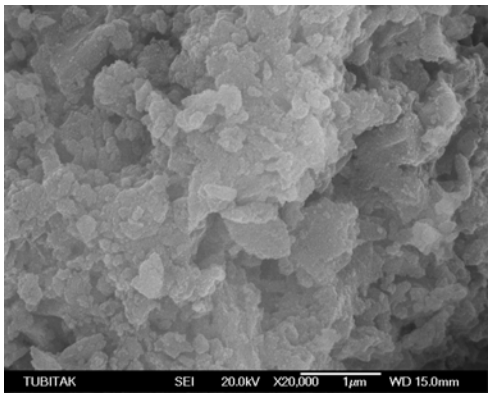

Figure B.10 SEM of Cu-HT(I)

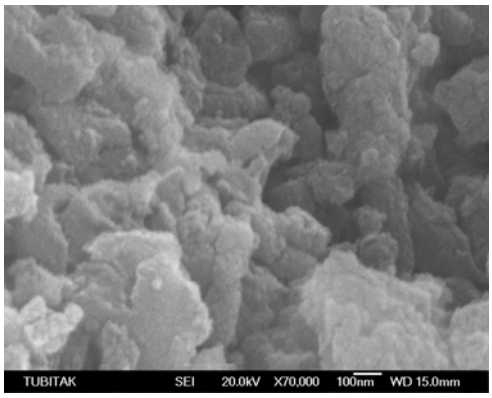

Figure B.11 SEM of Cu-HT(I)

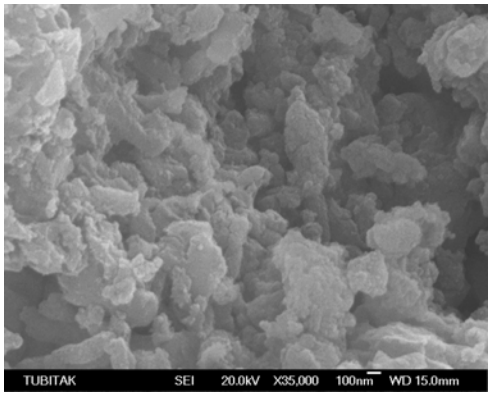

Figure B.12 SEM of Cu-LT(I)

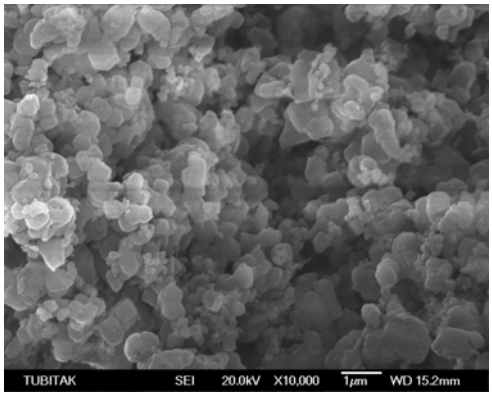

Figure B.13 SEM of Cu-LT(I)

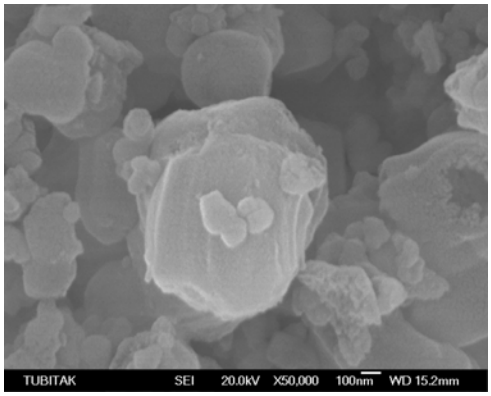

Figure B.14 SEM of Cu-LT(I)

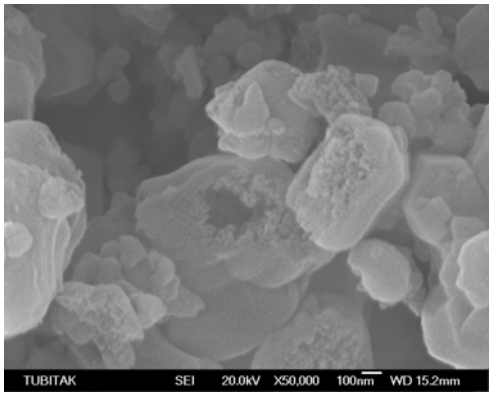

Figure B.15 SEM of Cu-LT(I)

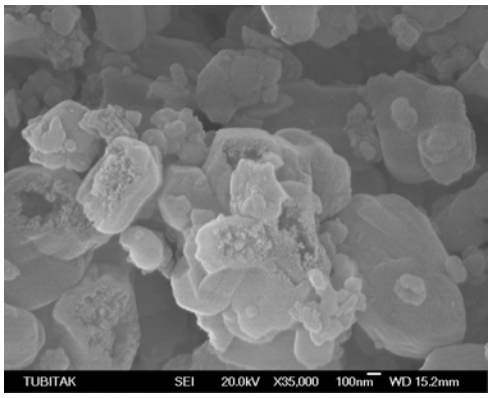

Figure B.16 SEM of Cu-LT(I)

B.5 X-ray Fluorescence

Table B.28 XRF analyses of Cu-MCM-41 type catalytic materials

Sample ID	CuO wt%	SiO_2 wt%	Cu (mol)	Si (mol)	Cu/Si mol ratio
Cu-Imp(I)	17.754	80.207	0.223	1.337	0.167
Cu-Imp(II)	19.100	79.190	0.240	1.320	0.182
Cu-HT(I)	22.651	76.924	0.285	1.282	0.222
Cu-HT(II)	23.600	72.400	0.297	1.207	0.246
Cu-LT(I)	0.519	98.988	0.007	1.650	0.004
Cu-LT(II)	5.100	87.880	0.064	1.465	0.044

Table B.29 XRF analyses of Ni-MCM-41 type catalytic materials

Sample ID	NiO wt%	SiO_2 wt%	Ni (mol)	Si (mol)	Ni/Si mol ratio
Ni-HT(I)	22.100	76.500	0.277	1.275	0.218
Ni-HT(II)	11.500	84.800	0.144	1.413	0.102
Ni-Imp(I)	6.100	90.800	0.077	1.513	0.051

B.6 Energy Dispersive Spectroscopy

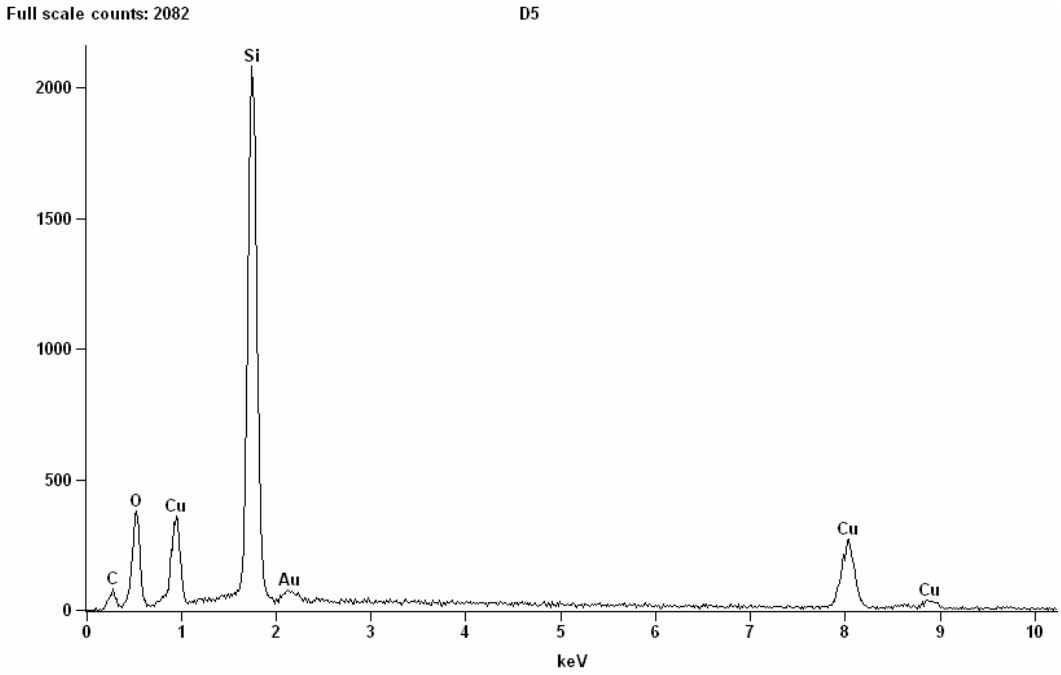

Figure B.17 EDS of Cu-Imp(I)

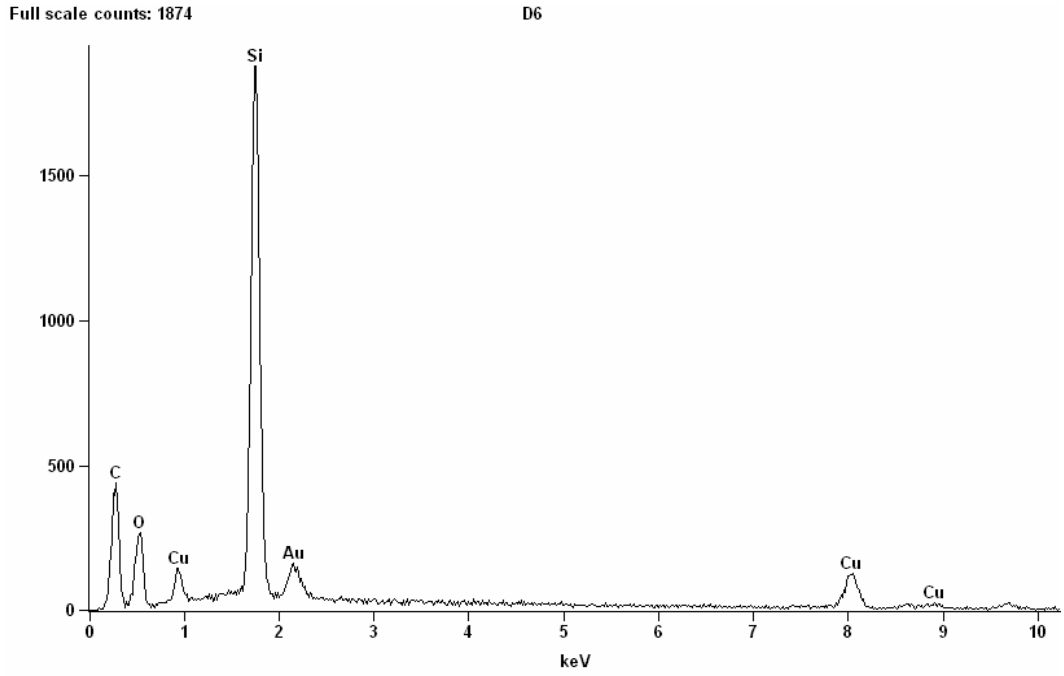

Figure B.18 EDS of Cu-Imp(II)

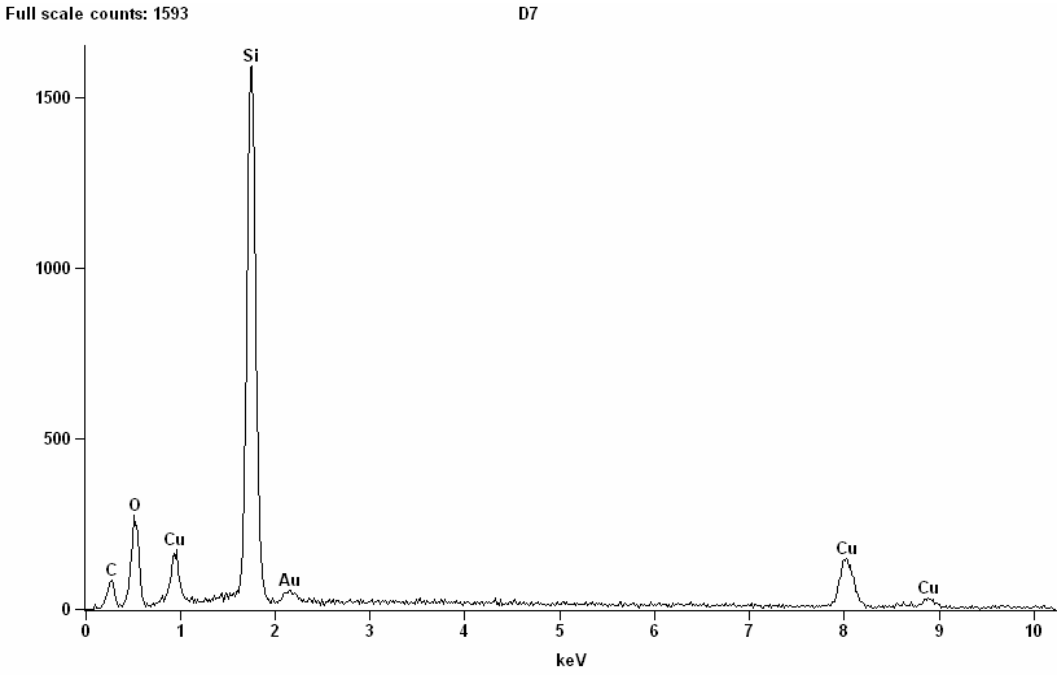

Figure B.19 EDS of Cu-HT(I)

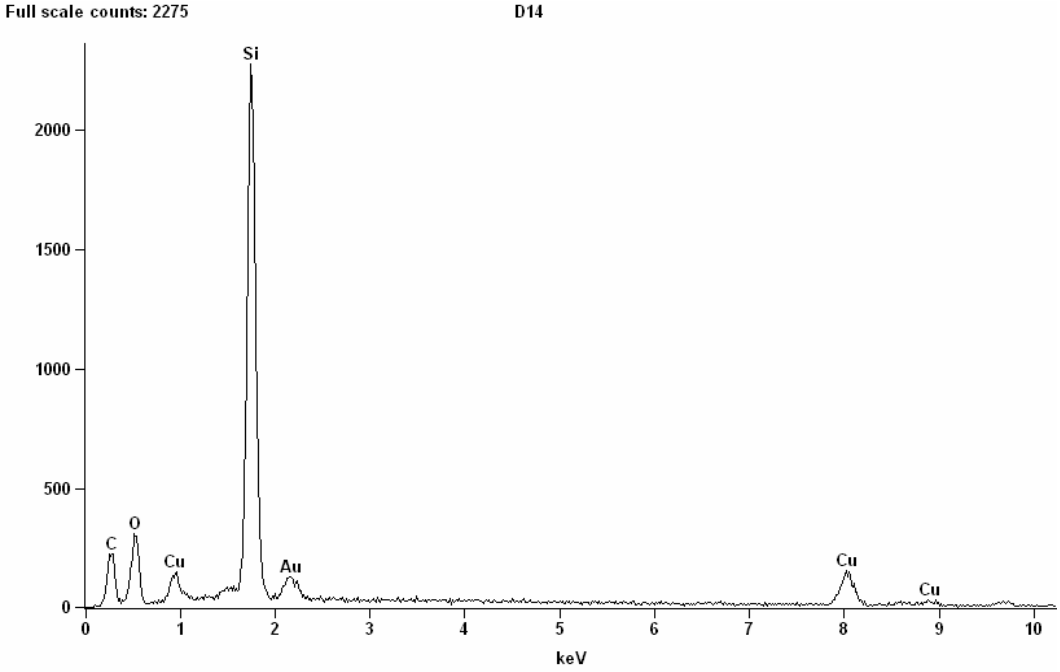

Figure B.20 EDS of Cu-HT(II)

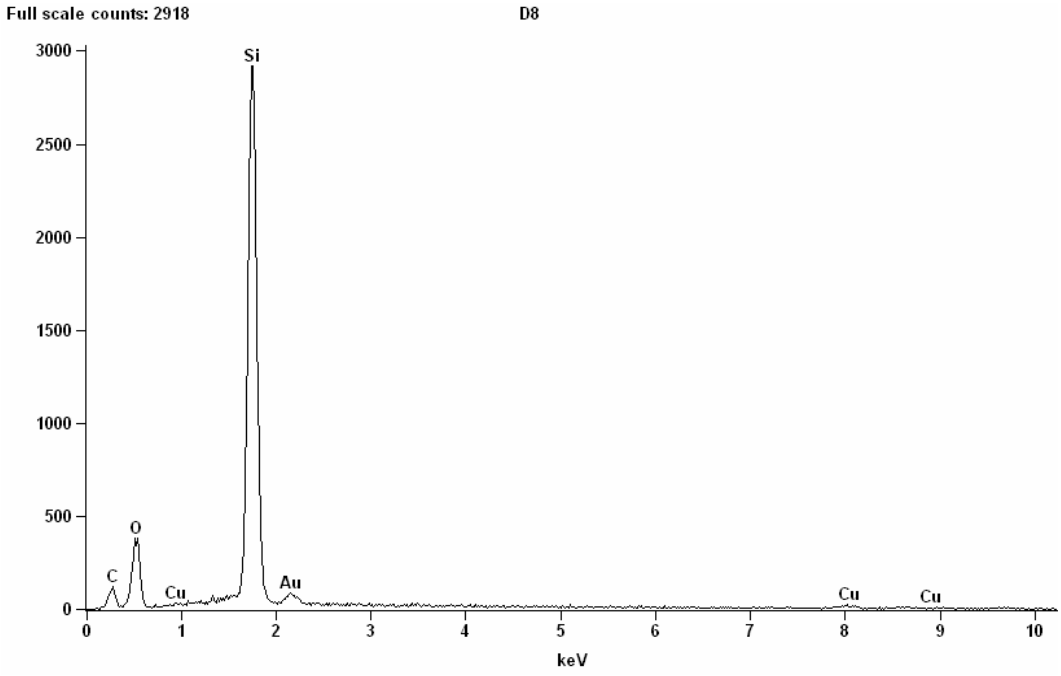

Figure B.21 EDS of Cu-LT(I)

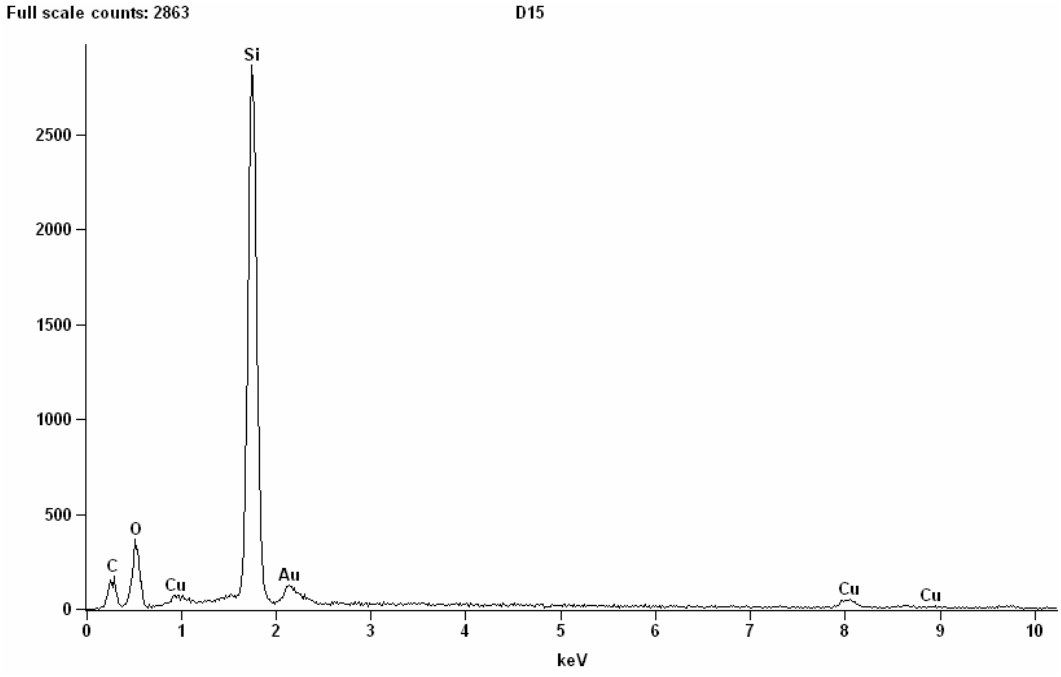

Figure B.22 EDS of Cu-LT(II)

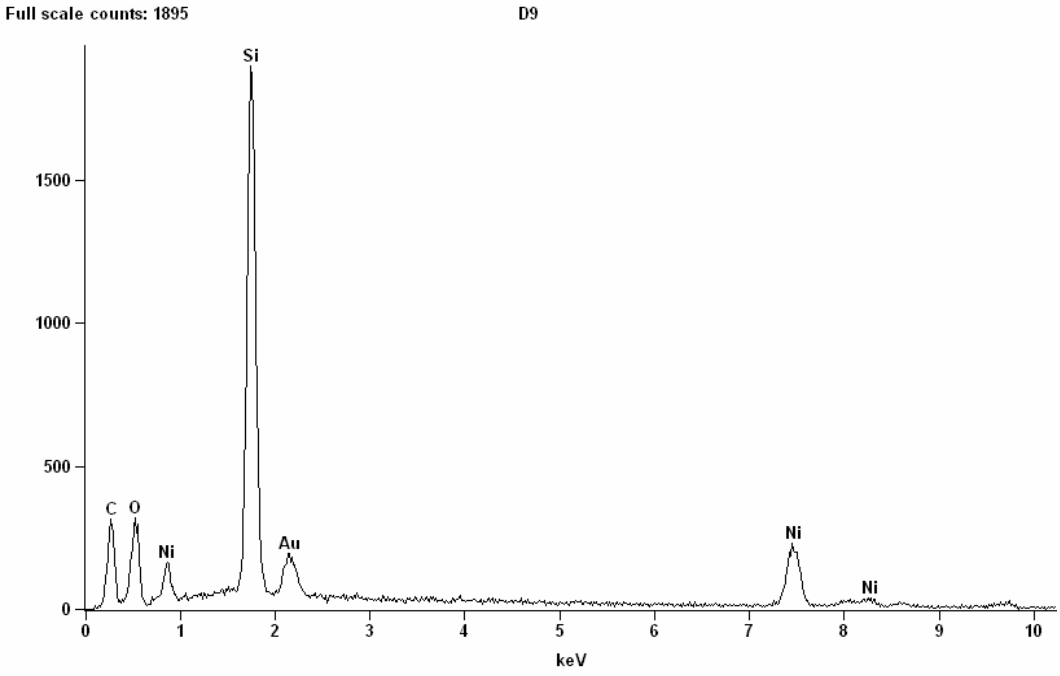

Figure B.23 EDS of Ni-HT(I)

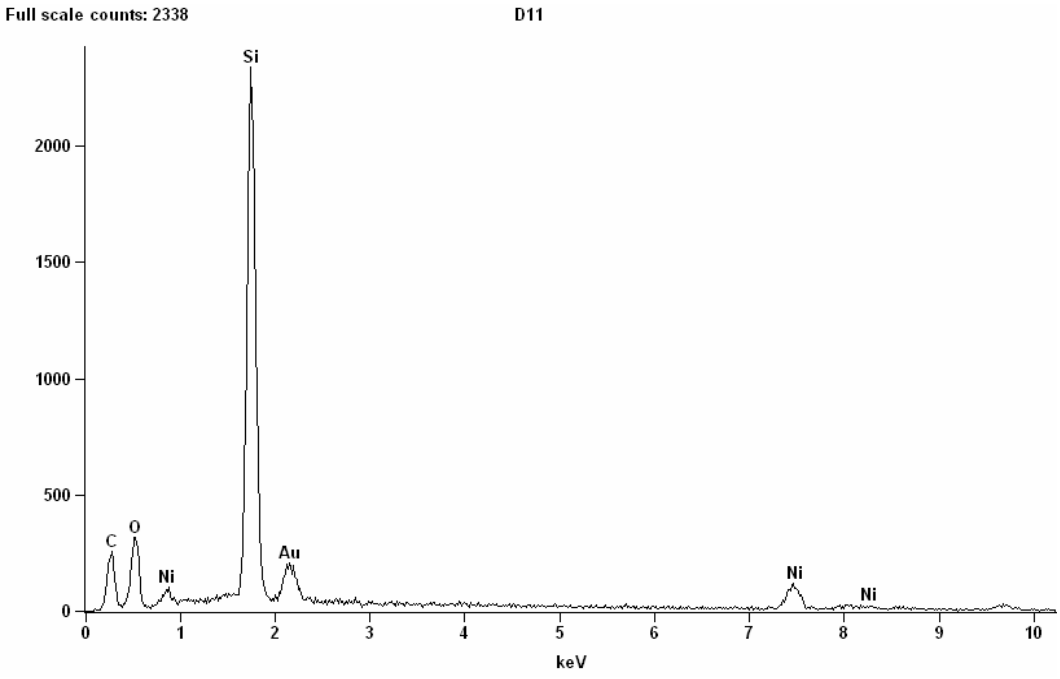

Figure B.24 EDS of Ni-HT(II)

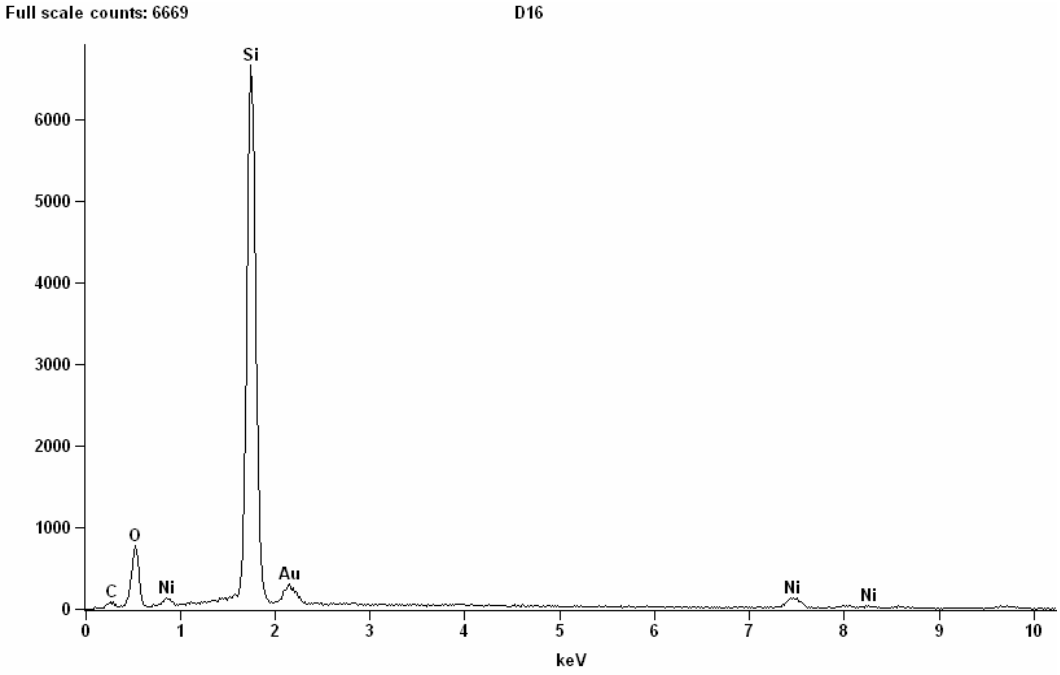

Figure B.25 EDS of Ni-Imp(I)

B.7 Atomic Absorption Spectroscopy

Table B.30 AAS analyses of Cu-MCM-41 type catalytic materials

Sample ID	Cu wt%	Cu (mol)	Si wt %	Si (mol)	Cu/Si mol ratio
Cu-Imp(I)	16.493	0.260	27.357	0.974	0.266
Cu-Imp(II)	13.714	0.216	26.855	0.956	0.226
Cu-HT(I)	13.440	0.212	28.801	1.025	0.206
Cu-HT(II)	10.883	0.171	31.614	1.126	0.152
Cu-LT(II)	2.042	0.032	41.122	1.464	0.022

Table B.31 AAS analyses of Ni-MCM-41 type catalytic materials

Sample ID	Ni wt%	Ni (mol)	Si wt %	Si (mol)	Ni/Si mol ratio
Ni-HT(I)	13.873	0.236	25.217	0.898	0.263
Ni-HT(II)	10.589	0.180	30.401	1.082	0.167
Ni-Imp(I)	6.081	0.104	27.652	0.985	0.105

B.8 Temperature Programmed Reduction

The TPR measurements in terms of temperatures are given in Figures B.26, B.27 and B.28, respectively.

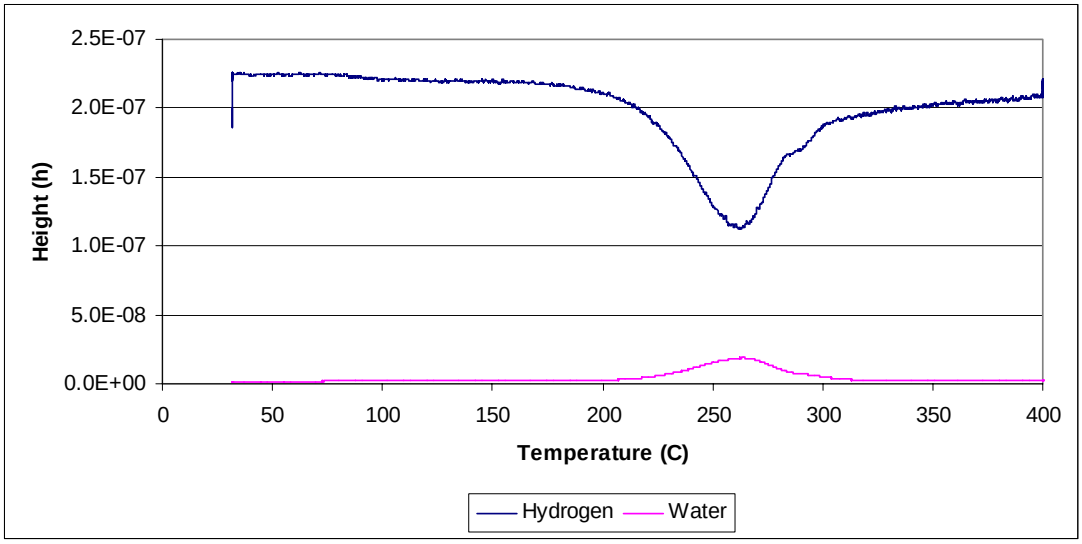

Figure B.26 TPR analysis of Cu-Imp(I)

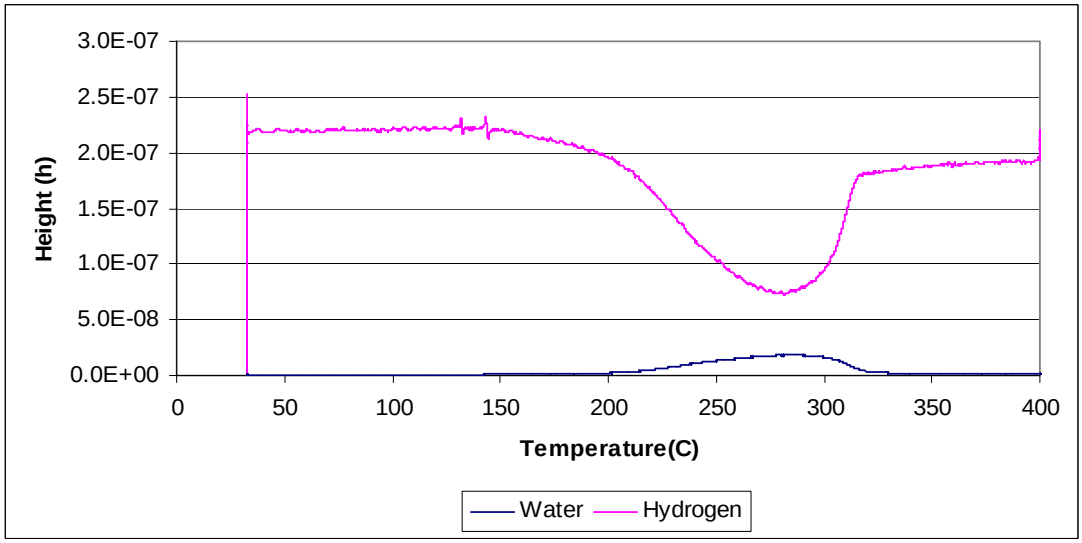

Figure B.27 TPR analysis of Cu-HT(I)

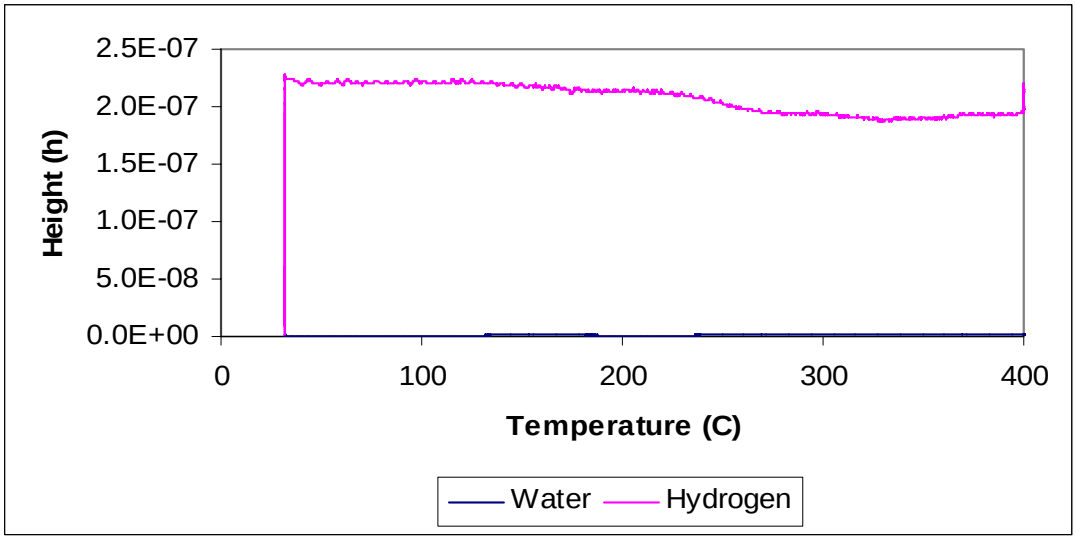

Figure B.28 TPR analysis of Cu-LT(II)